Metabolic Cancer Therapy Using Graphene Drug Carriers

A study of biguanide drug effects
in cellular and zebrafish larvae model systems

by

Abdelnour H. Alhourani

Thesis submitted in fulfillment of
the requirements for the degree of
PHILOSOPHIAE DOCTOR
(PhD)

University
of Stavanger

Faculty Science and Technology
Department of Chemistry, Bioscience and Environmental Engineering
2021

1

Acknowledgements

I would like to express my sincerest gratitude and appreciation to the following people who contributed to my knowledge and the completion of this work.

Associate professor Hanne R. Hagland, Main supervisor, for her unlimited support and assistance towards this work and for me personally as a Ph.D. candidate.

Professor Lars Harfindal, Co-Supervisor, for this critical insights and assistance that shaped this work for the better.

Professor Lutz Eichacker, for his generous contributions and advice to this work and my personal knowledge.

Jan-Lukas Førde, my friend and research collaborator throughout this project, with whom I had uncountable valuable discussions.

I would also like to thank my research group members and colleagues at the center for organelle research, especially *Marina Alexeeva, Tia Tidwell, Julie Nikolaisen, Mojdeh Khakiani, Ansooya Bokil, Martin Watson, and Marcus Roalsø,* for creating a great academic environment.

Finally, I would like to thank my partner and research collaborator at home, *Aleksandra Szwedo*, as well as my family members, for their patience and support in helping me finish this journey.

Contents

Abstract

Targeting cancer metabolism is an increasingly important strategy in the fight against cancer relapse. Metabolic drugs belonging to the biguanides family have gained attention in cancer treatment due to their ability to target the mitochondria of cancer cells and the chemo resistant cancer stem cells. However, improvements on the bioavailability of biguanides are still needed in order to incorporate them into a viable and effective treatment regimen.

To first test the effect of biguanide treatment in cancer cell lines, the effect of the metabolic drug metformin was studied in colorectal cell line models using high and low glucose concentration in growth media (paper I). The results showed that the potency of metformin was highly sensitive to the glucose concentration used *in vitro*. Furthermore, standard glucose concentrations used in cell cultures (25 mmol/L) masked the metformin response compared to physiological glucose concentration (5mmol/L) (paper I).

The bioavailability at target site can be enhanced using nanosized drug carriers to aid in the targeted delivery was studied. Graphene is a 2D carbon allotrope that has been gaining increased attention since its discovery due to its unique properties. Herein, non-oxidized graphene was modified using polyethylene glycol (PEG) to increase hydrophilicity and compared to graphene oxide (GO) as potential drug carriers for the biguanide phenformin. The pegylated graphene nano sheets (PGNS) offered good biocompatibility, high binding affinity, and a pH-responsive release of phenformin which was significantly improved compared to graphene oxide (paper II).

As the toxicity of drug carriers themselves may pose an issue, both PGNS and (GO) were tested for their inherent toxicity in different cell lines and in zebrafish larvae as an *in vivo* model. Additionally, both drug carriers were loaded with phenformin and tested for toxicity compared to free phenformin in the same model systems. The cytotoxicity and mitochondrial effects of PGNS were lower than that of GO in the cell models tested. PGNS also offered controlled release in acidic pH similar to that found in tumor microenvironments. Moreover, the ability of PGNS and GO to mitigate the side effects of phenformin was confirmed in the zebrafish larvae.

The presented data shows that PGNS have qualities that are sought after for cancer drug delivery, making it an exciting new drug carrier to be further explored for future metabolic treatments of cancers.

List of Figures

List of papers

- **Paper I**

Metformin Treatment Response Is Dependent on Glucose Growth Conditions and Metabolic Phenotype In Colorectal Cancer Cells.

Alhourani AH, Tidwell TR, Bokil AA, Røsland GV, Tronstad KJ, Søreide K, Hagland HR. Sci Rep. 2021;11:10487. doi:10.1038/s41598-021-89861-6.

- **Paper II**

Improved Ph-Responsive Release of Phenformin from Low-Defect Graphene Compared To Graphene Oxide.

Abdelnour Alhourani, Jan-Lukas Førde, Lutz Andreas Eichacker, Lars Herfindal, and Hanne Røland Hagland. ACS Omega. DOI: 10.1021/acsomega.1c03283

- **Paper III [manuscript]**

Graphene-Based Phenformin Carriers for Cancer Treatment, A Comparative Study Between Oxidized and Pegylated Pristine Graphene In Human Cells And Zebrafish.

Abdelnour Alhourani, Jan-Lukas Førde, Mojdeh Nasrollahzadeh, Lutz Andreas Eichacker, Lars Herfindal, Hanne Røland Hagland

8

1. Introduction

1.1. Drug delivery in cancer using nanoparticles.

The use of nanosized drug carriers to deliver chemotherapeutic agents in cancer treatment is a valuable avenue for research that requires further advancements. Nanosized drug carriers promise to offer increased efficacy and reduce the toxic effects of chemotherapeutics, relieving cancer sufferers from avoidable treatment side effects and increasing their quality of life. An ideal nanosized drug carrier (NDC) that can deliver on these promises is expected to bind considerable amounts of the drug that is retained until reaching the desired release location. The NDC should also have low cellular toxicity and be able to evade triggering an unwanted immune response. Additionally, the stability of the NDC should remain uncompromised during storage and when administered to a physiological system. To meet these expectations, careful tuning of the NDC dimensions and surface functionalization is needed, posing further challenges.

Constant efforts are put into producing standardized NDCs to ease predicting their effects and interactions in complex biological systems. Liposomes were the first NDC to reach clinical use as cancer drug carriers[1], offering a biocompatible delivery system that prolongs the drug circulation time and could reduce side effects[2]. However, the critical targeting potential of liposomes is compromised by aggregation and cargo leakage as well as cargo fusion, rendering low bioavailability at tumor location[3–7]. The permeable nature of the liposomal membranes could be exploited by hydrophobic drugs leading to their untargeted release [8]. Even though many liposomal-based drug formulations are now commercially available[9, 10], challenging storage requirements[10, 11] and minimal benefits in terms of patient survivals[12] have limited their broader use in cancer drug delivery.

Contrary to liposomes, which are made to mimic the phospholipid bilayer of cellular membranes in eukaryotes, synthetic nanoparticles have been developed from polymers that form a shell around its cargo. The properties of polymeric NDCs are highly dependable on the polymer unit used to manufacture them. Typical polymer units include polyethylene glycol (PEG),

9

polyvinylpyrrolidone, and polyethylenimine due to familiarity with their toxicity profile[13, 14]. However, issues regarding biodegradability, polydispersity, and low drug loading capacity hinder the clinical implementation of polymeric-NDCs[5, 15]. Other types of NDCs including, dendrimers, protein nanoparticles, and metallic nanoparticles, have been developed with their advantages and disadvantages[5]. However, continuous development and diversification of NDCs are deemed necessary by the complexity and diversity of cancers. Importantly, it is crucial to focus on making NDCs accessible to a broader range of patients by designing affordable NDCs with attainable manufacturing and storage requirements that cater to geographical regions with lower economic resources.

1.1.1   Passive targeting of tumors.

Cancer cells are driven to achieve continued growth and proliferation. Therefore, cancer cells acquire unique features and properties that set them aside from normal human tissues. Many of these properties, such as decreased pH, high redox homeostasis, often a solid tumor core, and rapid angiogenesis[9, 16], can be exploited to build NDCs that passively target these tumors increasing the drug delivery at its immediate location. As the tumor demand for nutrients grows, it promotes the rapid formation of a new, usually deformed vasculature to ensure sufficient blood supply[9] (Figure 1). The deformation gives rise to a leaky vessel structure surrounding the tumors[9]. Gap sizes observed in these vessels were widely heterogeneous, ranging from 100-2000 nm depending on the type of tumor [17].
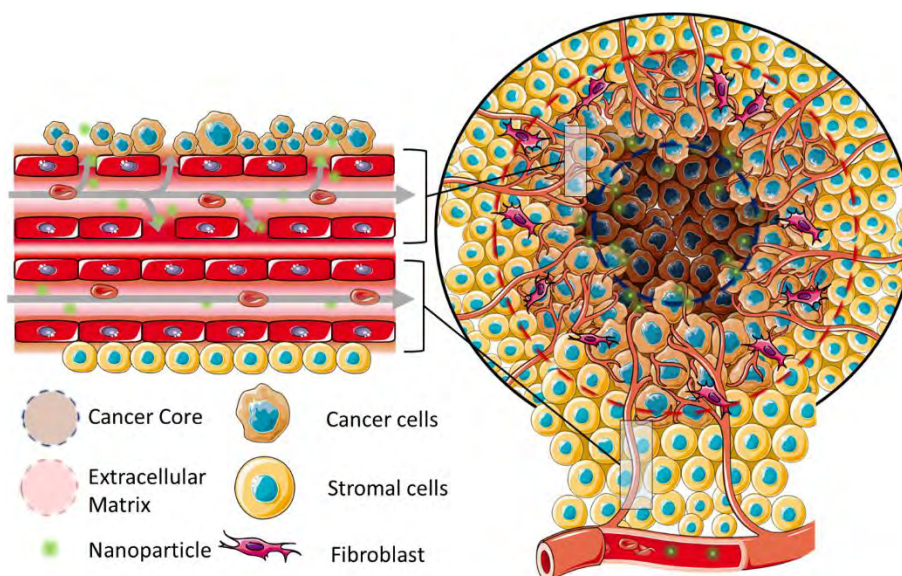
Figure 1 The tumor extracellular matrix (ECM) and nanoparticle accumulation.

A simplified schematic illustrating the increased angiogenesis in tumors, leading to an exploitable leaky vasculature by nanoparticles. The ECM surrounding the tumor that recruits additional components such as fibroblasts poses an added complexity to predict the accumulation of nanoparticles

Additionally, tumors with solid cores cause an increase in internal pressure that is exaggerated by the loss of an efficient interstitial relieving lymphatic system [10]. Therefore, larger particles that reach the inner regions of the tumor are retained for an extended period compared to smaller molecules[18]. The combination of these two phenomena is known as the enhanced permeability and retention effect (EPR), observed to occur in human tumors through biopsies and radiolabeled imaging [18]. Thus, NDCs could accumulate through vasculature gaps at the tumor site to a higher tendency than normal tissues and remain there for prolonged periods.

Production of appropriately size-controlled NDCs is critical to exploit the EPR effect[9]. However, the complexity of the tumor extracellular matrix can still form an additional obstacle layer against extravasating NDCs [9]. Therefore, it has been suggested that a further reduction in NDCs size than the approximate vasculature gap size is needed [19]. Alternatively, using non-typical spherical

shapes that are more flexible to change depending on the physical environment could also be explored to overcome this issue.

It is important to consider that the high expectations of the EPR effect alone are somewhat skewed by findings based on xenografts of highly permeable nature that do not comply with the highly heterogeneous tumor reality [9, 18]. Multivariant analysis surveying ten years of liposomal drug delivery to tumors showed that less than 1% of the nanoparticles end up at tumor location [20]. A high blood concentration of the nanoparticles needs to be maintained to prevent the backward efflux of NDCs in order to increase their tumor accumulation and efficacy [21]. This could explain the low survival benefits seen with liposome use in cancer therapy [12]. Nonetheless, reducing the side effects remains a compelling reason to continue using these nanoparticles even with cancers that do not seem to have a high EPR effect [18].

The decreased pH levels in tumors, ranging from 6.4 to 6.8, compared to the controlled 7.4 pH levels of blood and normal tissues [16, 22], is another advantageous property for targeted drug delivery. Lower pH levels are especially prevalent in highly glycolytic tumors that produce increased amounts of lactic acid, making the microenvironment more acidic [16, 23]. Therefore, it would be beneficial to formulate NDCs with pH-controlled release in relatively acidic conditions. This can be achieved by adding a pH-sensitive shell around the drug, which can be disturbed by the acidic environment. Alternatively, formulating NDCs with a pH-sensitive affinity towards the drug could also serve a controlled release in relevant pHs. To that end, several examples of pH-controlled drug carriers have been demonstrated with varying levels of pH sensitivity [24–29].

1.1.2 Graphene as a drug carrier

The discovery of graphene in 2008 [30] has revived the interest in carbon-based nanoparticles for drug delivery. However, carbon nanotubes (CNTs), a close relative to graphene, have not progressed to clinical use as a drug carrier after extensive research [31, 32], whereby toxicology studies revealed lung toxicity in humans [33] and carcinogenic effects [34, 35]. This was true for multi-walled CNTs, but the same was not observed with single-walled CNTs [32, 33, 36]. CNTs and graphene are both built of hexagonal SP^2 carbon

network, rolled up in a one-dimensional cylinder in the case of the CNTs but spread as a two-dimensional sheet making up graphene sheets [37, 38] (Figure 2). This gives graphene a more accessible surface area than CNTs for a similar number of carbon atoms. The unique properties of graphene have generated significant excitement about this 2D material, many of which are of particular interest to energy applications, including exceptional strength, thermal and electrical conductivity [38–40]. However, the high adsorbing surface area [39] and possibility for further functionalization [41], with low-cost production methods [42], are all attractive qualities, making graphene an important NDC option. The biomedical applications employing graphene properties extend beyond drug delivery, where graphene-based nanoparticles have also been studied for use in gene delivery [43, 44], photothermal therapy [45, 46], enhanced biomedical imaging [47, 48], and the fabrication of biosensors for medical applications [49, 50].
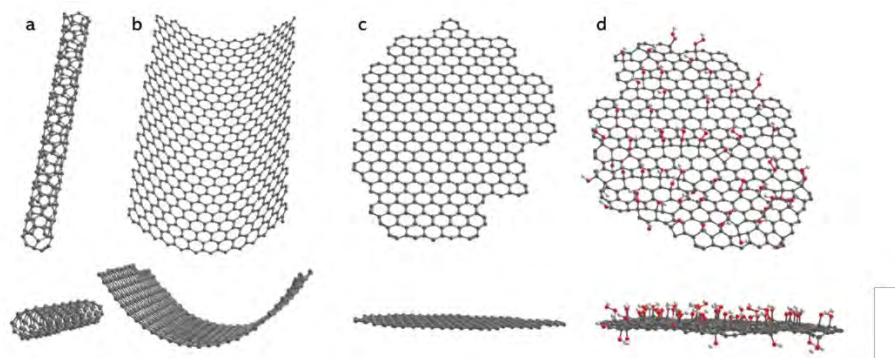
Figure 2 Schematic overview of carbon nanomaterials.

Top and side view of carbon nanotubes before (a) and after (b) unzipping into "pristine graphene" (c) compared to graphene oxide (d).

### 1.1.3 Production and functionalization of graphenes.

The oxidized form of graphene, Graphene oxide (GO), is the most studied graphene in biomedical applications. Available and inexpensive 3D graphite can be converted into high amounts of 2D graphene oxide using attainable lab production protocols in a "top-down" approach [51, 52]. GO comes with an abundance of oxygen-bearing functional groups [53], that provide

hydrophilicity [53, 54] and conveniently allows for further surface chemistry modifications [55].

However, oxidation of graphene to produce GO disturbs the SP^2 carbon network responsible for the unique functions that make graphene a "wonder material" (Figure 3), reducing its electrical and thermal conductivity significantly [53, 56]. Nonetheless, remaining "pristine areas" of pure carbon networks, i.e., non-oxidized regions, are thought to retain some of the original properties of graphene, which are essential for drug binding. These regions give GO the ability to form hydrophobic interactions with aromatic molecules [54]. However, the degree of "pristine graphene" area availability is questionable in light of the standard use of Hummer's method that relies on strong oxidizing agents such as potassium permanganate (KMnO4) and sodium nitrate (NaNO3) to form highly reactive bimetallic heptoxide dimanganese heptoxide (Mn2O7) in the presence of concentrated sulfuric acid (H_2SO_4) [51, 57, 58]. The produced GO is highly acidic and suffers from a largely defected basal plane with reaction contaminants such as residual manganese (Mn) [51, 59].
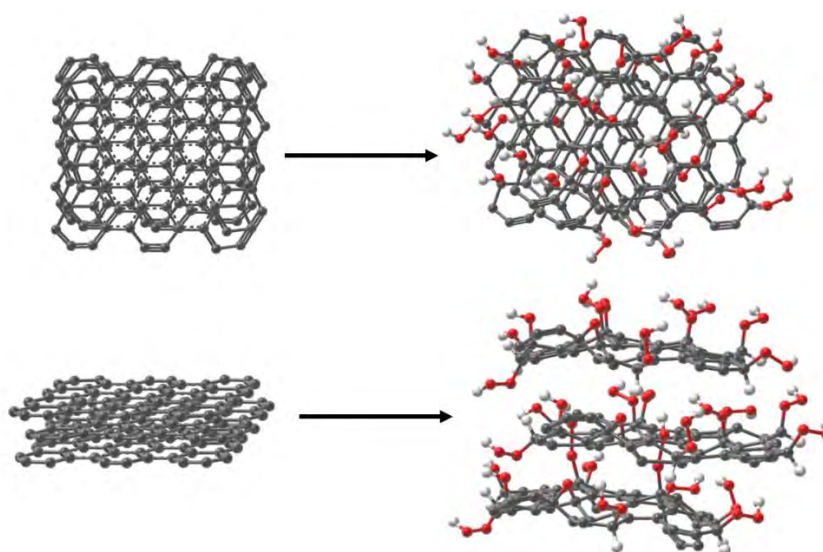

Figure 3 Exfoliation of graphite by chemical oxidation.

Top and side schematic views of stacked graphite sheets compared to their individual graphene oxide state after oxidation. The additional oxygen groups prevent the sheets from restacking into graphite.

Contrary to the mechanical methods of graphene production, GO synthesis by Hummer's method is an attainable process that can be performed in almost any laboratory. Therefore, enhancing the quality of the oxidized graphene by attempting to reverse the oxidation drawbacks of GO in a cheap and scalable manner is an attractive approach. The chemical reduction of GO to produce reduced graphene oxide (rGO) [60] is commonly used to produce sheets containing less oxygen in larger quantities than possible with mechanical production methods [61]. The chemically reduced rGO indeed contains less oxygen than GO [40, 62], enhancing electromechanical properties [55, 63], and is also similar to "pristine graphene," being highly hydrophobic and likely to aggregate [64]. Therefore, it requires stabilization either by surface modification or surfactants before use in aqueous solutions. However, a new set of problems arises from using reducing agents typically based on hydrazine [65–67], which are dangerous and pose high environmental risks [61, 68]. It is worth noting that safer and more environmentally friendly reduction reagents have been introduced [69]. However, they pose extra costs, further contaminations, and prolonged processing times that do not match the effectiveness of hydrazine [68].
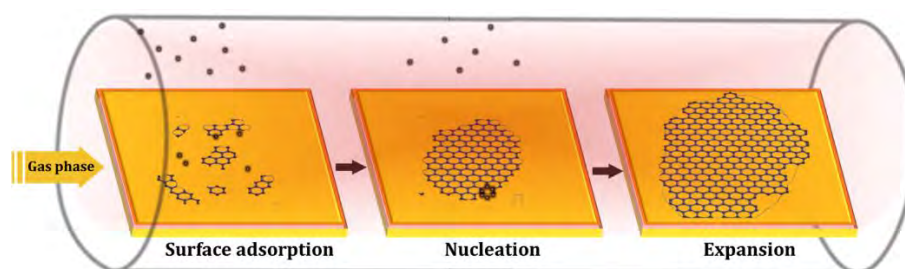
Figure 4 Graphene production by chemical vapor deposition.

Carbon deposition on a substrate from a carbon-containing gas phase under controlled conditions allowing the seeding and expansion of graphene sheets while avoiding spontaneous oxidation.

Graphene production by chemical vapor deposition (CVD) is a "bottom-up" approach that renders large single-layer graphene sheets from gaseous carbon precursors [70] (Figure 4). A defect-free growth of CVD graphene requires an energetically costly thermal treatment to block the spontaneous oxidation of the graphene sheets [53, 56]However, the potential for scaling up CVD graphene production method towards larger quantities of "pristine

graphene" makes it a promising approach. Plasma-enhanced treatment has come in as a promising alternative strategy to thermal treatment for the production of low defect "pristine graphene," allowing high scale production of Plasma-enhanced chemical vapor deposition (PE-CVD) graphene at lower costs [OBJ][71, 72]

The terms "graphene" and "pristine graphene" are used ambiguously in literature in the lack of international and regulatory standards and do not always conform to a pure graphene-based material [73, 74]. An example of using unspecific terminology is the use of "pegylated graphene" when the starting material is GO [75] or not clearly characterized material [76]. Such confusion leads to contrasting reports on biocompatibility, drug binding properties, and functionalization protocols [33, 77, 78].

1.1.4   Biocompatibility of graphenes.

Recent reports of graphene-based drug delivery have used GO/rGO with either DOX [26, 48, 79] or Paclitaxel [80, 81]. However, conflicting reports on the biocompatibility of graphene in these studies are probably due to the non-homogeneity of produced graphene oxide, including different oxygenation levels of the GO used. While "carbon-based material" might give the impression of biocompatibility with the human body, graphene sheets have a unique 2D structure that needs to be carefully evaluated before proceeding with clinical use, even if built up purely out of carbon atoms [82]. To that end, the toxicity of graphene-based drug carriers should consider impurities and contamination from production protocols and aseptic working conditions [83, 84] that can exert additional toxicity.

Lessons learned from CNTs show that careful purification and surface functionalization with polymers like PEG can mitigate some toxic effects and enhance biocompatibility [36, 75, 85]. PEGylation of GO has shown to half its liver accumulation, slightly decreasing its toxicity [86].

The toxicity and biodistribution of graphene material have been studied depending on the intended application. Assessments of oral [87], or subcutaneous administration [88], as well as inhalation [89–91], showed varying degrees of toxicity based on sheet size and oxidation levels [87–91]. However, of most relevance to cancer drug delivery is the intravenous

16

administration (i.v.). Agglomeration of intravenously administered GO was shown to cause accumulation in the lungs, whereas GO sheets end up in the liver, spleen, and bladder when well dispersed and stable [92, 93]. The relatively more hydrophobic rGO has been found to cross the blood-brain barrier and accumulate in the brain [94]. The sheet size is also a determining factor for the accumulation site, with the smaller sheets ending up in the liver to a greater extent than larger sheets [95]. However, evidence suggests that graphene sheets can be renally cleared if they do not agglomerate to critical sizes [96, 97].

On a cellular level, the most-reported mechanism of graphene cytotoxicity involves the generation of reactive oxygen species due to mitochondrial dysfunction and associated with a dissipated membrane potential [98–100]. Therefore, the assessment of cellular bioenergetics can be an essential tool to understand the interaction of graphene with the mitochondria and its potential to deliver drugs that target its energy-producing machinery.

1.2. Targeting cancer metabolism, a new avenue for treatments

Mitochondrial dysfunction is observed in many cancers [101, 102], and has been commonly portrayed as an expected consequence of cancer growth[103]. The focus on genetic roots and predisposition led to the production of chemotherapies that targets fast-dividing cells and inhibit their growth [104, 105]. However, as we look for more answers and ways to treat cancers effectively, more attention goes to the metabolism-targeted treatments in cancers. A developing understanding of the metabolic roots of cancers is a primary driver towards the increased investigation of cancer metabolism and its involvement in disease progression. This opens new avenues to use metabolic agents targeted at manipulating the mitochondria of cancer cells, making them more susceptible for cancer treatments [105, 106].

1.2.1   The altered metabolism of cancers.

Due to their excessive growth, cancer cells require increased amounts of proteins and fatty acids for continued cellular proliferation[101]. This constant

production of biomolecules dictates a shift in the metabolic priorities of the cell away from efficient use of glucose for energy production towards anabolic processes [101, 107]. In non-proliferating cells, oxygen availability is essential for the optimization of glucose metabolism in order to achieve a high energy outcome in terms of ATP[108]. This is done by channeling the glycolytic end-product pyruvate through the tricarboxylic acid (TCA) cycle, which provides the necessary NADH and $FADH_2$ for functionality of the electron transport chain (ETC) complexes through oxidative phosphorylation (OxPhos) to produce ATP at the final ATP-synthase complex[101] (Figure 5).
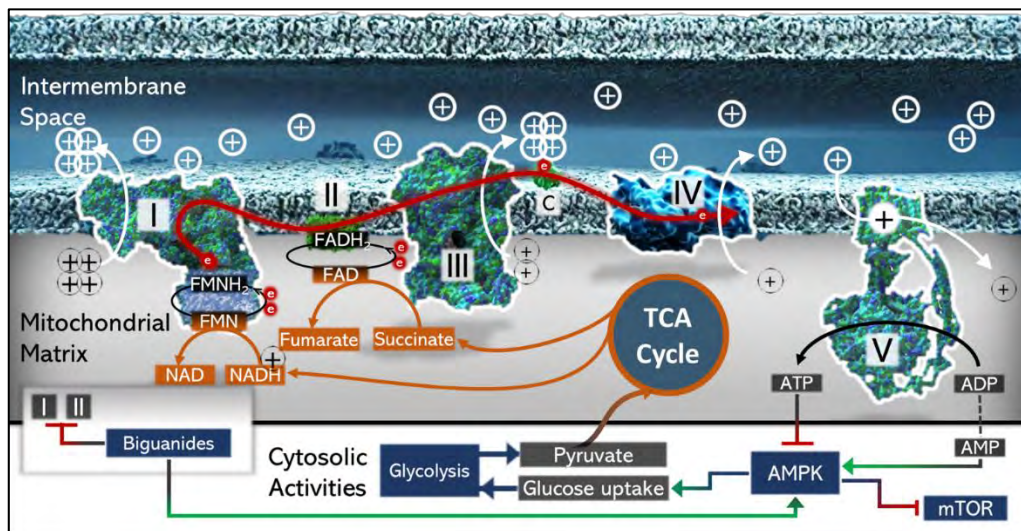
Figure 5 Respiratory chain modulators and the effect of biguanides.

The ETC consists of four complexes. Electrons donated from TCA cycle contribute to an electron across the ETC complexes, which is used to pump protons into the intermembrane space and are later channeled through complex V to produce ATP. AMPK regulates glucose uptake depending on the AMP/ATP and dictates the anabolic/catabolic state of the cell to ensure sufficient ATP supply. Biguanides can block the electron flow by inhibiting complexes I and II and subsequently activating AMPK signaling.

Cells under hypoxic may switch to anaerobic glycolysis producing lactate as a by-product of glucose breakdown to maintain ATP production exempt from the mitochondria[108]. The loss of OxPhos metabolism in cancer cells was first described by Otto Warburg in the 1920s, where he observed that some cancer cells, later termed to exhibit a "Warburg" metabolism, elevating their reliance on glycolysis to meet their energy needs, and consequently taking up

significantly higher amounts of glucose[109–111]. Cancer cells portraying the Warburg phenotype attempt at halting the mitochondrial utilization of glucose (as pyruvate), reducing oxidative phosphorylation and the high ATP yield of the ETC in favor of aerobic glycolysis[102, 108, 109]. Pyruvate is instead converted to lactic acid to oxidize NAD$^+$ from NADH[112]. Such metabolic maneuver allows sustaining the excessive growth levels by exploiting a continuous NAD$^+$ availability to maintain glycolysis and harvest its intermediates to synthesize biomolecules needed for cellular division[101, 112]. Both of the co-enzymes NAD(H) and FAD regulate the function of complex I and II of the ETC, respectively, which are mutated in many cancer cells [113–115]. This also gave these coenzymes, among others, increasing attention to understand their role in cancer progression[116].

1.2.2   Targeting the mitochondria in cancer treatment.

Increased understanding of metabolic adaptation in cancers can lead to new treatment methodologies aimed at overcoming chemotherapy resistance[117, 118]. To separate the energy regulation in cancers from biosynthesis, the ETC needs to be uncoupled from ATP production to maintain replenishment of the TCA cycle [119–121]. This is done by upregulating uncoupling proteins to increase the proton leak from the intermembrane space without going through ATP synthase and therefore controlling the consumption of the limiting adenosine diphosphate (ADP)[110, 120]. However, cancer cells can revert to OxPhos metabolism when under stressed conditions[122, 123], making some cancer cells more chemotherapy resistant by increasing their energetic flexibility in a similar fashion to cancer stem cells (CSCs)[111, 119, 124]. AMP-activated protein kinase (AMPK) acts as an energy sensor to regulate glucose intake by monitoring AMP/ATP ratio[111, 121]. AMPK controls anabolic/catabolic processes to maintain sufficient ATP levels by regulating the signaling of the mechanistic target of rapamycin (mTOR)[101] (Figure 5). Upregulating mTOR anabolic signaling allows cancer cells to boost their cellular growth[101], giving AMPK-mediated inhibition of mTOR signaling an antineoplastic effect in many cancers[121].

1.2.3   Biguanides mitochondrial effects in cancer cells.

Biguanides have been in clinical use as diabetes medication since the 1950s[125] giving researchers years of knowledge and information to understand their effects on a large segment of the population. Metformin (dimethylbiguanide), a first-line type-2 diabetes medication with an annual cohort of users that exceeds 150 millions[126], gained support as an alternative to phenformin (N-phenethylbiguanide) in treatment of diabetes due to its reduced side effects [125, 127]. More recently, meta-analysis on people treated with metformin revealed a potential protective effect against some cancers that were not associated with other in-use diabetes medications[128, 129]. The anti-tumor potential of metformin and its analog phenformin has been further confirmed *in vitro* and *in vivo*[130, 131]. Biguanides can activate AMPK signaling through mechanisms that are both dependent[132] and independent [133] of complex I inhibition.

Additionally, biguanides can inhibit the mitochondrial glycerophosphate dehydrogenase (mGPD), which is vital for regulating the cellular redox potential and production by cytosolic reducing equivalents[134, 135].   A disturbed AMP/ATP ratio due to complex I and II inhibition could be an important treatment target in many cancers that rely on OxPhos to evade chemotherapy[117, 136, 137]. Additionally, the inhibition of complex I deplete the critical metabolites of the TCA cycle for the tumor biosynthesis [136, 138].

Multiple clinical trials have tested the use of metformin as adjuvant treatment in cancers with promising results[139–141]. However, the efficacy of metformin within a therapeutic window is still a major bottleneck for its implementation in therapy[126, 142]. This could be a reason for its shortcomings as a sole treatment in trials using 850-2000 mg of metformin daily[143–145], compared to higher concentration treatments in successful preclinical studies[146, 147]. Activation of AMPK signaling *in vitro* by metformin was achieved at a concentration of 50 µmol/L[148]. In context, the plasma concentration of metformin after treatment is on average estimated to be 15 µmol/L[149] with an upper therapeutic window of ~55 µmol/L[150]. However, significantly higher concentrations are needed for the inhibition of complex I [151]. The accumulation of positively charged metformin, and similarly, phenformin in the mitochondrial matrix due to the negative

membrane potential could result in significantly increased mitochondrial concentrations relative serum, providing a partial inhibition of complex I by metformin[151]. Moreover, evidence of metformin accumulation in specific organs[152], mainly in the intestines[153], could explain the protective effect of metformin seen in some specific cancers, which could be due to the increased complex I inhibition that comes with higher concentrations in these tissues.

To utilize the benefits of complex I inhibition further, interest in phenformin as a metabolic anticancer medication has increased[154–159], with an ongoing clinical trial to determine its safe use as adjuvant therapy (NCT03026517). Phenformin has shown higher potency against cancer cells in cellular [160, 161] and animal models[162, 163]. The particular interest in adjuvant biguanides therapy in cancers comes from their ability to affect chemotherapeutic resistant cancer stem cells or quiescent cells [164, 165] to form an effective treatment with partner drugs that targets rapidly proliferating cells[166]. Before moving further in biguanide use in cancer therapy, experimental and biological factors affecting their efficacy need to be determined to ensure better consistency and understanding of their anti-tumor effects in future research.

2 Aims and objectives

The main goal of this work is to optimize the use of biguanides in a preclinical setting to target the mitochondria of cancer cells. A targeted therapy approach incorporating graphene-based drug carriers to improve the bioavailability of biguanides is investigated to overcome bottlenecks preventing their implementation in therapy. The following objectives are put forward to achieve these goals:

- Identify the experimental parameters that better represent the effect of biguanides in cancer cells in terms of mitochondrial dependency and glucose culturing conditions.
- Identify drug delivery candidates from biguanide derivates for use with graphene-based drug carriers.
- Achieve attainable production and characterization of aqueously stabilized graphene-based carriers to be used in drug delivery applications.
- Study the interaction dynamics between graphene and phenformin in regards to the oxidation level of graphene.
- Determine biotoxicity of novel graphene materials in cellular and animal models.
- Examine the effects of graphene-based drug carrier systems in a passive metabolic targeting approach against cancer cells while minimizing possible side effects.

3 Summary of Papers

Paper I

Metformin treatment response is dependent on glucose growth conditions and metabolic phenotype in colorectal cancer cells

Background

Metformin use in cancer treatment has stalled in the past years due to discrepancies in beneficial outcomes in clinical and preclinical studies. Earlier *in vitro* attempts at elucidating the anticancer effect of metformin have been conducted without proper consideration of critical factors, such as growth conditions, that could lead to inconsistent results. Therefore, we investigate metformin potency in cancer cells with different mitochondrial dependency levels and study the effects of non-physiological glucose versus physiological glucose concentrations on the experimental outcomes to elucidate how metformin can be used to its best potential.

Results and considerations

Metabolic phenotyping of the colon cancer cells SW948 and SW1116 showed that the prior is a closer representation of the "Warburg" phenotype while the latter can better utilize its mitochondria to overcome stress conditions such as metformin exposure. Glucose concentrations in the culture media played a pivotal role in deciding the outcome of metformin treatment in both cell lines. Adhering to the physiologically relevant concentrations (5mmol/L) was of utmost importance as the commonly used high glucose (25mmol/L) supplementation to the culture media masked the antiproliferative effects of metformin. Therefore, we implement the use of physiological concentration of glucose in culture media for further experimentation using metabolic drugs in the following work. Our results indicate that metformin could be better utilized as an adjuvant treatment in cellular phenotypes similar to SW1116 but highly potent against phenotypes similar to SW948 as an individual treatment.

Paper II

Improved pH-responsive release of phenformin from low defect graphene compared to graphene oxide

Background

Achieving effective concentrations of biguanides at tumor location is an important milestone towards its application in cancer treatment. Graphene-based drug carriers offer great potential, especially with the increased material accessibility in a broader range of qualities. Therefore, we investigate the drug carrier capabilities of two graphene-based carriers obtained by different production methods, PE-CVD graphene and GO, in combination with the metabolic drug phenformin.   The graphene-based drug carriers are assessed in terms of stability, binding affinity, and pH-dependent release of phenformin.

Results and considerations

The PEGylated graphene nanosheets (PGNS) prepared from low defect PE-CVD graphene were found to be less likely to agglomerate when loaded with phenformin than GO. The steric stabilization in PGNS showed better compatibility with phenformin compared to the repulsive stabilization in GO. In addition, an excess of 4-fold increase in the binding affinity to phenformin was observed in PGNS over GO. Increased surface defects due to a higher oxygen content (~5-fold higher) could explain the compromised affinity in GO compared to PGNS. Finally, phenformin release in acidic pH was elevated in both graphene-based drug carriers compared to physiological pH but was enhanced using the less defected PGNS sheets. This is attributed to the higher capacity to carry on pi interactions which are pH-responsive.

Paper III

Graphene-based phenformin carriers for cancer treatment, a comparative study between oxidized and pegylated pristine graphene in human cells and zebrafish

Background

Biocompatibility assessment in biological systems is an essential step towards implementing the use of nanoparticle drug carriers. Therefore, cellular viability and mitochondrial toxicity of GO and PGNS were assessed in cellular and zebrafish models. Furthermore, the efficacy of phenformin after loading onto GO and PGNS was tested for its ability to induce antiproliferative effects in cancer cells and whether its mitochondrial effect was sustained compared to free phenformin in a pH-responsive release mechanism.

Results and considerations

The stability of PGNS in culture media was better than that of GO. More importantly, PGNS exerted lower toxicity on all three cell models investigated in our tests. Lower concentrations (<25 µg/ml) of graphene seemed to be well tolerated by cells, with minimal effects on the mitochondria, although GO concentrations of 100 µg/ml induced a significant reduction in the spare respiratory capacity, indicating mitochondrial toxicity. Both GO and PGNS demonstrated a pH-responsive release of phenformin. However, PGNS mediated no additional toxicity, contrary to what was observed when using GO. Further testing on zebrafish *in vivo* models revealed successful mitigation of acute phenformin mitochondrial effects when loaded onto graphene. Our findings indicate that PGNS is the better candidate for further drug carrier exploration and may have promising potential for intravenous drug administration.

4. Discussion

4.1 Methodological considerations

The interdisciplinary nature of this work dictates the use of a wide range of analytical methodologies that incorporates material sciences with biological technology. Meeting the varied instrumentation demand presents a unique challenge in a biologically specialized facility. It also brought the need to utilize alternative methodologies to reach the experimental aims.

4.1.1 Graphene handling and safety

Even though most commercially available graphene is produced in microscale dimensions, it remains a 2D material, making it a nanoparticle due to a minimal (down to one atom only) third dimension. The 2D property puts graphene in the category of nanomaterials where special safety requirements apply, especially when working with dry material. Safety precautions, such as working in an enclosed environment (dust box), are critical as the toxicity of graphene is not fully explored in humans. Furthermore, PE-CVD graphene sheets are collected under inert conditions to reduce spontaneous oxygen functional groups formation. Therefore, further atmospheric exposure of graphene sheets needs to be performed in inert conditions.

4.1.2 Characterization of Graphene materials

A seemingly trivial but vital aspect of working with graphene is the ability to keep track of its concentration in solutions after dispersing. Due to the absence of characteristic absorption peaks in the visible range, the optical density of graphene is traditionally measured at 660 nm to estimate its dispersion concentration. However, the absorbance spectrum of graphene is highly dependent on its polydispersity and the thickness of graphene sheets (number of layers) [167]. We found that using the area under the curve in the visible range is a more stable metric to correlate with the concentration of graphene dispersion over a one-point measurement at 660 nm.

In terms of size, atomic force microscopy (AFM) and transmission electron microscopy (TEM) imaging are among the most accurate methods to estimate the lateral size of graphene sheets. However, both methods can be time-consuming and inconvenient to incorporate in fabrication methods development. Alternatively, Dynamic light scattering (DLS) is a high throughput technique that is very sensitive to particle shape as it measures particle diffusion in solution to estimate its size based on the Stokes-Einstein equation [168]. Therefore, DLS is not able to offer an accurate size estimation for 2D materials due to their non-spherical shape. However, Electrophoretic light scattering used for measuring the zeta potential is not affected by particle shape [169]. It therefore can be used to characterize graphene in different solutions rapidly and with different functionalization to indicate its stability and surface charge.

Another important aspect of graphene characterization is the Carbon/Oxygen ratio. While absolute measurements are mainly possible using X-ray photoelectron spectroscopy (XPS), and thus the most commonly used method, we found that the changes in Carbon/Oxygen can be consistently measured using x-ray fluorescence spectroscopy (XRF), offering an important alternative. The choice of method relies on the access to instrumentation during the project, and thus change of the carbon/oxygen ratio was presented in GO versus PGNS rather than absolute ratios.

4.1.3 Functionalization of graphene

Pegylation was used in this work to achieve aqueous stabilization of PE-CVD graphene while sparing the pi-interaction capacity of the graphene surface that the use of potential surfactants can otherwise occupy. Additionally, surfactants can have toxic effects on cells and be less biocompatible in a biological environment than PEG. The 2 kDa PEG used in this study to stabilize graphene was selected among different candidates with weights of 750, 2000, 5000, and 10000 Daltons. In our pilot experiments, the 2 kDa PEG offered better stabilization than smaller PEG and was small enough to conveniently wash off its excess using dialysis and filtration. Since we found that it offers minimal blockage of the graphene surface than larger PEGs, this was the PEG candidate used throughout the experiments.

4.1.4 Chemical and biological investigation using fluorescence lifetime.

The use of fluorescence lifetime imaging microscopy (FLIM) allows for a functional investigation within the nanometer dimension using a microscope. The technique offers superior reproducibility over intensity-based methods as the lifetime of a fluorophore is independent of the acquisition parameters. Using the quenching properties of graphene, FLIM can estimate the proximity of fluorescent molecules to graphene sheets by tracking the lifetime as it offers an alternative, faster route to dissipate the excitation energy. However, due to the statistical nature of fluorescence lifetime calculation and the measuring electronics limitation to a one-photon per laser pulse, a relatively slow acquisition procedure needs to be repeated to acquire enough data points to produce an accurate fluorescence lifetime decay. Thus, in the zebrafish lifetime experiments (paper III), ensuring sufficient data within collection while avoiding photobleaching the sample dictated the use of wider regions of interest (ROIs) that encompass multiple organs. Further precise segmentation of the zebrafish larvae organs can result in inconsistencies between the samples due to variations in Z-sampling of photons and inadequate quality of the lifetime decay due to lower number of photons.

4.2 Cancer metabolism and targeting of cancer stem cells.

The complete eradication of cancers is difficult to achieve due to the presence of a metabolically adaptable sub-set of cancer cells that evade most anticancer drugs [117, 136, 164]. These cells can switch between cancerous proliferation and quiescent survival modes in response to stress factors and could later trigger cancer relapse [117, 118, 123]. The need to target both metabolic phenotypes of cancer cells brings biguanides into use in cancer therapy. Its ability to halt the ETC, which is the exact machinery necessary for both energetic and biosynthesis processes [125, 132, 136, 151], offers an alternative path to enhance cancer treatment.

The use of metformin as an adjuvant drug in cancer therapy has been faced with conflicting reports on its effectiveness in preclinical tests [170, 171] and

high discrepancy in many *in vitro* model systems [142, 172, 173]. The high glucose levels (25 mmol/L) routinely used to accelerate subculturing could offer a reason for this as it masks the effects of metformin on cancer cells (Paper I). This further underscores the importance of evaluating drug responses in physiological glucose conditions (5 mmol/L). Adopting these glucose culturing conditions was critical to better reflect on the potency of biguanides in our experimental models. As drug loading onto NDC itself may interfere with the cellular uptake influencing its measured potency, thus a misrepresentation of the drug effectiveness due to high glucose levels needed to be avoided.

It is suggested that the greatest potential of biguanides is treating chemoresistant OxPhos phenotype exhibiting cancer cells [164, 165]. However, in a preclinical setting, the highly proliferative and more glycolytic (SW948) colorectal cancer cells were especially responsive to mono biguanide treatment (Paper I). Suggesting that an effective biguanide treatment could be sufficient alone in eliminating both proliferative and quiescent cancer cells. However, our results indicate that millimolar concentrations of metformin are needed to exert adequate antiproliferative effects, even in physiological glucose conditions (Paper I). Nonetheless, millimolar concentrations of metformin are difficult to achieve in many tissues [150]. Alternative strategies are needed to ensure or increase the concentration of metformin at the target location.

4.3.1   Targeted biguanide treatment using graphene carriers

Metformin has a low toxicity profile in combination with low potency, whereas its analog phenformin has a higher potency and is suggested to be a better candidate with a tolerable toxicity profile for cancer treatment [17, 155, 158, 174]. Phenformin has been shown to be effective against CSCs at concentrations much lower than metformin of 1 mM (~0.2 mg/ml) [17]. However, the plasma concentrations of phenformin, after a typical 50 mg dose treatment, peak at 0.0002 mg/ml with a bioavailability of 11 hours [175]. Although a liposomal-phenformin formulation has shown promising effects over the free form *in vivo* and *in vitro [176]*, the higher potency of phenformin can be further exploited when combined with an NDC that improves on the delivery profile, such as graphene. Moreover, the aromatic ring structure in

phenformin makes it a more suitable candidate to combine with graphene over metformin.

The high ionic strength of phenformin makes it challenging to use in combination with GO due to a noncompatible stabilization mechanism. The repulsive stabilization of GO stems from the negatively charged oxygen groups on its surface, subsequent to the chemical exfoliation of graphite by oxidizers [42, 64]. This stabilization mechanism grants GO good aqueous dispersibility. However, it leaves the GO sheets susceptible to agglomeration upon the dissolution with high concentrations of positive ions, such as phenformin (Paper II), posing a major hindrance to its drug delivery ability and subsequent clearance. Moreover, the high oxygen content in oxidized graphene is implicated in increased reactive oxidative species (ROS) generation in cells, causing toxicity. This incites the need for an alternative stabilization strategy that is more compatible with higher ionic strength solvents and less toxic to biological systems.

Therefore, PEGylated graphene nanosheets (PGNS), an NDC fabricated from a highly hydrophobic and less defected PE-CVD graphene, were used in this study as a graphene-based drug carrier after covalent functionalization with PEG. The improved aqueous stability and phenformin binding affinity of PGNS over GO make it a better suited NDC for phenformin delivery. The use of a PE-CVD-based graphene carrier is of greater relevance considering the increased availability of "pristine" graphene. Importantly, the improved binding affinity of PGNS highlighted the significance of Pi-interactions for phenformin loading, being responsible for over four-fold increased affinity compared to GO. As the oxygenation level in PGNS was measured to be significantly lower than GO, the proportion of "pristine graphene islands" containing delocalized electrons and consequently capable of participating in Pi-interactions, should be relatively higher. Thus, PGNS was more capable of binding phenformin (Paper II).

The benefits of using less oxidized graphene also extended to a decrease in cytotoxicity, as observed in several cell models (paper III). Previous studies have shown a correlation between cellular mitotoxicity and increased oxygen levels in graphene [177], resulting in the generation of reactive oxidative species (ROS) causing mitotoxicity. This is supported by our data indicating significant mitochondrial stress in SW948 cell line after 0.1 mg/ml GO

exposure that is not observed with similar doses of PGNS (paper III). It is unclear whether the mitotoxic effect of GO would add to the therapeutic values of phenformin in cancer cells. However, given the expected longer circulation time of graphene itself [33, 92, 94], it would be wise to limit the toxic contribution of the drug carrier itself, in this case, graphene, to a minimum.

By having a pH-dependent amphiphilicity property, graphene oxide became an attractive choice for use as an NDC in cancer treatment [24, 29, 178]. However, the underlying causes for surface changes in GO by pH, leading to drug release, are not fully understood. The pH-dependent binding affinity of GO has been previously attributed to weakened hydrogen bonding [24, 27–29], "interruption" of pi-pi interactions [26], and the protonation of the carboxylic groups on graphene oxide [25]. Most of which predict that the binding affinity of non-oxidized graphene would be less affected by changes in acidity. However, these claims are indirectly inferred, and we found that PGNS had increased pH responsiveness in terms of binding affinity compared to GO, highlighting the importance of the dominant Pi-interactions of PGNS over other hydrophobic interactions in controlling the pH responsiveness (Paper II).

Even though these findings are based on the interaction kinetics with only one drug represented by phenformin, both the enhanced adsorption capacity and the pH responsiveness can apply to other drugs and molecules subject to pi interactions. Thus, making "pristine graphene" use in future biomedical applications more advantageous compared to heavily oxidized forms, such as GO. *In vitro* application of the pH-responsive release confirmed that PGNS loaded phenformin had a decreased toxicity than free phenformin at pH 7.4, but the opposite was confirmed at the lower pH of 6 (Paper III). This could suggest that phenformin would remain retained to PGNS to a higher degree in tissues with physiological pH potentially reducing harmful side effects while being selectively released in lower pH environments. Similar results were not observed using GO as an NDC for phenformin, likely due to GOs own toxicity on the cells in our *in vitro* setting, which has also been previously reported by others[85]. However, *in vivo* testing of both PGNS and GO revealed no acute toxic effects in zebrafish larvae. Moreover, both were able to minimize the side effects of phenformin compared to the free drug (Paper III). Free

phenformin induced a significant increase in, what we believe to be, oxidized FMN and FAD 24 hours after the injection, consistent with mitochondrial toxicity [179, 180]. This toxicity appeared to be mitigated by loading phenformin on either GO or PGNS, thus providing a promising platform for the re-introduction of phenformin in clinical use as a cancer treatment.

4.3.2   Conclusion and future perspectives

The use of an attainable fabrication process to utilize non-oxidized graphene as a drug carrier for phenformin shows considerable improvements over many NDC systems and opens an interesting field for further investigation. The example of PGNS being a better alternative to graphene oxide in terms of biocompatibility and drug binding ability, should bring the implementation of graphene in drug delivery closer to reality. Further *in vivo* testing of the ability of non-oxidized graphene-based carriers to enhance the effects of the metabolic drugs at the target site while limiting its side effects to normal cells in more advanced models is still needed.

The use of zebrafish larvae as an *in vivo* model is an accessible approach that does not require elaborate laboratory resources. It offers a promising early testing system for assessing drug and nanoparticle toxicity. However, further genetic modification to the zebrafish could help better understand system effects are still needed. For example, using macrophage fluorescent zebrafish could prove advantageous to localize graphene biodegradation pathways within the organism. Moreover, tumor-bearing zebrafish in-vivo model would be a logical next step to further test a graphene-based phenformin system in order to confirm its properties *in vivo.*

Future concerns regarding the biomedical use of graphene need to be carefully evaluated to reach feasibility for clinical use. In terms of biocompatibility, a more comprehensive understanding is needed of the toxic effect of graphene sheets under shear stress applied by the physiological blood flow. Additionally, the by-products of graphene degradation need to be considered for their toxicity *in vitro* and *in vivo* models. While this is an area of active investigation for graphene oxide [36, 181], parallel evaluation is needed for less oxidized graphene as the lack of functional groups that modulate GO's interactions with proteins. Furthermore, the effect of pristine

graphene on the mitochondrial membrane potential still needs to be better understood.

Investing in the determination of metabolic treatment susceptibility in cancer patients could offer an improved fighting chance for chemoresistant and re-occurrent cancer sufferers. Careful evaluation of patients' tumors is needed in order to define viable treatment options. Metabolic flux analysis to determine the preferred energetic pathways of cancer cells is the current method used in research settings. However, it lacks a standardized operational procedure approved for clinical use. Alternative strategies that include identifying metabolically sensitive biomarkers that may guide treatment predictions could be necessary to achieve this transition. Moreover, not all cancers exhibit significant levels of enhanced permeability and retention that are necessary for the passive accumulation of the NDC[182]. However, longitudinal PET imaging may be used to determine the degree of EPR effect in tumors prior to NDC use.

Overall, the strategy to load phenformin onto PGNS shows that it may overcome multiple bottlenecks currently limiting the use of metabolic treatments targeting cancers, offering a unique and much needed repurposing of a familiar and well-studied drug that could improve the lives of cancer sufferers.

5   References

1. Barenholz Y. Doxil®--the first FDA-approved nano-drug: lessons learned. J Control Release. 2012;160:117–34. doi:10.1016/j.jconrel.2012.03.020.
2. Sercombe L, Veerati T, Moheimani F, Wu SY, Sood AK, Hua S. Advances and Challenges of Liposome Assisted Drug Delivery. Front Pharmacol. 2015;6:286. doi:10.3389/fphar.2015.00286.
3. Akbarzadeh A, Rezaei-Sadabady R, Davaran S, Joo SW, Zarghami N, Hanifehpour Y, et al. Liposome: classification, preparation, and applications. Nanoscale Res Lett. 2013;8:102. doi:10.1186/1556-276X-8-102.
4. Chen C, Han D, Cai C, Tang X. An overview of liposome lyophilization and its future potential. J Control Release. 2010;142:299–311. doi:10.1016/j.jconrel.2009.10.024.
5. Ageitos JM, Chuah J-A, Numata K. Chapter 1. Design Considerations for Properties of Nanocarriers on Disposition and Efficiency of Drug and Gene Delivery. In: Braddock M, editor. Nanomedicines: Design, delivery and detection / edited by Martin Braddock, AstraZeneca Research and Development, Macclesfield, UK. Cambridge, UK: Royal Society of Chemistry; 2016. p. 1–22. doi:10.1039/9781782622536-00001.
6. Moosavian SA, Bianconi V, Pirro M, Sahebkar A. Challenges and pitfalls in the development of liposomal delivery systems for cancer therapy. Semin Cancer Biol. 2021;69:337–48. doi:10.1016/j.semcancer.2019.09.025.
7. Nel AE, Mädler L, Velegol D, Xia T, Hoek EMV, Somasundaran P, et al. Understanding biophysicochemical interactions at the nano-bio interface. Nat Mater. 2009;8:543–57. doi:10.1038/nmat2442.
8. Noble CO, Guo Z, Hayes ME, Marks JD, Park JW, Benz CC, et al. Characterization of highly stable liposomal and immunoliposomal formulations of vincristine and vinblastine. Cancer Chemother Pharmacol. 2009;64:741–51. doi:10.1007/s00280-008-0923-3.
9. Rosenblum D, Joshi N, Tao W, Karp JM, Peer D. Progress and challenges towards targeted delivery of cancer therapeutics. Nat Commun. 2018;9:1410. doi:10.1038/s41467-018-03705-y.

10. Byrne JD, Betancourt T, Brannon-Peppas L. Active targeting schemes for nanoparticle systems in cancer therapeutics. Advanced Drug Delivery Reviews. 2008;60:1615–26. doi:10.1016/j.addr.2008.08.005.

11. Sydykov B, Oldenhof H, Sieme H, Wolkers WF. Storage stability of liposomes stored at elevated subzero temperatures in DMSO/sucrose mixtures. PLoS ONE. 2018;13:e0199867. doi:10.1371/journal.pone.0199867.

12. Petersen GH, Alzghari SK, Chee W, Sankari SS, La-Beck NM. Meta-analysis of clinical and preclinical studies comparing the anticancer efficacy of liposomal versus conventional non-liposomal doxorubicin. J Control Release. 2016;232:255–64. doi:10.1016/j.jconrel.2016.04.028.

13. Naahidi S, Jafari M, Edalat F, Raymond K, Khademhosseini A, Chen P. Biocompatibility of engineered nanoparticles for drug delivery. Journal of Controlled Release. 2013;166:182–94. doi:10.1016/j.jconrel.2012.12.013.

14. Begines B, Ortiz T, Pérez-Aranda M, Martínez G, Merinero M, Argüelles-Arias F, Alcudia A. Polymeric Nanoparticles for Drug Delivery: Recent Developments and Future Prospects. Nanomaterials (Basel) 2020. doi:10.3390/nano10071403.

15. Han J, Zhao D, Li D, Wang X, Jin Z, Zhao K. Polymer-Based Nanomaterials and Applications for Vaccines and Drugs. Polymers 2018. doi:10.3390/polym10010031.

16. Zhang X, Li X, You Q, Zhang X. Prodrug strategy for cancer cell-specific targeting: A recent overview. Eur J Med Chem. 2017;139:542–63. doi:10.1016/j.ejmech.2017.08.010.

17. Jiang W, Finniss S, Cazacu S, Xiang C, Brodie Z, Mikkelsen T, et al. Repurposing phenformin for the targeting of glioma stem cells and the treatment of glioblastoma. Oncotarget. 2016;7:56456–70. doi:10.18632/oncotarget.10919.

18. Björnmalm M, Thurecht KJ, Michael M, Scott AM, Caruso F. Bridging Bio-Nano Science and Cancer Nanomedicine. ACS Nano. 2017;11:9594–613. doi:10.1021/acsnano.7b04855.

19. Wong C, Stylianopoulos T, Cui J, Martin J, Chauhan VP, Jiang W, et al. Multistage nanoparticle delivery system for deep penetration into tumor tissue. Proc Natl Acad Sci U S A. 2011;108:2426–31. doi:10.1073/pnas.1018382108.

20. Wilhelm S, Tavares AJ, Dai Q, Ohta S, Audet J, Dvorak HF, Chan WCW. Analysis of nanoparticle delivery to tumours. Nat Rev Mater 2016. doi:10.1038/natrevmats.2016.14.

21. Bertrand N, Wu J, Xu X, Kamaly N, Farokhzad OC. Cancer nanotechnology: the impact of passive and active targeting in the era of modern cancer biology. Advanced Drug Delivery Reviews. 2014;66:2–25. doi:10.1016/j.addr.2013.11.009.

22. Gillies RJ, Raghunand N, Karczmar GS, Bhujwalla ZM. MRI of the tumor microenvironment. J Magn Reson Imaging. 2002;16:430–50. doi:10.1002/jmri.10181.

23. Gatenby RA, Gillies RJ. Why do cancers have high aerobic glycolysis? Nat Rev Cancer. 2004;4:891–9. doi:10.1038/nrc1478.

24. Tao C, Wang J, Qin S, Lv Y, Long Y, Zhu H, Jiang Z. Fabrication of pH-sensitive graphene oxide–drug supramolecular hydrogels as controlled release systems. J Mater Chem. 2012;22:24856. doi:10.1039/c2jm34461k.

25. Yang X, Wang Y, Huang X, Ma Y, Huang Y, Yang R, et al. Multi-functionalized graphene oxide based anticancer drug-carrier with dual-targeting function and pH-sensitivity. Journal of Materials Chemistry. 2011;21:3448–54. doi:10.1039/c0jm02494e.

26. Yang Z, Yang D, Zeng K, Li D, Qin L, Cai Y, Jin J. Simultaneous Delivery of antimiR-21 and Doxorubicin by Graphene Oxide for Reducing Toxicity in Cancer Therapy. ACS Omega. 2020;5:14437–43. doi:10.1021/acsomega.0c01010.

27. Depan D, Shah J, Misra R. Controlled release of drug from folate-decorated and graphene mediated drug delivery system: Synthesis, loading efficiency, and drug release response. Mater. Sci. Eng., C. 2011;31:1305–12. doi:10.1016/j.msec.2011.04.010.

28. Fong YT, Chen C-H, Chen J-P. Intratumoral Delivery of Doxorubicin on Folate-Conjugated Graphene Oxide by In-Situ Forming Thermo-Sensitive Hydrogel for Breast Cancer Therapy. Nanomaterials (Basel, Switzerland) 2017. doi:10.3390/nano7110388.

29. Yang X, Zhang X, Liu Z, Ma Y, Huang Y, Chen Y. High-Efficiency Loading and Controlled Release of Doxorubicin Hydrochloride on Graphene Oxide. J. Phys. Chem. C. 2008;112:17554–8. doi:10.1021/jp806751k.

30. Novoselov KS, Geim AK, Morozov SV, Jiang D, Zhang Y, Dubonos SV, et al. Electric field effect in atomically thin carbon films. Science. 2004;306:666–9. doi:10.1126/science.1102896.

31. Marchesan S, Kostarelos K, Bianco A, Prato M. The winding road for carbon nanotubes in nanomedicine. Mater Today (Kidlington). 2015;18:12–9. doi:10.1016/j.mattod.2014.07.009.

32. Saito N, Haniu H, Usui Y, Aoki K, Hara K, Takanashi S, et al. Safe clinical use of carbon nanotubes as innovative biomaterials. Chem Rev. 2014;114:6040–79. doi:10.1021/cr400341h.

33. Fadeel B, Bussy C, Merino S, Vázquez E, Flahaut E, Mouchet F, et al. Safety Assessment of Graphene-Based Materials: Focus on Human Health and the Environment. ACS Nano. 2018;12:10582–620. doi:10.1021/acsnano.8b04758.

34. Barbarino M, Giordano A. Assessment of the Carcinogenicity of Carbon Nanotubes in the Respiratory System. Cancers (Basel) 2021. doi:10.3390/cancers13061318.

35. Liu XT, Mu XY, Wu XL, Meng LX, Guan WB, Ma YQ, et al. Toxicity of multi-walled carbon nanotubes, graphene oxide, and reduced graphene oxide to zebrafish embryos. Biomed Environ Sci. 2014;27:676–83. doi:10.3967/bes2014.103.

36. Bhattacharya K, Mukherjee SP, Gallud A, Burkert SC, Bistarelli S, Bellucci S, et al. Biological interactions of carbon-based nanomaterials: From coronation to degradation. Nanomedicine-Nanotechnology Biology and Medicine. 2016;12:333–51. doi:10.1016/j.nano.2015.11.011.

37. Rodríguez-Pérez L, Herranz MÁ, Martín N. The chemistry of pristine graphene. Chem Commun (Camb). 2013;49:3721–35. doi:10.1039/c3cc38950b.

38. Novoselov KS, Fal'ko VI, Colombo L, Gellert PR, Schwab MG, Kim K. A roadmap for graphene. Nature. 2012;490:192–200. doi:10.1038/nature11458.

39. Stoller MD, Park S, Zhu Y, An J, Ruoff RS. Graphene-based ultracapacitors. Nano Letters. 2008;8:3498–502. doi:10.1021/nl802558y.

40. Bagri A, Mattevi C, Acik M, Chabal YJ, Chhowalla M, Shenoy VB. Structural evolution during the reduction of chemically derived graphene oxide. Nat Chem. 2010;2:581–7. doi:10.1038/nchem.686.

41. Kuila T, Bose S, Mishra AK, Khanra P, Kim NH, Lee JH. Chemical functionalization of graphene and its applications. Progress in Materials Science. 2012;57:1061–105. doi:10.1016/j.pmatsci.2012.03.002.

42. Ikram R, Jan BM, Ahmad W. An overview of industrial scalable production of graphene oxide and analytical approaches for synthesis and characterization. Journal of Materials Research and Technology. 2020;9:11587–610. doi:10.1016/j.jmrt.2020.08.050.

43. Imani R, Emami SH, Faghihi S. Synthesis and characterization of an octaarginine functionalized graphene oxide nano-carrier for gene delivery applications. Phys. Chem. Chem. Phys. 2015;17:6328–39. doi:10.1039/C4CP04301D.

44. Feng L, Yang X, Shi X, Tan X, Peng R, Wang J, Liu Z. Polyethylene glycol and polyethylenimine dual-functionalized nano-graphene oxide for photothermally enhanced gene delivery. Small. 2013;9:1989–97. doi:10.1002/smll.201202538.

45. Chen J, Liu H, Zhao C, Qin G, Xi G, Li T, et al. One-step reduction and PEGylation of graphene oxide for photothermally controlled drug delivery. Biomaterials. 2014;35:4986–95. doi:10.1016/j.biomaterials.2014.02.032.

46. Sahu A, Choi WI, Lee JH, Tae G. Graphene oxide mediated delivery of methylene blue for combined photodynamic and photothermal therapy. Biomaterials. 2013;34:6239–48. doi:10.1016/j.biomaterials.2013.04.066.

47. Chen D, Dougherty CA, Zhu K, Hong H. Theranostic applications of carbon nanomaterials in cancer: Focus on imaging and cargo delivery. Journal of Controlled Release. 2015;210:230–45. doi:10.1016/j.jconrel.2015.04.021.

48. Ma X, Tao H, Yang K, Feng L, Cheng L, Shi X, et al. A functionalized graphene oxide-iron oxide nanocomposite for magnetically targeted drug delivery, photothermal therapy, and magnetic resonance imaging. Nano Research. 2012;5:199–212. doi:10.1007/s12274-012-0200-y.

49. Yang G, Zhu C, Du D, Zhu J, Lin Y. Graphene-like two-dimensional layered nanomaterials: Applications in biosensors and nanomedicine. Nanoscale. 2015;7:14217–31. doi:10.1039/c5nr03398e.

50. Xue T, Cui X, Guan W, Wang Q, Liu C, Wang H, et al. Surface plasmon resonance technique for directly probing the interaction of DNA and

graphene oxide and ultra-sensitive biosensing. Biosens Bioelectron. 2014;58:374–9. doi:10.1016/j.bios.2014.03.002.

51. Del Lavin-Lopez MP, Romero A, Garrido J, Sanchez-Silva L, Valverde JL. Influence of Different Improved Hummers Method Modifications on the Characteristics of Graphite Oxide in Order to Make a More Easily Scalable Method. Ind. Eng. Chem. Res. 2016;55:12836–47. doi:10.1021/acs.iecr.6b03533.

52. Alam SN, Sharma N, Kumar L. Synthesis of Graphene Oxide (GO) by Modified Hummers Method and Its Thermal Reduction to Obtain Reduced Graphene Oxide (rGO)*. Graphene. 2017;06:1–18. doi:10.4236/graphene.2017.61001.

53. Tian W, Li W, Yu W, Liu X. A Review on Lattice Defects in Graphene: Types, Generation, Effects and Regulation. Micromachines (Basel) 2017. doi:10.3390/mi8050163.

54. Kim J, Cote LJ, Kim F, Yuan W, Shull KR, Huang J. Graphene Oxide Sheets at Interfaces. J Am Chem Soc. 2010;132:8180–6. doi:10.1021/ja102777p.

55. Yang K, Feng L, Shi X, Liu Z. Nano-graphene in biomedicine: theranostic applications. Chem Soc Rev. 2013;42:530–47. doi:10.1039/c2cs35342c.

56. Banhart F, Kotakoski J, Krasheninnikov AV. Structural defects in graphene. ACS Nano. 2011;5:26–41. doi:10.1021/nn102598m.

57. Marcano DC, Kosynkin DV, Berlin JM, Sinitskii A, Sun Z, Slesarev A, et al. Improved synthesis of graphene oxide. ACS Nano. 2010;4:4806–14. doi:10.1021/nn1006368.

58. Hummers WS, Offeman RE. Preparation of Graphitic Oxide. J Am Chem Soc. 1958;80:1339. doi:10.1021/ja01539a017.

59. Yue H, Wei W, Yue Z, Wang B, Luo N, Gao Y, et al. The role of the lateral dimension of graphene oxide in the regulation of cellular responses. Biomaterials. 2012;33:4013–21. doi:10.1016/j.biomaterials.2012.02.021.

60. Stankovich S, Dikin DA, Piner RD, Kohlhaas KA, Kleinhammes A, Jia Y, et al. Synthesis of graphene-based nanosheets via chemical reduction of exfoliated graphite oxide. Carbon. 2007;45:1558–65. doi:10.1016/j.carbon.2007.02.034.

61. Fan Z-J, Kai W, Yan J, Wei T, Zhi L-J, Feng J, et al. Facile synthesis of graphene nanosheets via Fe reduction of exfoliated graphite oxide. ACS Nano. 2011;5:191–8. doi:10.1021/nn102339t.

62. Azizighannad S, Mitra S. Stepwise Reduction of Graphene Oxide (GO) and Its Effects on Chemical and Colloidal Properties. Sci Rep. 2018;8:10083. doi:10.1038/s41598-018-28353-6.

63. Robinson JT, Tabakman SM, Liang Y, Wang H, Casalongue HS, Vinh D, Dai H. Ultrasmall Reduced Graphene Oxide with High Near-Infrared Absorbance for Photothermal Therapy. J Am Chem Soc. 2011;133:6825–31. doi:10.1021/ja2010175.

64. Gudarzi MM. Colloidal Stability of Graphene Oxide: Aggregation in Two Dimensions. Langmuir. 2016;32:5058–68. doi:10.1021/acs.langmuir.6b01012.

65. Zhu P, Shen M, Xiao S, Zhang D. Experimental study on the reducibility of graphene oxide by hydrazine hydrate. Physica B Condens Matter. 2011;406:498–502. doi:10.1016/j.physb.2010.11.022.

66. Furst A, Berlo RC, Hooton S. Hydrazine as a Reducing Agent for Organic Compounds (Catalytic Hydrazine Reductions). Chem Rev. 1965;65:51–68. doi:10.1021/cr60233a002.

67. Tung VC, Allen MJ, Yang Y, Kaner RB. High-throughput solution processing of large-scale graphene. Nat Nanotechnol. 2009;4:25–9. doi:10.1038/nnano.2008.329.

68. Aunkor MTH, Mahbubul IM, Saidur R, Metselaar HSC. The green reduction of graphene oxide. Rsc Advances. 2016;6:27807–28. doi:10.1039/C6RA03189G.

69. Silva K de, Huang H-H, Joshi RK, Yoshimura M. Chemical reduction of graphene oxide using green reductants. Carbon. 2017;119:190–9. doi:10.1016/j.carbon.2017.04.025.

70. Zhang Y, Zhang L, Zhou C. Review of chemical vapor deposition of graphene and related applications. Acc Chem Res. 2013;46:2329–39. doi:10.1021/ar300203n.

71. Boyd DA, Lin W-H, Hsu C-C, Teague ML, Chen C-C, Lo Y-Y, et al. Single-step deposition of high-mobility graphene at reduced temperatures. Nat Commun. 2015;6:6620. doi:10.1038/ncomms7620.

72. USPTO.report. Apparatus and Method for Large-Scale Production of Graphene Patent Application. 14/06/2021. https://uspto.report/patent/app/20190144283. Accessed 14 Jun 2021.

73. Bianco A, Cheng H-M, Enoki T, Gogotsi Y, Hurt RH, Koratkar N, et al. All in the graphene family – A recommended nomenclature for two-

dimensional carbon materials. Carbon. 2013;65:1–6. doi:10.1016/j.carbon.2013.08.038.

74. Wick P, Louw-Gaume AE, Kucki M, Krug HF, Kostarelos K, Fadeel B, et al. Classification framework for graphene-based materials. Angew Chem Int Ed Engl. 2014;53:7714–8. doi:10.1002/anie.201403335.

75. Yang K, Wan J, Zhang S, Zhang Y, Lee S-T, Liu Z. In vivo pharmacokinetics, long-term biodistribution, and toxicology of PEGylated graphene in mice. ACS Nano. 2011;5:516–22. doi:10.1021/nn1024303.

76. Begum P, Fugetsu B. Induction of cell death by graphene in Arabidopsis thaliana (Columbia ecotype) T87 cell suspensions. J Hazard Mater. 2013;260:1032–41. doi:10.1016/j.jhazmat.2013.06.063.

77. Lalwani G, D'Agati M, Khan AM, Sitharaman B. Toxicology of graphene-based nanomaterials. Adv Drug Deliv Rev. 2016;105:109–44. doi:10.1016/j.addr.2016.04.028.

78. Sanchez VC, Jachak A, Hurt RH, Kane AB. Biological Interactions of Graphene-Family Nanomaterials: An Interdisciplinary Review. Chemical Research in Toxicology. 2012;25:15–34. doi:10.1021/tx200339h.

79. Wang Y, Wang K, Zhao J, Liu X, Bu J, Yan X, Huang R. Multifunctional Mesoporous Silica-Coated Graphene Nanosheet Used for Chemo-Photothermal Synergistic Targeted Therapy of Glioma. J Am Chem Soc. 2013;135:4799–804. doi:10.1021/ja312221g.

80. Deng W, Qiu J, Wang S, Yuan Z, Jia Y, Tan H, et al. Development of biocompatible and VEGF-targeted paclitaxel nanodrugs on albumin and graphene oxide dual-carrier for photothermal-triggered drug delivery in vitro and in vivo. Int J Nanomedicine. 2018;13:439–53. doi:10.2147/IJN.S150977.

81. Zhuang W, He L, Wang K, Ma B, Ge L, Wang Z, et al. Combined Adsorption and Covalent Linking of Paclitaxel on Functionalized Nano-Graphene Oxide for Inhibiting Cancer Cells. ACS Omega. 2018;3:2396–405. doi:10.1021/acsomega.7b02022.

82. Bianco A, Prato M. Safety concerns on graphene and 2D materials: a Flagship perspective. 2D Mater. 2015;2:30201. doi:10.1088/2053-1583/2/3/030201.

83. Pumera M, Ambrosi A, Chng ELK. Impurities in graphenes and carbon nanotubes and their influence on the redox properties. Chem Sci. 2012;3:3347. doi:10.1039/c2sc21374e.

84. Mukherjee SP, Lozano N, Kucki M, Del Rio-Castillo AE, Newman L, Vázquez E, et al. Detection of Endotoxin Contamination of Graphene Based Materials Using the TNF-α Expression Test and Guidelines for Endotoxin-Free Graphene Oxide Production. PLoS ONE. 2016;11:e0166816. doi:10.1371/journal.pone.0166816.

85. Liao K-H, Lin Y-S, Macosko CW, Haynes CL. Cytotoxicity of Graphene Oxide and Graphene in Human Erythrocytes and Skin Fibroblasts. ACS Appl Mater Interfaces. 2011;3:2607–15. doi:10.1021/am200428v.

86. Li B, Zhang X-Y, Yang J-Z, Zhang Y-J, Li W-X, Fan C-H, Huang Q. Influence of polyethylene glycol coating on biodistribution and toxicity of nanoscale graphene oxide in mice after intravenous injection. International Journal of Nanomedicine. 2014;9:4697–707. doi:10.2147/IJN.S66591.

87. Yang K, Gong H, Shi X, Wan J, Zhang Y, Liu Z. In vivo biodistribution and toxicology of functionalized nano-graphene oxide in mice after oral and intraperitoneal administration. Biomaterials. 2013;34:2787–95. doi:10.1016/j.biomaterials.2013.01.001.

88. Sydlik SA, Jhunjhunwala S, Webber MJ, Anderson DG, Langer R. In vivo compatibility of graphene oxide with differing oxidation states. ACS Nano. 2015;9:3866–74. doi:10.1021/acsnano.5b01290.

89. Li B, Yang J, Huang Q, Zhang Y, Peng C, Zhang Y, et al. Biodistribution and pulmonary toxicity of intratracheally instilled graphene oxide in mice. NPG Asia Mater. 2013;5:e44-e44. doi:10.1038/am.2013.7.

90. Mao L, Hu M, Pan B, Xie Y, Petersen EJ. Biodistribution and toxicity of radio-labeled few layer graphene in mice after intratracheal instillation. Part Fibre Toxicol. 2016;13:7. doi:10.1186/s12989-016-0120-1.

91. Czarny B, Georgin D, Berthon F, Plastow G, Pinault M, Patriarche G, et al. Carbon nanotube translocation to distant organs after pulmonary exposure: insights from in situ (14)C-radiolabeling and tissue radioimaging. ACS Nano. 2014;8:5715–24. doi:10.1021/nn500475u.

92. Wen K-P, Chen Y-C, Chuang C-H, Chang H-Y, Lee C-Y, Tai N-H. Accumulation and toxicity of intravenously-injected functionalized graphene oxide in mice. J Appl Toxicol. 2015;35:1211–8. doi:10.1002/jat.3187.

93. Qu G, Wang X, Liu Q, Liu R, Yin N, Ma J, et al. The ex vivo and in vivo biological performances of graphene oxide and the impact of surfactant

on graphene oxide's biocompatibility. J Environ Sci (China). 2013;25:873–81. doi:10.1016/S1001-0742(12)60252-6.

94. Syama S, Paul W, Sabareeswaran A, Mohanan PV. Raman spectroscopy for the detection of organ distribution and clearance of PEGylated reduced graphene oxide and biological consequences. Biomaterials. 2017;131:121–30. doi:10.1016/j.biomaterials.2017.03.043.

95. Liu J-H, Yang S-T, Wang H, Chang Y, Cao A, Liu Y. Effect of size and dose on the biodistribution of graphene oxide in mice. Nanomedicine (Lond). 2012;7:1801–12. doi:10.2217/nnm.12.60.

96. Jasim DA, Murphy S, Newman L, Mironov A, Prestat E, McCaffrey J, et al. The Effects of Extensive Glomerular Filtration of Thin Graphene Oxide Sheets on Kidney Physiology. ACS Nano. 2016;10:10753–67. doi:10.1021/acsnano.6b03358.

97. Jasim DA, Boutin H, Fairclough M, Ménard-Moyon C, Prenant C, Bianco A, Kostarelos K. Thickness of functionalized graphene oxide sheets plays critical role in tissue accumulation and urinary excretion: A pilot PET/CT study. Appl Mater Today. 2016;4:24–30. doi:10.1016/j.apmt.2016.04.003.

98. Pelin M, Fusco L, Martín C, Sosa S, Frontiñán-Rubio J, González-Domínguez JM, et al. Graphene and graphene oxide induce ROS production in human HaCaT skin keratinocytes: the role of xanthine oxidase and NADH dehydrogenase. Nanoscale. 2018;10:11820–30. doi:10.1039/c8nr02933d.

99. Jaworski S, Strojny B, Sawosz E, Wierzbicki M, Grodzik M, Kutwin M, et al. Degradation of Mitochondria and Oxidative Stress as the Main Mechanism of Toxicity of Pristine Graphene on U87 Glioblastoma Cells and Tumors and HS-5 Cells. Int J Mol Sci 2019. doi:10.3390/ijms20030650.

100. Jarosz A, Skoda M, Dudek I, Szukiewicz D. Oxidative Stress and Mitochondrial Activation as the Main Mechanisms Underlying Graphene Toxicity against Human Cancer Cells. Oxid Med Cell Longev. 2016;2016:5851035. doi:10.1155/2016/5851035.

101. Counihan JL, Grossman EA, Nomura DK. Cancer Metabolism: Current Understanding and Therapies. Chemical Reviews. 2018;118:6893–923. doi:10.1021/acs.chemrev.7b00775.

102. Vander Heiden MG, DeBerardinis RJ. Understanding the Intersections between Metabolism and Cancer Biology. Cell. 2017;168:657–69. doi:10.1016/j.cell.2016.12.039.

103. Seyfried TN, Flores RE, Poff AM, D'Agostino DP. Cancer as a metabolic disease: implications for novel therapeutics. Carcinogenesis. 2014;35:515–27. doi:10.1093/carcin/bgt480.

104. Seyfried TN. Cancer as a metabolic disease: On the origin, management, and prevention of cancer / by Thomas N. Seyfried. Hoboken, N.J.: Wiley; 2012.

105. Luengo A, Gui DY, Vander Heiden MG. Targeting Metabolism for Cancer Therapy. Cell Chem Biol. 2017;24:1161–80. doi:10.1016/j.chembiol.2017.08.028.

106. Vasan K, Werner M, Chandel NS. Mitochondrial Metabolism as a Target for Cancer Therapy. Cell Metab. 2020;32:341–52. doi:10.1016/j.cmet.2020.06.019.

107. Vander Heiden MG, Locasale JW, Swanson KD, Sharfi H, Heffron GJ, Amador-Noguez D, et al. Evidence for an alternative glycolytic pathway in rapidly proliferating cells. Science. 2010;329:1492–9. doi:10.1126/science.1188015.

108. Lunt SY, Vander Heiden MG. Aerobic glycolysis: meeting the metabolic requirements of cell proliferation. Annu Rev Cell Dev Biol. 2011;27:441–64. doi:10.1146/annurev-cellbio-092910-154237.

109. WARBURG O. On the origin of cancer cells. Science. 1956;123:309–14. doi:10.1126/science.123.3191.309.

110. Carracedo A, Cantley LC, Pandolfi PP. Cancer metabolism: fatty acid oxidation in the limelight. Nat Rev Cancer. 2013;13:227–32. doi:10.1038/nrc3483.

111. Thorsten Cramer, Clemens A. Schmitt. Metabolism in Cancer. Switzerland: Springer International Publishing; 2016.

112. Fantin VR, St-Pierre J, Leder P. Attenuation of LDH-A expression uncovers a link between glycolysis, mitochondrial physiology, and tumor maintenance. Cancer Cell. 2006;9:425–34. doi:10.1016/j.ccr.2006.04.023.

113. Birsoy K, Possemato R, Lorbeer FK, Bayraktar EC, Thiru P, Yucel B, et al. Metabolic determinants of cancer cell sensitivity to glucose limitation and biguanides. Nature. 2014;508:108–12. doi:10.1038/nature13110.

114. Calabrese C, Iommarini L, Kurelac I, Calvaruso MA, Capristo M, Lollini P-L, et al. Respiratory complex I is essential to induce a Warburg profile in mitochondria-defective tumor cells. Cancer & Metabolism. 2013;1:11. doi:10.1186/2049-3002-1-11.

115. Zhao T, Mu X, You Q. Succinate: An initiator in tumorigenesis and progression. Oncotarget. 2017;8:53819–28. doi:10.18632/oncotarget.17734.

116. Thapa M, Dallmann G. Role of coenzymes in cancer metabolism. Semin Cell Dev Biol. 2020;98:44–53. doi:10.1016/j.semcdb.2019.05.027.

117. Kharkar PS. Cancer Stem Cell (CSC) Inhibitors in Oncology-A Promise for a Better Therapeutic Outcome: State of the Art and Future Perspectives. J Med Chem. 2020;63:15279–307. doi:10.1021/acs.jmedchem.0c01336.

118. Xu Y, Xue D, Bankhead A, Neamati N. Why All the Fuss about Oxidative Phosphorylation (OXPHOS)? J Med Chem. 2020;63:14276–307. doi:10.1021/acs.jmedchem.0c01013.

119. Baffy G. Mitochondrial uncoupling in cancer cells: Liabilities and opportunities. Biochim Biophys Acta Bioenerg. 2017;1858:655–64. doi:10.1016/j.bbabio.2017.01.005.

120. Krauss S, Zhang C-Y, Lowell BB. The mitochondrial uncoupling-protein homologues. Nat Rev Mol Cell Biol. 2005;6:248–61. doi:10.1038/nrm1592.

121. van Nostrand JL, Hellberg K, Luo E-C, van Nostrand EL, Dayn A, Yu J, et al. AMPK regulation of Raptor and TSC2 mediate metformin effects on transcriptional control of anabolism and inflammation. Genes & Development. 2020;34:1330–44. doi:10.1101/gad.339895.120.

122. Pelicano H, Zhang W, Liu J, Hammoudi N, Dai J, Xu R-H, et al. Mitochondrial dysfunction in some triple-negative breast cancer cell lines: role of mTOR pathway and therapeutic potential. Breast Cancer Res. 2014;16:434. doi:10.1186/s13058-014-0434-6.

123. Lu C-L, Qin L, Liu H-C, Candas D, Fan M, Li JJ. Tumor cells switch to mitochondrial oxidative phosphorylation under radiation via mTOR-mediated hexokinase II inhibition--a Warburg-reversing effect. PLoS ONE. 2015;10:e0121046. doi:10.1371/journal.pone.0121046.

124. Viale A, Pettazzoni P, Lyssiotis CA, Ying H, Sánchez N, Marchesini M, et al. Oncogene ablation-resistant pancreatic cancer cells depend on

mitochondrial function. Nature. 2014;514:628–32. doi:10.1038/nature13611.

125. Pollak M. Metformin and other biguanides in oncology: advancing the research agenda. Cancer Prevention Research. 2010;3:1060–5. doi:10.1158/1940-6207.CAPR-10-0175.

126. He L, Wondisford FE. Metformin action: concentrations matter. Cell Metab. 2015;21:159–62. doi:10.1016/j.cmet.2015.01.003.

127. Bailey CJ. Metformin: historical overview. Diabetologia. 2017;60:1566–76. doi:10.1007/s00125-017-4318-z.

128. Evans JMM, Donnelly LA, Emslie-Smith AM, Alessi DR, Morris AD. Metformin and reduced risk of cancer in diabetic patients. BMJ. 2005;330:1304–5. doi:10.1136/bmj.38415.708634.F7.

129. Morales DR, Morris AD. Metformin in cancer treatment and prevention. Annual Review of Medicine. 2015;66:17–29. doi:10.1146/annurev-med-062613-093128.

130. Vancura A, Bu P, Bhagwat M, Zeng J, Vancurova I. Metformin as an Anticancer Agent. Trends Pharmacol Sci. 2018;39:867–78. doi:10.1016/j.tips.2018.07.006.

131. Kulkarni AS, Gubbi S, Barzilai N. Benefits of Metformin in Attenuating the Hallmarks of Aging. Cell Metab. 2020;32:15–30. doi:10.1016/j.cmet.2020.04.001.

132. Wheaton WW, Weinberg SE, Hamanaka RB, Soberanes S, Sullivan LB, Anso E, et al. Metformin inhibits mitochondrial complex I of cancer cells to reduce tumorigenesis. Elife. 2014;3:e02242. doi:10.7554/eLife.02242.

133. Zhang C-S, Li M, Ma T, Zong Y, Cui J, Feng J-W, et al. Metformin Activates AMPK through the Lysosomal Pathway. Cell Metab. 2016;24:521–2. doi:10.1016/j.cmet.2016.09.003.

134. Madiraju AK, Erion DM, Rahimi Y, Zhang X-M, Braddock DT, Albright RA, et al. Metformin suppresses gluconeogenesis by inhibiting mitochondrial glycerophosphate dehydrogenase. Nature. 2014;510:542–6. doi:10.1038/nature13270.

135. Di Magno L, Manni S, Di Pastena F, Coni S, Macone A, Cairoli S, et al. Phenformin Inhibits Hedgehog-Dependent Tumor Growth through a Complex I-Independent Redox/Corepressor Module. Cell Rep. 2020;30:1735-1752.e7. doi:10.1016/j.celrep.2020.01.024.

136. Janzer A, German NJ, Gonzalez-Herrera KN, Asara JM, Haigis MC, Struhl K. Metformin and phenformin deplete tricarboxylic acid cycle and glycolytic intermediates during cell transformation and NTPs in cancer stem cells. Proc Natl Acad Sci U S A. 2014;111:10574–9. doi:10.1073/pnas.1409844111.

137. Zhao H, Swanson KD, Zheng B. Therapeutic Repurposing of Biguanides in Cancer. Trends Cancer 2021. doi:10.1016/j.trecan.2021.03.001.

138. Griss T, Vincent EE, Egnatchik R, Chen J, Ma EH, Faubert B, et al. Metformin Antagonizes Cancer Cell Proliferation by Suppressing Mitochondrial-Dependent Biosynthesis. PLoS Biol. 2015;13:e1002309. doi:10.1371/journal.pbio.1002309.

139. DeCensi A, Puntoni M, Gandini S, Guerrieri-Gonzaga A, Johansson HA, Cazzaniga M, et al. Differential effects of metformin on breast cancer proliferation according to markers of insulin resistance and tumor subtype in a randomized presurgical trial. Breast Cancer Research and Treatment. 2014;148:81–90. doi:10.1007/s10549-014-3141-1.

140. Niraula S, Dowling RJO, Ennis M, Chang MC, Done SJ, Hood N, et al. Metformin in early breast cancer: a prospective window of opportunity neoadjuvant study. Breast Cancer Research and Treatment. 2012;135:821–30. doi:10.1007/s10549-012-2223-1.

141. Hadad SM, Coates P, Jordan LB, Dowling RJO, Chang MC, Done SJ, et al. Evidence for biological effects of metformin in operable breast cancer: biomarker analysis in a pre-operative window of opportunity randomized trial. Breast Cancer Research and Treatment. 2015;150:149–55. doi:10.1007/s10549-015-3307-5.

142. Alhourani AH, Tidwell TR, Bokil AA, Røsland GV, Tronstad KJ, Søreide K, Hagland HR. Metformin treatment response is dependent on glucose growth conditions and metabolic phenotype in colorectal cancer cells. Sci Rep. 2021;11:10487. doi:10.1038/s41598-021-89861-6.

143. Kalinsky K, Crew KD, Refice S, Xiao T, Wang A, Feldman SM, et al. Presurgical trial of metformin in overweight and obese patients with newly diagnosed breast cancer. Cancer Investigation. 2014;32:150–7. doi:10.3109/07357907.2014.889706.

144. Mark M, Klingbiel D, Mey U, Winterhalder R, Rothermundt C, Gillessen S, et al. Impact of Addition of Metformin to Abiraterone in Metastatic Castration-Resistant Prostate Cancer Patients With Disease Progressing

47

While Receiving Abiraterone Treatment (MetAb-Pro): Phase 2 Pilot Study. Clin Genitourin Cancer. 2019;17:e323-e328. doi:10.1016/j.clgc.2018.12.009.

145. Pimentel I, Lohmann AE, Ennis M, Dowling RJO, Cescon D, Elser C, et al. A phase II randomized clinical trial of the effect of metformin versus placebo on progression-free survival in women with metastatic breast cancer receiving standard chemotherapy. Breast. 2019;48:17–23. doi:10.1016/j.breast.2019.08.003.

146. Chandel NS, Avizonis D, Reczek CR, Weinberg SE, Menz S, Neuhaus R, et al. Are Metformin Doses Used in Murine Cancer Models Clinically Relevant? Cell Metab. 2016;23:569–70. doi:10.1016/j.cmet.2016.03.010.

147. Dowling RJO, Niraula S, Stambolic V, Goodwin PJ. Metformin in cancer: translational challenges. J Mol Endocrinol. 2012;48:R31-43. doi:10.1530/JME-12-0007.

148. Cao J, Meng S, Chang E, Beckwith-Fickas K, Xiong L, Cole RN, et al. Low concentrations of metformin suppress glucose production in hepatocytes through AMP-activated protein kinase (AMPK). J. Biol. Chem. 2014;289:20435–46. doi:10.1074/jbc.M114.567271.

149. Gottlieb B, AULD WH. Metformin in treatment of diabetes mellitus. Br Med J. 1962;1:680–2. doi:10.1136/bmj.1.5279.680.

150. Graham GG, Punt J, Arora M, Day RO, Doogue MP, Duong JK, et al. Clinical pharmacokinetics of metformin. Clin Pharmacokinet. 2011;50:81–98. doi:10.2165/11534750-000000000-00000.

151. Bridges HR, Jones AJY, Pollak MN, Hirst J. Effects of metformin and other biguanides on oxidative phosphorylation in mitochondria. Biochemical Journal. 2014;462:475–87. doi:10.1042/BJ20140620.

152. Gormsen LC, Sundelin EI, Jensen JB, Vendelbo MH, Jakobsen S, Munk OL, et al. In Vivo Imaging of Human 11C-Metformin in Peripheral Organs: Dosimetry, Biodistribution, and Kinetic Analyses. J Nucl Med. 2016;57:1920–6. doi:10.2967/jnumed.116.177774.

153. Bailey CJ, Wilcock C, Scarpello JHB. Metformin and the intestine. Diabetologia. 2008;51:1552–3. doi:10.1007/s00125-008-1053-5.

154. Chong CR, Chabner BA. Mysterious metformin. Oncologist. 2009;14:1178–81. doi:10.1634/theoncologist.2009-0286.

155. Berstein LM. Modern approach to metabolic rehabilitation of cancer patients: Biguanides (phenformin and metformin) and beyond. Future Oncol. 2010;6:1313–23. doi:10.2217/fon.10.87.

156. Jackson AL, Sun W, Kilgore J, Guo H, Fang Z, Yin Y, et al. Phenformin has anti-tumorigenic effects in human ovarian cancer cells and in an orthotopic mouse model of serous ovarian cancer. Oncotarget. 2017;8:100113–27. doi:10.18632/oncotarget.22012.

157. Kim SH, Li M, Trousil S, Zhang Y, Di Pasca Magliano M, Swanson KD, Zheng B. Phenformin Inhibits Myeloid-Derived Suppressor Cells and Enhances the Anti-Tumor Activity of PD-1 Blockade in Melanoma. J Invest Dermatol. 2017;137:1740–8. doi:10.1016/j.jid.2017.03.033.

158. Trousil S, Chen S, Mu C, Shaw FM, Yao Z, Ran Y, et al. Phenformin Enhances the Efficacy of ERK Inhibition in NF1-Mutant Melanoma. J Invest Dermatol. 2017;137:1135–43. doi:10.1016/j.jid.2017.01.013.

159. Zhang J, Nannapaneni S, Wang D, Liu F, Wang X, Jin R, et al. Phenformin enhances the therapeutic effect of selumetinib in KRAS-mutant non-small cell lung cancer irrespective of LKB1 status. Oncotarget. 2017;8:59008–22. doi:10.18632/oncotarget.19779.

160. Shackelford DB, Abt E, Gerken L, Vasquez DS, Seki A, Leblanc M, et al. LKB1 inactivation dictates therapeutic response of non-small cell lung cancer to the metabolism drug phenformin. Cancer Cell. 2013;23:143–58. doi:10.1016/j.ccr.2012.12.008.

161. Yuan P, Ito K, Perez-Lorenzo R, Del Guzzo C, Lee JH, Shen C-H, et al. Phenformin enhances the therapeutic benefit of BRAF(V600E) inhibition in melanoma. Proc Natl Acad Sci U S A. 2013;110:18226–31. doi:10.1073/pnas.1317577110.

162. Huang X, Wullschleger S, Shpiro N, McGuire VA, Sakamoto K, Woods YL, et al. Important role of the LKB1-AMPK pathway in suppressing tumorigenesis in PTEN-deficient mice. Biochemical Journal. 2008;412:211–21. doi:10.1042/BJ20080557.

163. Vara-Ciruelos D, Dandapani M, Russell FM, Grzes KM, Atrih A, Foretz M, et al. Phenformin, But Not Metformin, Delays Development of T Cell Acute Lymphoblastic Leukemia/Lymphoma via Cell-Autonomous AMPK Activation. Cell Rep. 2019;27:690-698.e4. doi:10.1016/j.celrep.2019.03.067.

164. Hirsch HA, Iliopoulos D, Tsichlis PN, Struhl K. Metformin selectively targets cancer stem cells, and acts together with chemotherapy to block tumor growth and prolong remission. Cancer Res. 2009;69:7507–11. doi:10.1158/0008-5472.CAN-09-2994.

165. Lee K, Giltnane JM, Balko JM, Schwarz LJ, Guerrero-Zotano AL, Hutchinson KE, et al. MYC and MCL1 Cooperatively Promote Chemotherapy-Resistant Breast Cancer Stem Cells via Regulation of Mitochondrial Oxidative Phosphorylation. Cell Metab. 2017;26:633-647.e7. doi:10.1016/j.cmet.2017.09.009.

166. Elgogary A, Xu Q, Poore B, Alt J, Zimmermann SC, Zhao L, et al. Combination therapy with BPTES nanoparticles and metformin targets the metabolic heterogeneity of pancreatic cancer. Proceedings of the National Academy of Sciences. 2016;113:E5328-36. doi:10.1073/pnas.1611406113.

167. Backes C, Abdelkader AM, Alonso C, Andrieux-Ledier A, Arenal R, Azpeitia J, et al. Production and processing of graphene and related materials. 2D Mater. 2020;7:22001. doi:10.1088/2053-1583/ab1e0a.

168. Lotya M, Rakovich A, Donegan JF, Coleman JN. Measuring the lateral size of liquid-exfoliated nanosheets with dynamic light scattering. Nanotechnology. 2013;24:265703. doi:10.1088/0957-4484/24/26/265703.

169. Corbett JCW, McNeil-Watson F. Electrophoretic Light Scattering. In: Roberts G, Watts A, editors. Encyclopedia of Biophysics. Berlin, Heidelberg: Springer Berlin Heidelberg; 2018. p. 1–10. doi:10.1007/978-3-642-35943-9_288-1.

170. Coyle C, Cafferty FH, Vale C, Langley RE. Metformin as an adjuvant treatment for cancer: a systematic review and meta-analysis. Ann Oncol. 2016;27:2184–95. doi:10.1093/annonc/mdw410.

171. Tsilidis KK, Capothanassi D, Allen NE, Rizos EC, Lopez DS, van Veldhoven K, et al. Metformin does not affect cancer risk: a cohort study in the U.K. Clinical Practice Research Datalink analyzed like an intention-to-treat trial. Diabetes Care. 2014;37:2522–32. doi:10.2337/dc14-0584.

172. Ma L, Wei J, Wan J, Wang W, Wang L, Yuan Y, et al. Low glucose and metformin-induced apoptosis of human ovarian cancer cells is connected to ASK1 via mitochondrial and endoplasmic reticulum stress-

associated pathways. J Exp Clin Cancer Res. 2019;38:77. doi:10.1186/s13046-019-1090-6.

173. Zordoky BNM, Bark D, Soltys CL, Sung MM, Dyck JRB. The anti-proliferative effect of metformin in triple-negative MDA-MB-231 breast cancer cells is highly dependent on glucose concentration: implications for cancer therapy and prevention. Biochim Biophys Acta. 2014;1840:1943–57. doi:10.1016/j.bbagen.2014.01.023.

174. García Rubiño ME, Carrillo E, Ruiz Alcalá G, Domínguez-Martín A, A Marchal J, Boulaiz H. Phenformin as an Anticancer Agent: Challenges and Prospects. Int J Mol Sci 2019. doi:10.3390/ijms20133316.

175. Alkalay D, Khemani L, Wagner WE, Bartlett MF. Pharmacokinetics of phenformin in man. J Clin Pharmacol. 1975;15:446–8. doi:10.1002/j.1552-4604.1975.tb02367.x.

176. Krishnamurthy S, Ng VWL, Gao S, Tan M-H, Yang YY. Phenformin-loaded polymeric micelles for targeting both cancer cells and cancer stem cells in vitro and in vivo. Biomaterials. 2014;35:9177–86. doi:10.1016/j.biomaterials.2014.07.018.

177. Pelin M, Fusco L, León V, Martín C, Criado A, Sosa S, et al. Differential cytotoxic effects of graphene and graphene oxide on skin keratinocytes. Sci Rep. 2017:40572. doi:10.1038/srep40572.

178. Paulista Neto AJ, Fileti EE. Elucidating the amphiphilic character of graphene oxide. Phys. Chem. Chem. Phys. 2018;20:9507–15. doi:10.1039/C8CP00797G.

179. Kahl A, Stepanova A, Konrad C, Anderson C, Manfredi G, Zhou P, et al. Critical Role of Flavin and Glutathione in Complex I-Mediated Bioenergetic Failure in Brain Ischemia/Reperfusion Injury. Stroke. 2018;49:1223–31. doi:10.1161/STROKEAHA.117.019687.

180. Stepanova A, Sosunov S, Niatsetskaya Z, Konrad C, Starkov AA, Manfredi G, et al. Redox-Dependent Loss of Flavin by Mitochondrial Complex I in Brain Ischemia/Reperfusion Injury. Antioxid Redox Signal. 2019;31:608–22. doi:10.1089/ars.2018.7693.

181. Hu W, Peng C, Lv M, Li X, Zhang Y, Chen N, et al. Protein corona-mediated mitigation of cytotoxicity of graphene oxide. ACS Nano. 2011;5:3693–700. doi:10.1021/nn200021j.

182. Chauhan VP, Jain RK. Strategies for advancing cancer nanomedicine. Nat Mater. 2013;12:958–62. doi:10.1038/nmat3792.

Bibliography

Paper I - Metformin treatment response is dependent on glucose growth conditions and metabolic phenotype in colorectal cancer cells

scientific reports

OPEN

Metformin treatment response is dependent on glucose growth conditions and metabolic phenotype in colorectal cancer cells

Abdelnour H. Alhourani[1,5], Tia R. Tidwell[1,5], Ansooya A. Bokil[1], Gro V. Røsland[2,3], Karl Johan Tronstad[2], Kjetil Søreide[4] & Hanne R. Hagland[1]

Cancer cells exhibit altered metabolism, a phenomenon described a century ago by Otto Warburg. However, metabolic drug targeting is considered an underutilized and poorly understood area of cancer therapy. Metformin, a metabolic drug commonly used to treat type 2 diabetes, has been associated with lower cancer incidence, although studies are inconclusive concerning effectiveness of the drug in treatment or cancer prevention. The aim of this study was to determine how glucose concentration influences cancer cells' response to metformin, highlighting why metformin studies are inconsistent. We used two colorectal cancer cell lines with different growth rates and clinically achievable metformin concentrations. We found that fast growing SW948 are more glycolytic in terms of metabolism, while the slower growing SW1116 are reliant on mitochondrial respiration. Both cell lines show inhibitory growth after metformin treatment under physiological glucose conditions, but not in high glucose conditions. Furthermore, SW1116 converges with SW948 at a more glycolytic phenotype after metformin treatment. This metabolic shift is supported by changed GLUT1 expression. Thus, cells having different metabolic phenotypes, show a clear differential response to metformin treatment based on glucose concentration. This demonstrates the importance of growth conditions for experiments or clinical studies involving metabolic drugs such as metformin.

Nearly a century ago, Otto Warburg described a commonality among many cancers that is still under intense study[1]. What Warburg described was the cancer cells' ability to consume glucose, even in the presence of oxygen, later termed the Warburg effect. Cancer cells that have perfected this ability are avid glucose consumers supporting a high proliferation rate, with many cell signalling pathways primed to maintain this rapid growth[2]. Thus, many studies show that calorie restriction and nutrient deprivation may be both cancer preventative and may enhance treatment response[3]. However, lowering blood glucose within fasting range (< 5 mmol/L) seems to not be enough to prevent cancer growth[4–6], as cancer cells express high affinity glucose receptors[4–6], which even at fasting glucose levels, as low as 1 mmol/L, are able to import glucose[7]. However, lowering glucose levels may compromise the metabolic flexibility of these cells under stress[8]. Therefore targeting cancer metabolism is an interesting avenue to pursue, and has prompted many recent studies testing the efficacy of metabolic drugs for cancer treatment[9]. One drug that has spurred great interest is metformin, normally used to treat type 2 diabetes (T2D). Metformin use in diabetes is associated with lower incidence in many cancer groups worldwide compared to diabetic patients not using metformin[10–13]. It has since been studied in pre-clinical settings using in vitro cancer cell models[14–16], animal models[17–21], and consequently over 300 clinical trials are found when searching "metformin AND cancer" in clinicaltrial.gov. The high number of initiated clinical trials reflect both the low cost of the drug and the extensive use with minimal side effects reported since it was approved as a drug nearly 60 years ago[22,23]. However, many of these studies have so far been inconclusive, and have not shown major treatment effects nor improved survival[23–26]. The low success rate may be due to many reasons, but lack of patient stratification, metformin dosage, and mode of delivery seem to be areas to address. A regular metformin treatment in diabetic patients starts at 500–850 mg administered orally every 12 h, increasing to, but no more

[1]Department of Chemistry, Bioscience and Environmental Engineering, University of Stavanger, Stavanger, Norway. [2]Department of Biomedicine, University of Bergen, Bergen, Norway. [3]Department of Oncology and Medical Physics, Haukeland University Hospital, Bergen, Norway. [4]Department of Gastrointestinal Surgery, Stavanger University Hospital, Stavanger, Norway. [5]These authors contributed equally to this work: Abdelnour H. Alhourani and Tia R. Tidwell. email: hanne.r.hagland@uis.no
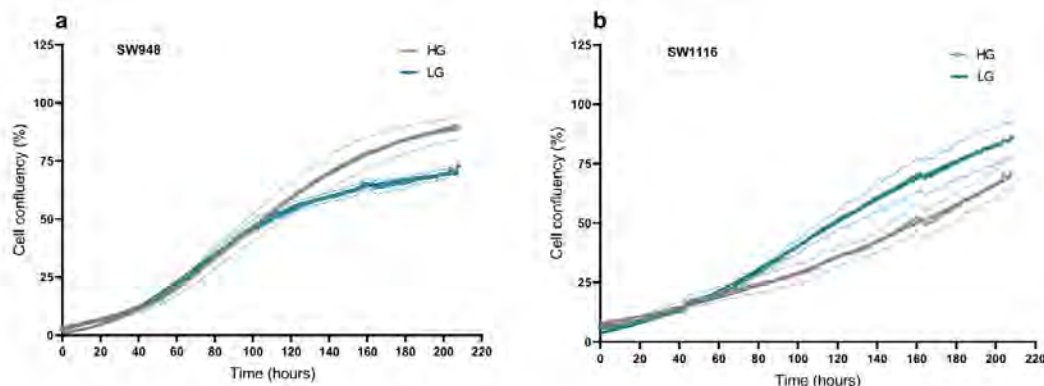
Figure 1. Cell growth recording of SW948 and SW1116 in HG and LG over 9 days continuous monitoring using Incucyte ZOOM. Cell confluency was analyzed in the Incucyte ZOOM software and plotted here as confluency (%) over time (hours). **(a)** SW948, initial seeding density of 10,000 cells/well. **(b)** SW1116, initial seeding density of 20,000 cells/well. Complete growth medium was exchanged at day 2 and 7 of the culture period. Grey solid line depicts growth in high glucose (HG) conditions, whereas blue solid line represents growth in low glucose conditions (LG). The dotted lines represent standard deviation from the average of N = 8 for each condition.

than 2550 mg/day, achieving a steady state concentration of 1.4 mg/L (10.8 µM)[27]. As an orally ingested drug, its highest concentration is found in the gastrointestinal (GI) tract, and GI derived tumours would most likely be affected[28], which further indicates that achieved drug concentration play a major role in tumour responses. This is recapitulated in its various mode of action ranging from influence on microbiota[29], immune modulation[30], and direct intracellular effect[31].

Metformin became an interest in the cancer field due to studies reporting that diabetic colorectal cancer (CRC) patients taking metformin had a better overall survival compared to those treated with other glucose lowering drugs[14,26,32,33]. This effect has largely been tied to the lowering of insulin growth factor and activation of AMPK[22,34-36]. Hence, the potential anticancer effect of metformin is most likely not due to expected lowering of blood glucose, but rather due to intracellular effects of metformin in the tumour cells[37]. Once inside the cell, the exact target of metformin has been difficult to pinpoint, although a change in mitochondrial function is one major effect seen[34-36], attributed to its inhibition of the electron transport chain (ETC)[37]. Metformin has also been shown to reduce GLUT1 expression alongside HIF-1α[38]. GLUT1 is a rate limiting transporter for glucose metabolism and involved in maintaining higher levels of glycolysis intermediates[39,40]. Clinically, its increased expression has been correlated with tumour aggressiveness and is correlated with increased proliferation activity and poor survival[5]. However, this increase could be either due to an oncogenic transformation in cells or indirectly due to high glucose consumption of cancer cells and resulting low intracellular glucose levels[40]. On the other hand, reduced glycolysis due to lower levels of GLUT1 has been associated with less malignancy[40]. Monitoring GLUT1 levels under the previously mentioned conditions could be an indicator of the adaptive mechanisms different metabolic phenotypes undergo in their response to glucose levels and metformin treatment.

In the last decades, there have been a few major breakthroughs in cancer drug discovery[41], however a fundamental issue for drug development is the discrepancy in drugs' effects once they reach efficacy testing in humans, despite promising results in earlier pre-clinical model systems[42]. One major challenge relates to the unphysiological metabolic conditions normally applied in cell cultures, often using supraphysiological levels of glucose in the growth medium. Moreover, most studies investigating metformin have applied higher concentrations than what is achievable in vivo[14,34,37,43]. Metformin is administered orally, typically achieving concentrations at up to 300 times higher in the GI tract than that found in plasma[44]. The aim of this study was therefore to test how colorectal cancer cells responded to metformin at a concentration typically found in the GI tract and grown in physiological glucose media. We show that using physiologically relevant glucose levels in cell growth media could provide a response to metformin that is more representative to in vivo conditions and that GLUT1 may be used as a metabolic biomarker for studying these responses.

Results

Glucose concentration in culture media affect cellular proliferation rates. A glucose concentration of 25 mmol/L is commonly used for in vitro cell culture, and this is from here-on referred to as high glucose (HG). The physiological glucose concentration in blood at fasting state is around 5 mmol/L, here referred to as low glucose (LG). We found that glucose concentration in the growth media directly affects the proliferation rates of two cell lines SW948 (Fig. 1a) and SW1116 (Fig. 1b) with differential metabolic phenotypes (Fig. 3). By culturing them in HG and LG over 9 days with two full media changes (day 2 and 7), we found that the doubling time of SW948 is 25.1 ± 1.2 h and 25.0 ± 0.4 h in HG and LG, respectively. Whilst for SW1116 the doubling time is 74.0 ± 10.1 h in HG and 41.8 ± 2.4 h in LG (p < 0.0001). The glucose effect is not immediate in either cell line,

54

where in SW948 the effect on proliferation becomes apparent only when the stationary growth phase begins, thus showing lower cell confluency in LG. In contrast, glucose has a significant effect on the exponential growth of SW1116, with low glucose conditions resulting in increased proliferation.

Metformin predominantly suppressed the proliferation of SW948 and SW1116 cells under physiological glucose conditions in comparison to high glucose culture conditions.

To see if the concentration of glucose in the growth media affects the cellular response to metformin treatment, we tested a range of metformin concentrations up to the clinically achievable range and higher only achievable in vitro. Since many proliferation assays measure metabolic activity (Alamar blue, WST-1), which may be affected by metformin treatment directly, the two assays we used were compared to nuclei count for verification of results. We found that after 48 h of metformin treatment, the SW948 cells (Fig. 2a) exhibit a concentration-dependent reduction in viability in HG up to 42% in 24 mM metformin treatment compared to HG control, which is consistent with corresponding cell counts. However, in LG, the CCK-8 measured viability of SW948 is reduced to 40% in comparison to LG control, even at the lowest metformin concentration (1.5 mM). At metformin treatments of 6 mM and lower there are discrepancies between the two viability measurements, whereas both cellular viability and cell numbers show more than 90% reduction in viability to control during metformin treatment of 12 mM.

There is no observed reduction in the viability of SW1116 cells (Fig. 2b) in HG using metformin concentrations up to 6 mM, while 12 and 24 mM concentrations result in viabilities of 86% and 72%, respectively. Cell numbers are lower than control across all treatments but follow the same trends as the CCK-8 assay results. In LG, the metformin effect is again found to be concentration-dependent with a reduction in viability from 61% (1.5 mM) to 11% (24 mM). The reduction in cell numbers is also consistent in a stepwise fashion with the increasing metformin concentrations and corresponds to CCK-8 viability results.

Metabolic phenotype plays a role in response to metformin.

Metformin is thought to affect mitochondrial function, although its specific target in the mitochondria has been a source of debate. To investigate effects of metformin on mitochondrial respiration and glycolysis in the two cell lines, we measured the cellular oxygen consumption rate (OCR) and lactate production assessed via extracellular acidification rate (ECAR). Specific protocols involving sequential addition of modulators were used to test key functions of oxidative phosphorylation in the metabolic flux analyzer Seahorse XFe96 (see "Methods"). In SW948, there is no significant change in oxygen consumption rate (OCR) between high (7.953 ± 0.905 pmol O_2/min/µg protein) or low glucose (7.791 ± 0.407 pmol O_2/min/µg protein) medium (Fig. 3a). However, 48 h metformin treatment causes a significant drop in OCR levels in both glucose conditions (HG: 1.571 ± 0.216 pmol O_2/min/µg protein, $p < 0.0001$; LG: 1.862 ± 0.182 pmol O_2/min/µg protein, $p < 0.0001$) (Fig. 3a). In SW1116 cells there is a significant drop in OCR when cells are grown in low glucose compared to high glucose conditions (9.839 ± 0.598 and 7.175 ± 0.522 pmol O_2/min/µg protein, respectively, $p = 0.0018$). Like SW948, the metformin treatment in SW1116 also causes a drop in OCR in these cells under both glucose conditions (HG: 1.979 ± 0.342 pmol O_2/min/µg protein, $p < 0.0001$; LG: 1.737 ± 0.179 pmol O_2/min/µg protein, $p < 0.0001$) (Fig. 3a). Both cell lines exhibit similar normalized basal respiratory levels in control conditions and after 48 h with metformin treatment (Fig. 3a), when compared to one another. The ATP-linked respiration (Fig. 3b), revealed by oligomycin inhibition of ATP-synthase, was not significantly affected by high and low glucose concentrations in either cell line. While after metformin treatment, this is lower albeit not significant compared to the control. CCCP was used to uncouple the mitochondria and measure respiration under mild stress conditions. This CCCP-uncoupled respiration increases in both cell lines when grown in low glucose media and is further increased after metformin treatment (Fig. 3c). In SW1116, the increase in CCCP-uncoupled respiration (HG: $p = 0.0191$; LG: $p = 0.0314$) is significant compared to control. To see if HG or LG media and metformin influenced the cells' ability to use glycolysis, we performed a glycolysis stress test. We found that in SW948 there is no significant change in the cells' ability to use glycolysis under any of the conditions nor after metformin treatment (Fig. 3d), while metformin treated SW1116 cells show significantly increased glycolysis compared to control (HG: $p = 0.0027$; LG: $p = 0.0083$) (Fig. 3d). To see if either cell line had spare glycolytic capacity, we added oligomycin to block ATP synthesis in the mitochondria. We found that SW948 did not have increased glycolytic capacity, whereas SW1116 cells increased glycolytic capacity by over 170% in both high and low glucose control conditions. However, this glycolytic capacity is significantly lower after 48 h metformin treatment (HG: $p < 0.0001$; LG: $p < 0.0001$) (Fig. 3e). The absolute levels of normalized OCR and ECAR in each condition are included in supplementary information (Supplementary Fig. S2). The metabolic profiles based on basal levels of OCR and ECAR (Fig. 3f) show the differences and comparative shift of the cell lines in both glucose concentrations and metformin treatment. Untreated, SW948 are more glycolytic, while SW1116 are more aerobic. Following metformin treatment, both cell lines are less energetic, but perhaps more noteworthy is that SW1116 converges with SW948 at a more glycolytic phenotype.

Glut1 is affected by growth media and metformin treatment.

We analyzed protein expression of one of the major glucose import proteins, glucose transporter protein 1 (GLUT1), and how it correlates to the mitochondrial and glycolytic changes found in the metabolic flux analysis. GLUT1 significantly increases in SW948 cells under low glucose conditions compared to high glucose conditions. The corresponding change after metformin treatment is, however, not significant in these cells and follows the same pattern as glucose response (Fig. 4a). Similarly, in SW1116 grown in low glucose concentration, the GLUT1 expression increases compared to high glucose. Furthermore, no further increase is seen after metformin treatment (Fig. 4a). To verify location of GLUT1 expression and mitochondrial detection throughout the different growth conditions and metformin treatment we performed a multi-stained confocal analysis (Fig. 4b,c) for both cell lines, identifying GLUT1 in
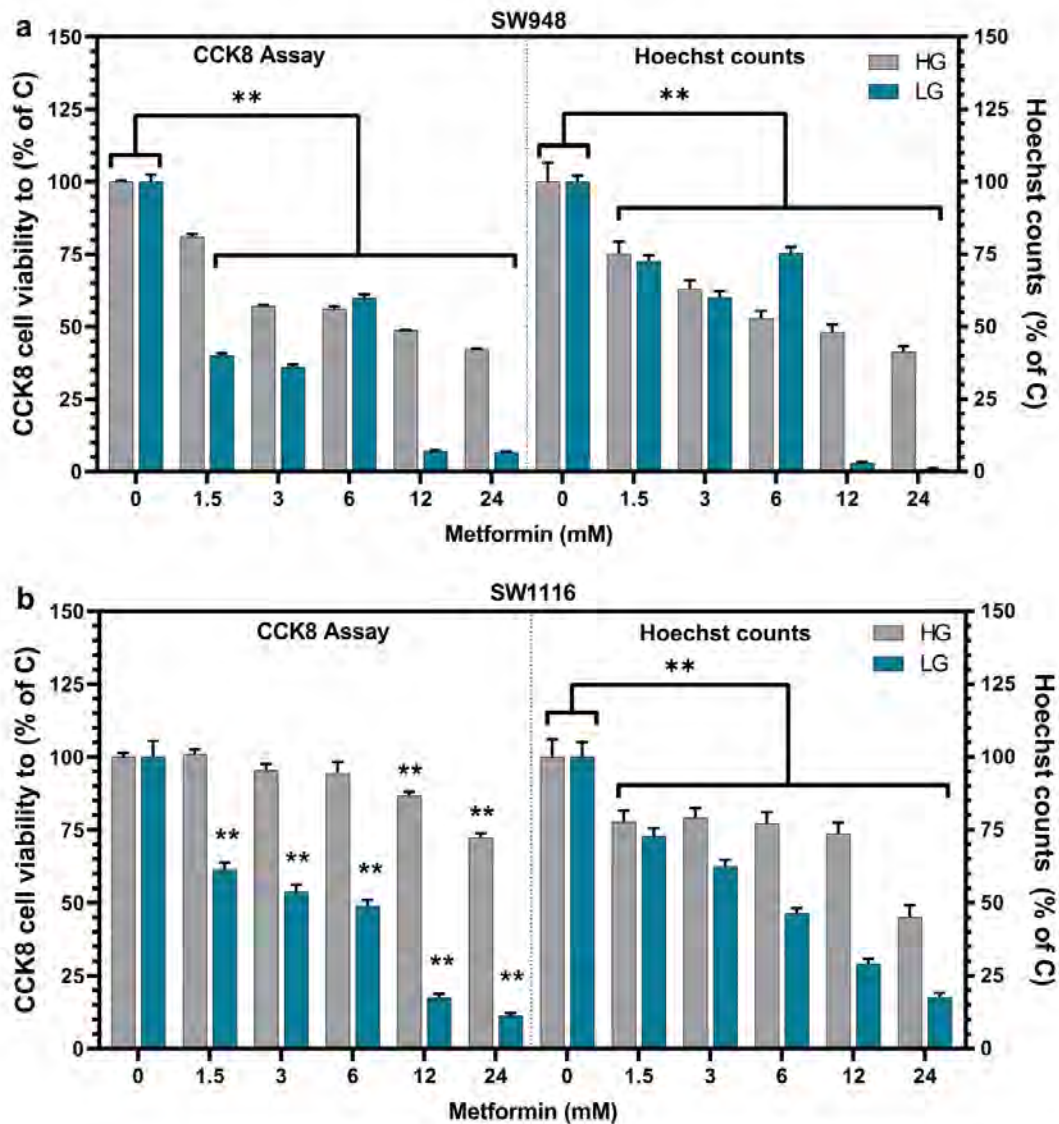
Figure 2. Viability assays of SW948 and SW1116 after metformin treatment for 48 h. The effect on the viability of (**a**) SW948 cells and (**b**) SW1116 in HG (25 mmol/L) and LG (5 mmol/L) is presented. Viability was calculated using CCK-8 (left) and cell counts were scored using fluorescent microscopy on Hoechst stained cells (right). CCK-8 absorbance values and the calculated cell numbers for all metformin treatments (1.5–24 mM) were compared to high glucose control (25 mmol/L, 0 mM Metformin) to show relative viability and cell numbers. Error bars denotes s.e.m, and statistical analysis was calculated using two-way ANOVA (** is $p < 0.05$) in GraphPad Prism (N = 3). C Control, *HG* high glucose, *LG* low glucose.

the cell plasma membrane during all conditions. We found no apparent change in mitochondrial morphology, nor in intracellular localization across the different treatments in either of the cell lines.
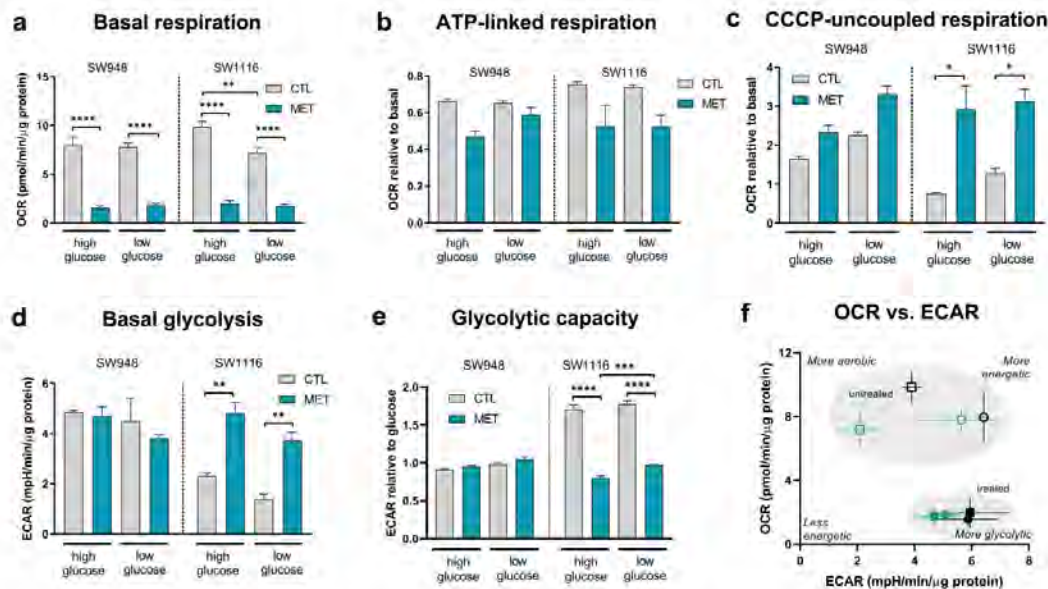
Figure 3. OCR and ECAR were measured in the Seahorse XF96 instrument, with injections of sequential compounds and concentrations according to the assays detailed in the methods section. Mitochondrial stress test assay: (**a**) Basal respiration, before any injections. (**b**) ATP-linked respiration, after oligomycin injection, shown relative to basal OCR level. (**c**) CCCP-uncoupled respiration, shown relative to basal OCR level. Glycolysis stress test assay: (**d**) Basal glycolysis, after glucose injection. (**e**) Glycolytic capacity, after oligomycin injection, shown relative to glycolysis level after glucose injection. Error bars denote s.e.m. Statistical analysis was performed using one-way ANOVA in GraphPad Prism (*p < 0.05; **p < 0.01; ***p < 0.001; ****p < 0.0001) (N = 2–8) (**f**) OCR vs ECAR from the mitochondrial stress test assay. Squares: SW948; Circles: SW116. Metabolic phenotypes of untreated (open symbols square, circle: control) and treated (closed symbols circle, square: 3 mM metformin) samples. Black: high glucose (25 mmol/L); Teal: low glucose (5 mmol/L). Error bars denote s.d. OCR Oxygen concentration rate, ECAR extracellular acidification rate, CTL control 0 mM metformin, MET metformin 3 mM pre-treatment for 48h.

Discussion

Here we show how growth conditions influence the metformin response in different cell lines, specifically concentration of glucose in the cell growth media. Using clinically achievable levels of metformin and changing the glucose concentration in the growth media for colorectal cell lines, SW948 and SW1116, resulted in changes in cell growth, metabolic flux, and protein expression. The glucose concentration directly influenced the growth rate in SW1116, where doubling time decreased in low glucose (5 mmol/L) media compared to high glucose (25 mmol/L), suggesting that glucose itself imposes an inhibitory growth effect in these cells. Comparatively, for SW948 there was no change in doubling rate between high glucose versus low glucose media. Most standard growth medias are formulated with high glucose content to avoid nutrient deprivation over time, however the finding that high glucose levels may mask true drug responses is not well considered.

We found that SW948 and SW1116 colon cancer cell lines were distinguishable in their ability to use their mitochondria, as shown in results from metabolic flux analysis. SW948 is, under non-stressed conditions (basal), running at maximum glycolytic capacity, further supported by our finding that under low glucose growth conditions these cells increased their expression of GLUT1 receptors. This could be a compensatory response for keeping up the high glucose flux through glycolysis with the lower amount of glucose available in the media as previously described[45], thus supporting rapid proliferation. As SW948 resemble Warburg's phenotype, i.e. rapid proliferation and are avid glucose consumers, they show an inability to maintain rapid proliferation under the mitochondrial-inhibiting effects of metformin even with an abundance of glucose, since glycolysis alone cannot support a high proliferation rate without mitochondrial contribution of biomolecules[2]. This is contrary to SW1116 cells that utilize their metabolic flexibility to overcome the effects of metformin by upregulating glycolysis, supporting their lower proliferation rate. In both glucose concentrations, SW1116 cells exhibit low to no additional respiration under CCCP stress; however, when treated with metformin, the relative rates of CCCP-uncoupled respiration to basal OCR increases significantly.

The abundance of glucose in culture media seems to affect the way both investigated metabolic phenotypes of cancer cells react to metformin. SW948 is more glucose dependent and able to thrive and grow exponentially in both glucose concentrations by altering their GLUT1 expression response to adapt to different conditions.
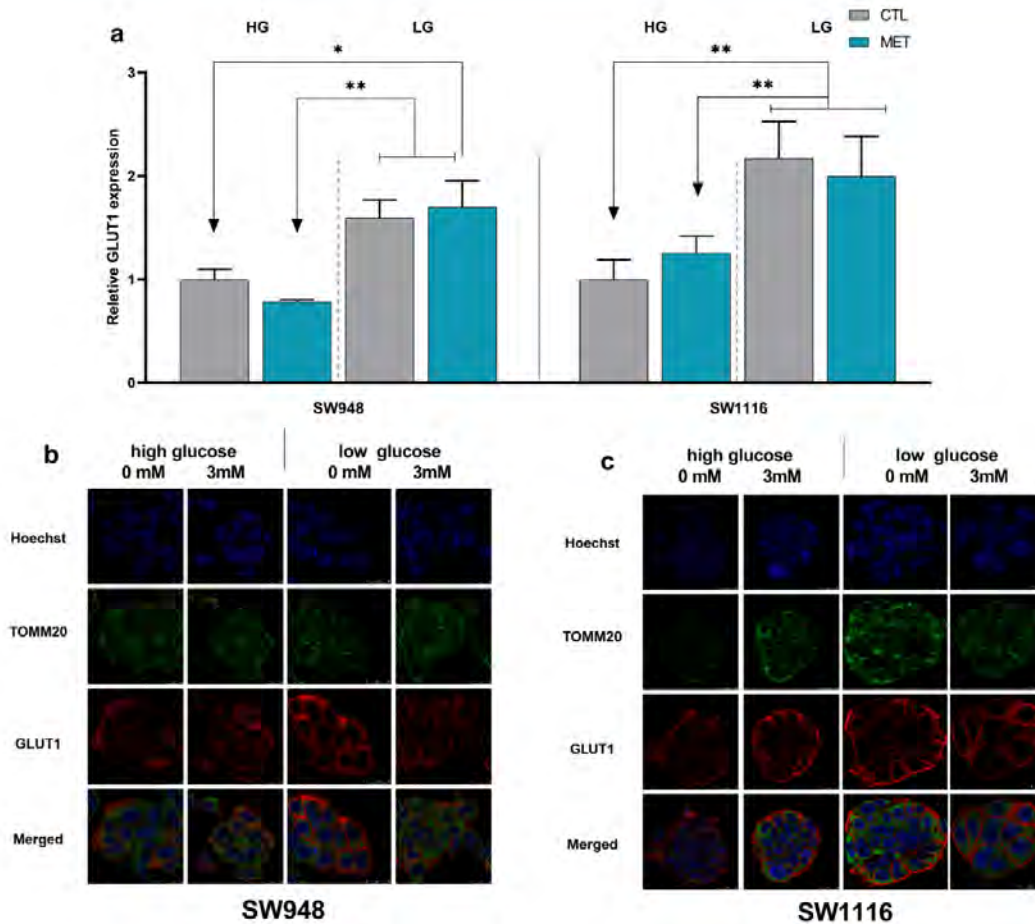
Figure 4. Protein expression analysis of GLUT1 in response to metformin treatment under different glucose culturing conditions. (**a**) Bars represent the relative GLUT1 fold inductions, measured by flow cytometry after 48 h metformin treatment in SW948 and SW1116, compared to respective controls at same glucose culturing conditions. Representative confocal images of (**b**) SW948 and (**c**) SW1116 using Hoechst for nuclei staining in blue, TOMM20 for the mitochondria in green, and GLUT-1 Antibody in red. Error bars denotes s.e.m. and statistical analysis was calculated using two-way ANOVA (*$p < 0.05$, **$p < 0.01$) (N = 3). *MET* Metformin, *CTL* control, *GLUT1* glucose transporter 1.

SW1116 is more metabolically adaptable to glucose concentration considering its GLUT1 and metabolic flux response. Here we found that after treatment in high glucose concentration, SW1116 show a slight increase in GLUT1 which could be due to their attempt to shift their metabolism towards glycolysis upon mitochondrial stress induced by metformin. SW948 had reduced GLUT1 expression in high glucose with treatment. Both cell lines had increased GLUT1 expression in the low glucose concentration, however SW1116 had a much larger increase, in line with their significant increase in basal glycolysis. In general, SW948 keep their glycolytic dependency in low glucose compared to high glucose, but the cell proliferation ultimately slows, which could mean they have less adaptability to glucose concentration compared to SW1116. In high glucose and with metformin treatment, there is a significant drop in OCR due to the inhibition of the ETC in both cell lines; similar results have been shown elsewhere[16]. Inhibition of complex I causes a drop in the ATP-linked respiration under metformin treatment. This could mean there is an unmet need of ATP production, which could cause a drop in proliferation or an increase in glycolysis. A higher uncoupled respiration in the metformin treated samples points to remaining functionality in the mitochondria, but it is reserved for acute stress, as induced by the mitochondrial uncoupler CCCP. The SW1116 cells showed a decreased response to metformin when cultured in high glucose media. This could be due to a metabolic shift towards glycolysis in a likely attempt to compensate for the metformin-driven inhibition of the ETC and TCA and resulting decrease of ATP-production in the mitochondria. However, in

both cell lines physiological glucose levels reveal an underlying concentration-dependent response to metformin. Three different assays were used here to assess the metformin response in our cell lines, presented by CCK-8 assay and direct cell counts (Fig. 2), and an Alamar blue assay (Supplementary Fig. S1). The Alamar blue assay, also known as resazurin assay, is commonly used to assess viability, however in our experimental set up did not correlate with counted cell numbers from the same assay wells. The CCK-8 assay which also measures metabolic activity, however with a different chemical reaction, showed good correlation to actual cell counts. We would thus advise caution when using viability assays that rely on metabolic activity to measure responses of metabolic treatments, without including a second confirming analysis as presented here by Hoechst cell counts (Fig. 2). This is well supported by previous studies who have found the same effect when using resazurin[47,48]. The sensitivity of cancer cells to drug treatments in different glucose concentrations is not only relevant for in vitro testing, but also clinically where many patients may present with T2D and elevated blood glucose levels, which has been associated with chemoresistance[19].

Not all cancer cells exhibit Warburg metabolism. This is becoming increasingly documented, both in vitro and clinically[50–52]. The results we see here of the difference in response of cell lines with different metabolic phenotypes, could explain the lack of response in the many clinical trials studying metformin. If only metabolically compatible cancers will respond and there are no criteria for treatment based on this, then it is unlikely a clear response would be seen when studying a mixed-phenotype clinical cohort. We found that metformin treated SW1116 shift toward a more glycolytic profile resembling that of the SW948 cell line. Fast proliferation is what is being targeted by cytotoxic chemotherapy drugs and SW948 is documented as being more susceptible to these, exhibiting lower IC50 to both 5-fluorouracil and oxaliplatin (GDSC2)[53]. However, cytotoxic drugs do seem to be targeting more than just proliferation[54], with one possible target being metabolic reprogramming. If this is the case, the metabolic shift of SW116 to be more like SW948 could then also result in increased vulnerability to chemotherapy. In this vein, metformin may be used a neoadjuvant agent in an effort to increase response[55–58]. If patient tumours are assessed for their metabolic phenotypes, either by metabolic analysis of biopsy tissue[59] or advanced tumour imaging[60–62], this can be directly translated to the clinic for improved course of treatment.

Methods

Cell culture, proliferation, and viability assessments. SW948 and SW1116 were purchased from ETCC and cultured under humidified conditions in a 5% CO_2 incubator at 37 °C. The culture media DMEM contained no glucose, (Corning, New York, USA) and was supplemented with 10% fetal bovine serum (FBS) (BioWest, Nuaillé, France), 2 mM (0.584 g/L) L-glutamine (Corning, New York, USA), penicillin (100 U/mL) and streptomycin (100 µg/mL) (Merck Millipore Corporation, Burlington, USA). For glucose experiments the DMEM media was supplemented with 25 mmol/L or 5 mmol/L glucose (Sigma-Aldrich, St. Louis, USA) concentrations for high glucose (HG) and low glucose (LG) culture conditions, respectively. The cells were acclimated to the glucose levels by being cultured and passaged several times in the respective glucose concentrations prior to metformin experiments. *Proliferation:* Cells were seeded in 96-well plates in 25 mmol/L or 5 mmol/L glucose supplemented media at a density of 20,000 cells/well or 10,000 cells/well for SW1116 and SW948, respectively. The plates were placed in the Incucyte ZOOM system (Essen Bioscience, Newark, United Kingdom) and monitored for 9 days with phase contrast images captured every 2 h. Media was exchanged on days 2 and 7. Growth was measured by analyzing the confluence of the cells over time using the Incucyte ZOOM software and reported as percent of image area covered. Doubling times were calculated during their respective log phases: 24–74 h for SW948 and 50–100 h for SW1116. Statistical analysis was performed as described in methods using an unpaired Student's t-test. *Viability:* Both cell lines were treated in 96-well plates at an initial seeding density of 10,000 cells/well using increasing concentrations of 1.5–24 mM of metformin hydrochloride (Sigma-Aldrich, St. Louis, USA) to determine the cellular viability after 48 h. Both Alamar blue (Resorufin) and CCK-8 (CCK-8; Dojindo Laboratories, Kumamoto, Japan) assays were carried out according to the manufacturer's protocol to estimate cell viability using fluorescence (Ex: 540 nm, Em:590 nm) and absorbance (450 nm) respectively via SpectraMax Paradigm plate reader (Molecular Devices, San Jose, USA). Cells in the Alamar blue plates were post-stained with Hoechst 33,342 (5 µg/mL) after fixation using 4% paraformaldehyde for 30 min, upon imaging using Leica SP8 Florescence microscope (Leica Microsystems, Mannheim, Germany). Image analysis using density counting of the nucleus was performed using ilastik[63]. Statistical analysis was calculated using two-way ANOVA.

Metabolic analysis. Mitochondrial respiration and glycolysis were measured using the Seahorse XF96e flux analyzer (Agilent Technologies, Santa Clara, USA). Cells were seeded in XF96e cell culture plates at a density of 20,000 cells/well or 10,000 cells/well for SW1116 and SW948, respectively. They were allowed to attach overnight before treatment with 3 mM metformin hydrochloride for 48 h. Prior to the mitochondrial respiration assay, culture media was exchanged for unbuffered, serum-free DMEM, composed of DMEM 8.3 g/L (D5030, Sigma-Aldrich, St. Louis, USA) pH 7.4, NaCl 1.85 g/L (Sigma-Aldrich, St. Louis, USA), 2 mM L-glutamine (Corning, New York, USA), and glucose (concentration dependent on condition as described in results) (Sigma-Aldrich, St. Louis, USA). For the glycolysis assays, the assay media contained no glucose. The plates were then incubated at 37 °C in a CO_2-free incubator for 1 h prior to running the assay. Oxygen Consumption Rate (OCR) and ExtraCellular Acidification Rate (ECAR) were measured over 100 min (15 mix and measure cycles), with compounds being injected every 3 cycles. For the mitochondrial respiration assays, the following compounds (Sigma-Aldrich, St. Louis, USA) were injected sequentially (final concentrations in the wells): Oligomycin (3 µM), CCCP (0.25 µM), Rotenone (1 µM), and Antimycin A (1 µM). For the glycolysis assays, the following compounds (Sigma-Aldrich, St. Louis, USA) were injected sequentially (final concentrations in the wells): glucose (10 mM), oligomycin (3 µM), CCCP[64,65] (0.25 µM), 2-deoxy-D-glucose (100 mM). Protein concentration

was measured in each well for normalization using a Pierce BCA assay (ThermoFisher Scientific, Rockford, USA) according to manufacturer's instructions. Statistical analysis was performed using one-way ANOVA.

Flow cytometry quantification of Glut1. SW948 and SW1116 cells were treated with 3 mM of metformin for 48 h at a seeding density of 1.0×10^6 cells per well using HG and LG media. After treatment, cells were trypsinized and washed twice with PBS before adding 4% Paraformaldehyde (PFA) fixation and incubating on ice. The fixed cells were subsequently incubated with GLUT1 primary antibody (Abcam, Cambridge, United Kingdom) at the concentration 1:500 for 1 h at room temperature. GLUT1 labelled cells were washed twice in PBS and labelled with Alexa fluor 647 conjugated Donkey anti-rabbit secondary antibody (Abcam, Cambridge, United Kingdom) for another 30 min before analysing with Accuri C6 flow cytometer (BD Biosciences, San Jose, USA).

Confocal imaging. Both cell lines were seeded in Ibidi µ-Slide 8-well chambered coverslips (Ibidi GmbH, Munich, Germany) at a density of 30,000 cells/well and were allowed to attach overnight in HG and LG media. 3 mM metformin treatment was added for 48 h before the cells were washed with PBS and fixed using 4% PFA. After 1 h of incubation with 20% FCS blocking solution, the cells were incubated overnight with GLUT1 Alexa fluor 647 conjugated antibody (Abcam, Cambridge, United Kingdom) (1:1000 in blocking solution). The next day, the wells were washed again and the cells permeabilized using 0.5% triton X in PBS for 15 min at room temperature, before another incubation step using TOMM20 antibody (Abcam, Cambridge, United Kingdom) 1:1000 in blocking solution overnight. The next day, cells were counterstained with Hoechst 33342 (ThermoFisher Scientific, Rockford, USA) (15 µg/ml solution) for 2 min, then washed 3 times with PBS. The cells were then imaged on a Leica TCS SP8 confocal microscope (Leica Microsystems, Mannheim, Germany).

Statistical analysis. Statistical comparisons were made using GraphPad PRISM (version 8, GraphPad Software, Inc., USA) software with one-way or two-way ANOVA to determine significant differences between several treatment groups. Post-hoc corrections for multiple comparisons were applied according to recommendations by GraphPad for each experimental data set (viability: Dunnett; metabolic analysis: Sidak; flow cytometry: Tukey). A student's unpaired t-test was employed when only two groups were compared. The number of biological replicates (N) are given in the figures and legends. Values that follow ± within the results section are standard deviation (s.d.).

Data availability

References

1. Warburg, O. The metabolism of carcinoma cells. *J. Cancer Res.* **9**, 148–163. https://doi.org/10.1158/jcr.1925.148 (1925).
2. Heiden, M. G. V., Cantley, L. C. & Thompson, C. B. Understanding the Warburg effect: The metabolic requirements of cell proliferation. *Science (New York, N.Y.)* **324**, 1029–1033. https://doi.org/10.1126/science.1160809 (2009).
3. Brandhorst, S. & Longo, V. D. Fasting and caloric restriction in cancer prevention and treatment. *Recent Results Cancer Res. Fortschritte der Krebsforschung Progres dans les recherches sur le cancer* **207**, 241–266. https://doi.org/10.1007/978-3-319-42118-6_12 (2016).
4. Navale, A. M. & Paranjape, A. N. Glucose transporters: Physiological and pathological roles. *Biophys. Rev.* **8**, 5–9. https://doi.org/10.1007/s12551-015-0186-2 (2016).
5. Carvalho, K. C. *et al.* GLUT1 expression in malignant tumors and its use as an immunodiagnostic marker. *Clinics (Sao Paulo, Brazil)* **66**, 965–972. https://doi.org/10.1590/S1807-59322011000600008 (2011).
6. Barron, C., Tsiani, E. & Tsakiridis, T. Expression of the glucose transporters GLUT1, GLUT3, GLUT4 and GLUT12 in human cancer cells. *BMC Proc.* https://doi.org/10.1186/1753-6561-6-S3-P4 (2012).
7. Karlish, S., Lieb, W. R., Ram, D. & Stein, W. D. Kinetic parameters of glucose efflux from human red blood cells under zero-trans conditions. *Biochim. Biophys. Acta (BBA) Biomembr.* **255**, 126–132. https://doi.org/10.1016/0005-2736(72)90014-4 (1972).
8. Menendez, J. A. *et al.* Metformin is synthetically lethal with glucose withdrawal in cancer cells. *Cell cycle (Georgetown, Tex.)* **11**, 2782–2792. https://doi.org/10.4161/cc.20948 (2012).
9. Andrzejewski, S., Siegel, P. M. & St-Pierre, J. Metabolic profiles associated with metformin efficacy in cancer. *Front. Endocrinol.* **9**, 372. https://doi.org/10.3389/fendo.2018.00372 (2018).
10. Kim, H. J. *et al.* Metformin reduces the risk of cancer in patients with type 2 diabetes: An analysis based on the Korean National Diabetes Program Cohort. *Medicine* **97**, e0036. https://doi.org/10.1097/MD.0000000000010036 (2018).
11. Libby, G. *et al.* New users of metformin are at low risk of incident cancer: A cohort study among people with type 2 diabetes. *Diabetes Care* **32**, 1620–1625. https://doi.org/10.2337/dc08-2175 (2009).
12. Yao, L. *et al.* Metformin use and lung cancer risk in diabetic patients: A systematic review and meta-analysis. *Dis. Mark.* https://doi.org/10.1155/2019/6230162 (2019).
13. Sehdev, A. *et al.* Metformin for primary colorectal cancer prevention in patients with diabetes: A case-control study in a US population. *Cancer* **121**, 1071–1078. https://doi.org/10.1002/cncr.29165 (2015).
14. Bizjak, M. *et al.* Combined treatment with Metformin and 2-deoxy glucose induces detachment of viable MDA-MB-231 breast cancer cells in vitro. *Sci. Rep.* **7**, 1761. https://doi.org/10.1038/s41598-017-01801-5 (2017).
15. Riaz, M. A. *et al.* Metformin enhances the radiosensitizing effect of cisplatin in non-small cell lung cancer cell lines with different cisplatin sensitivities. *Sci. Rep.* **9**, 38. https://doi.org/10.1038/s41598-018-38004-5 (2019).
16. Song, C. W. *et al.* Metformin kills and radiosensitizes cancer cells and preferentially kills cancer stem cells. *Sci. Rep.* **2**, 362. https://doi.org/10.1038/srep00362 (2012).
17. William, W. W., Samuel, E. W., Gokhan, M. M., Budigner, G. R. S. & Navdeep, S. C. Metformin inhibits mitochondrial complex I of cancer cells to reduce tumorigenesis. *Elife* https://doi.org/10.7554/eLife.02242.001 (2014).

60

Paper I - Metformin treatment response is dependent on glucose growth conditions and metabolic phenotype in colorectal cancer cells

18. Kim, J. H. *et al.* Effects of metformin on colorectal cancer stem cells depend on alterations in glutamine metabolism. *Sci. Rep.* **8**, 409. https://doi.org/10.1038/s41598-017-18762-4 (2018).
19. Shehata, M. *et al.* Identifying the murine mammary cell target of metformin exposure. *Commun. Biol.* **2**, 192. https://doi.org/10.1038/s42003-019-0439-x (2019).
20. Birsoy, K. *et al.* Metabolic determinants of cancer cell sensitivity to glucose limitation and biguanides. *Nature* **508**, 108–112. https://doi.org/10.1038/nature13110 (2014).
21. Cho, K. *et al.* Antihyperglycemic mechanism of metformin occurs via the AMPK/LXRα/POMC pathway. *Sci. Rep.* **5**, 8145. https://doi.org/10.1038/srep08145 (2015).
22. Cantoria, M. J., Patel, H., Boros, L. G. & Meuillet, E. J. Metformin and pancreatic cancer metabolism. In *Pancreatic Cancer—Insights into Molecular Mechanisms and Novel Approaches to Early Detection and Treatment* (ed. McCall, K. D.) (InTech, 2014).
23. Coyle, C., Cafferty, F. H., Vale, C. & Langley, R. E. Metformin as an adjuvant treatment for cancer: A systematic review and meta-analysis. *Ann. Oncol.* **27**, 2184–2195. https://doi.org/10.1093/annonc/mdw410 (2016).
24. Tsilidis, K. K. *et al.* Metformin does not affect cancer risk: a cohort study in the U.K. Clinical Practice Research Datalink analyzed like an intention-to-treat trial. *Diabetes Care* **37**, 2522–2532. https://doi.org/10.2337/dc14-0584 (2014).
25. Wu, L., Zhu, J., Prokop, L. J. & Murad, M. H. Pharmacologic therapy of diabetes and overall cancer risk and mortality: A meta-analysis of 265 studies. *Sci. Rep.* **5**, 10147. https://doi.org/10.1038/srep10147 (2015).
26. Decensi, A. *et al.* Metformin and cancer risk in diabetic patients: A systematic review and meta-analysis. *Cancer Prev. Res. (Philadelphia, Pa.)* **3**, 1451–1461. https://doi.org/10.1158/1940-6207.CAPR-10-0157 (2010).
27. Graham, G. G. *et al.* Clinical pharmacokinetics of metformin. *Clin. Pharmacokinet.* **50**, 81–98. https://doi.org/10.2165/11534750-000000000-00000 (2011).
28. Buse, J. B. *et al.* The primary glucose-lowering effect of metformin resides in the gut, not the circulation: Results from short-term pharmacokinetic and 12-week dose-ranging studies. *Diabetes Care* **39**, 198–205. https://doi.org/10.2337/dc15-0488 (2016).
29. Huang, X. *et al.* Metformin elicits antitumour effect by modulation of the gut microbiota and rescues Fusobacterium nucleatum-induced colorectal tumourigenesis. *EBioMedicine* https://doi.org/10.1016/j.ebiom.2020.103037 (2020).
30. Saito, A. *et al.* Metformin changes the immune microenvironment of colorectal cancer in patients with type 2 diabetes mellitus. *Cancer Sci.* **111**, 4012–4020. https://doi.org/10.1111/cas.14615 (2020).
31. Seo, Y. *et al.* Metformin suppresses cancer stem cells through AMPK activation and inhibition of protein prenylation of the mevalonate pathway in colorectal cancer. *Cancers* https://doi.org/10.3390/cancers12092554 (2020).
32. Bayraktar, S. *et al.* Effect of metformin on survival outcomes in diabetic patients with triple receptor-negative breast cancer. *Cancer* **118**, 1202–1211. https://doi.org/10.1002/cncr.26439 (2012).
33. Tian, S., Lei, H.-B., Liu, Y.-L., Chen, Y. & Dong, W.-G. The association between metformin use and colorectal cancer survival among patients with diabetes mellitus: An updated meta-analysis. *Chronic Dis. Transl. Med.* **3**, 169–175. https://doi.org/10.1016/j.cdtm.2017.06.001 (2017).
34. Dowling, R. J. O., Niraula, S., Stambolic, V. & Goodwin, P. J. Metformin in cancer: Translational challenges. *J. Mol. Endocrinol.* **48**, R31-43. https://doi.org/10.1530/JME-12-0007 (2012).
35. Luengo, A., Gui, D. Y. & Vander Heiden, M. G. Targeting metabolism for cancer therapy. *Cell Chem. Biol.* **24**, 1161–1180. https://doi.org/10.1016/j.chembiol.2017.08.028 (2017).
36. Viollet, B. *et al.* Cellular and molecular mechanisms of metformin: An overview. *Clin. Sci. (London, England: 1979)* **122**, 253–270. https://doi.org/10.1042/CS20110386 (2012).
37. Bridges, H. R., Jones, A. J. Y., Pollak, M. N. & Hirst, J. Effects of metformin and other biguanides on oxidative phosphorylation in mitochondria. *Biochem. J.* **462**, 475–487. https://doi.org/10.1042/BJ20140620 (2014).
38. Zhou, X. *et al.* Metformin suppresses hypoxia-induced stabilization of HIF-1α through reprogramming of oxygen metabolism in hepatocellular carcinoma. *Oncotarget* **7**, 873–884 (2015).
39. Yu, H. *et al.* Metabolic reprogramming and AMPKalpha1 pathway activation by caulerpin in colorectal cancer cells. *Int. J. Oncol.* **50**, 161–172. https://doi.org/10.3892/ijo.2016.3794 (2017).
40. Macheda, M. L., Rogers, S. & Best, J. D. Molecular and cellular regulation of glucose transporter (GLUT) proteins in cancer. *J. Cell. Physiol.* **202**, 654–662. https://doi.org/10.1002/jcp.20166 (2005).
41. Danovi, S. & Sadanand, S. Nature Milestones: Cancer. https://www.nature.com/collections/ccegecjiif (2020).(Accessed 17 Dec 2020)
42. Scannell, J. W., Blanckley, A., Boldon, H. & Warrington, B. Diagnosing the decline in pharmaceutical R&D efficiency. *Nat. Rev. Drug Discov.* **11**, 191–200. https://doi.org/10.1038/nrd3681 (2012).
43. Griss, T. *et al.* Metformin antagonizes cancer cell proliferation by suppressing mitochondrial-dependent biosynthesis. *PLoS Biol.* **13**, e1002309. https://doi.org/10.1371/journal.pbio.1002309 (2015).
44. Bailey, C. J., Wilcock, C. & Scarpello, J. H. B. Metformin and the intestine. *Diabetologia* **51**, 1552–1553. https://doi.org/10.1007/s00125-008-1053-5 (2008).
45. Hay, N. Reprogramming glucose metabolism in cancer: Can it be exploited for cancer therapy?. *Nat. Rev. Cancer* **16**, 635–649. https://doi.org/10.1038/nrc.2016.77 (2016).
46. Ariaans, G., Jalving, M., de Vries, E. G. E. & de Jong, S. Anti-tumor effects of everolimus and metformin are complementary and glucose-dependent in breast cancer cells. *BMC Cancer* **17**, 232. https://doi.org/10.1186/s12885-017-3230-8 (2017).
47. Erikstein, B. S. *et al.* Cellular stress induced by resazurin leads to autophagy and cell death via production of reactive oxygen species and mitochondrial impairment. *J. Cell. Biochem.* **111**, 574–584. https://doi.org/10.1002/jcb.22741 (2010).
48. Rampersad, S. N. Multiple applications of Alamar Blue as an indicator of metabolic function and cellular health in cell viability bioassays. *Sensors (Basel, Switzerland)* **12**, 12347–12360. https://doi.org/10.3390/s120912347 (2012).
49. Yang, I. P. *et al.* High blood sugar levels but not diabetes mellitus significantly enhance oxaliplatin chemoresistance in patients with stage III colorectal cancer receiving adjuvant FOLFOX6 chemotherapy.*Ther Adv Med Oncol.* **11**, 1–13 https://doi.org/10.1177/1758835919866964 (2019).
50. Xie, J. *et al.* Beyond Warburg effect—dual metabolic nature of cancer cells. *Sci. Rep.* **4**, 4927. https://doi.org/10.1038/srep04927 (2014).
51. Chen, P.-H. *et al.* Metabolic Diversity in Human Non-Small Cell Lung Cancer Cells. *Molecular Cell.* **76**, 838–851.e5 https://doi.org/10.1016/j.molcel.2019.08.028 (2019).
52. Faubert, B. *et al.* Lactate metabolism in human lung tumors. *Cell* **171**, 358–371. https://doi.org/10.1016/j.cell.2017.09.019 (2017).
53. Yang, W. *et al.* Genomics of Drug Sensitivity in Cancer (GDSC): A resource for therapeutic biomarker discovery in cancer cells. *Nucleic Acids Res.* **41**, D955–D961. https://doi.org/10.1093/nar/gks1111 (2013).
54. Mitchison, T. J. The proliferation rate paradox in antimitotic chemotherapy. *Mol. Biol. Cell* **23**, 1–6. https://doi.org/10.1091/mbc.E10-04-0335 (2012).
55. Lord, S. R. *et al.* Integrated pharmacodynamic analysis identifies two metabolic adaption pathways to metformin in breast cancer. *Cell Metab.* **28**, 679–688. https://doi.org/10.1016/j.cmet.2018.08.021 (2018).
56. Miranda, V. C. *et al.* A phase II trial of metformin and fluorouracil (MetFU) for patients (pts) with metastatic colorectal cancer (mCRC) refractory to standard treatment. *JCO* **32**, 601. https://doi.org/10.1200/jco.2014.32.3_suppl.601 (2014).
57. Saif, M. W. *et al.* A phase I delayed-start, randomized and pharmacodynamic study of metformin and chemotherapy in patients with solid tumors. *Cancer Chemother. Pharmacol.* **84**, 1323–1331. https://doi.org/10.1007/s00280-019-03967-3 (2019).

Paper I - Metformin treatment response is dependent on glucose growth conditions and metabolic phenotype in colorectal cancer cells

58. Tsakiridis, T. *et al.* Initial reporting of NRG-LU001 (NCT02186847), randomized phase II trial of concurrent chemoradiotherapy (CRT) +/- metformin in locally advanced Non-Small Cell Lung Cancer (NSCLC). *JCO* 37, 8502. https://doi.org/10.1200/JCO.2019.37.15_suppl.8502 (2019).
59. Russell, S., Wojtkowiak, J., Neilson, A. & Gillies, R. J. Metabolic profiling of healthy and cancerous tissues in 2D and 3D. *Sci. Rep.* 7, 15285. https://doi.org/10.1038/s41598-017-15325-5 (2017).
60. Walker-Samuel, S. *et al.* In vivo imaging of glucose uptake and metabolism in tumors. *Nat. Med.* 19, 1067–1072. https://doi.org/10.1038/nm.3252 (2013).
61. de Feyter, H. M. *et al.* Science Journals—AAAS//Deuterium metabolic imaging (DMI) for MRI-based 3D mapping of metabolism in vivo. *Sci. Adv.* 4, eaat7314. https://doi.org/10.1126/sciadv.aat7314 (2018).
62. Maher, E. A. *et al.* Metabolism of U-13 Cglucose in human brain tumors in vivo. *NMR Biomed.* 25, 1234–1244. https://doi.org/10.1002/nbm.2794 (2012).
63. Berg, S., Kutra, D., Kroeger, T. *et al.* Ilastik: interactive machine learning for (bio)image analysis. *Nat Methods.* 16, 1226–1232 https://doi.org/10.1038/s41592-019-0582-9 (2019).
64. Sundstrøm, T. *et al.* Inhibition of mitochondrial respiration prevents BRAF-mutant melanoma brain metastasis. *Acta Neuropathol. Commun.* 7, 55. https://doi.org/10.1186/s40478-019-0712-8 (2019).
65. Mookerjee, S. A., Nicholls, D. G. & Brand, M. D. Determining maximum glycolytic capacity using extracellular flux measurements. *PLoS ONE* 11, e0152016. https://doi.org/10.1371/journal.pone.0152016 (2016).

Competing interests
The authors declare no competing interests.

Additional information
Supplementary Information The online version contains supplementary material available at https://doi.org/10.1038/s41598-021-89861-6.

Correspondence and requests for materials should be addressed to H.R.H.

Reprints and permissions information is available at www.nature.com/reprints.

Publisher's note Springer Nature remains neutral with regard to jurisdictional claims in published maps and institutional affiliations.

Paper II - Improved pH-responsive release of phenformin from low defect graphene compared to graphene oxide

Paper II - Improved pH-responsive release of phenformin from low defect graphene compared to graphene oxide

Improved pH-Responsive Release of Phenformin from Low-Defect Graphene Compared to Graphene Oxide

Abdelnour Alhourani, Jan-Lukas Førde, Lutz Andreas Eichacker, Lars Herfindal, and Hanne Røland Hagland*

Cite This: https://doi.org/10.1021/acsomega.1c03283

Read Online

ACCESS | Metrics & More | Article Recommendations | Supporting Information

ABSTRACT: Graphene-based drug carriers provide a promising addition to current cancer drug delivery options. Increased accessibility of high-quality graphene made by plasma-enhanced chemical vapor deposition (PE-CVD) makes it an attractive material to revisit in comparison to the widely studied graphene oxide (GO) in drug delivery. Here, we show the potential of repurposing the metabolic drug phenformin for cancer treatment in terms of stability, binding, and pH-responsive release. Using covalent attachment of poly(ethylene glycol) (PEG) onto pristine (PE-CVD) graphene, we show that PEG stabilized graphene nanosheets (PGNS) are stable in aqueous solutions and exhibit higher binding affinity toward phenformin than GO. Moreover, we experimentally demonstrate an improved drug release from PGNS than GO at pH levels lower than physiological conditions, yet comparable to that found in tumor microenvironments.
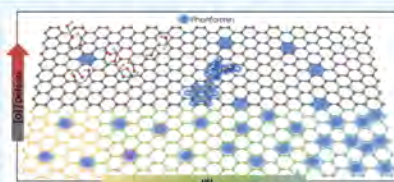
INTRODUCTION

Graphene, a two-dimensional (2D) hexagonal carbon isolated from graphite crystals,[1,2] has been investigated as a possible carrier of drugs and genomic materials for enhanced therapeutic effect.[1,3,4] Using graphene as a drug carrier is possible because of the large surface area of graphene sheets containing pi electrons,[1] which allows for high adsorption of hydrophobic and aromatic drugs by noncovalent interactions, such as pi–pi interactions.[3,5]

Graphene oxide (GO) has been particularly tested for cancer drug delivery,[3,6–8] due to its stability in aqueous solutions[9] caused by basal plane defects resulting in a high number of oxygen-rich groups on its surface.[10] GO is often produced via liquid-phase exfoliation of graphite, usually based on Hummer's method.[11,12] However, its high acidity and abundance of reactive functional groups, such as epoxides and carboxylic acids,[2,13,14] lead to low compatibility with physiological buffers,[3,15] as well as cytotoxicity by increasing intracellular levels of reactive oxygen species (ROS).[16–18] On the other hand, graphene produced by chemical vapor deposition (CVD) renders fewer sheet defects and, therefore, lower oxygen content,[9,12] especially under high temperatures[19] or plasma-enhanced (PE-CVD) production.[19] The lower number of defects, however, increases the hydrophobicity of graphene and thereby lowers the dispersibility in aqueous solutions.[20]

One of the main purposes of dedicated drug delivery systems is to allow for controlled drug delivery and release at a target tissue or organ. This minimizes unwanted side effects and increases exposure of drug at the tissue of interest, which makes the therapy more efficient compared to conventional drug-based therapy.[4,21,22] Graphene possesses preferred properties over the clinically used liposomes, as its carbon-based structure is impermeable to other molecules, reducing the risk of cargo leakage while requiring less demanding storage conditions.[23–28] However, its inability to form a stable dispersion in aqueous solutions, especially for nonoxidized graphene, has hampered its use compared to other drug delivery platforms.

Besides size limitations due to intravenous administration, delivery of nanosized carriers requires that graphene sheets are small enough to pass the leaky vessel endothelium in tumors to accumulate utilizing the enhanced permeability and retention (EPR) effect.[21,29,30] While the production of graphene usually renders polydisperse sheet sizes, multiple protocols to obtain a narrow size separation of graphene down to a nanometer range have been described previously,[31–36] making graphene an ideal candidate to fully exploit the EPR potential. Furthermore, the lower pH found in tumor microenvironments as a result of rapid cancer cell growth[37] can be used for targeted drug release. GO has previously shown amphiphilic properties

A

stemming from hydrophobic basal regions among the hydrophilic functional groups,[38,39] allowing for targeted release of loaded drugs at lower pH.[6,40,41] However, in contrast to GO, this ability remains to be investigated for CVD graphene, with its lower defect levels and fewer functional groups, as the pH-dependent release from GO has been attributed to the lower binding with these groups[9,42] affected by the protonation of the loaded drug in lower pH.[41,43,44]

To test graphene's potential as a drug carrier, we used phenformin, a biguanide antidiabetic drug,[45,46] that has previously been tested in cancer models using micelles as a drug carrier.[45] The analogue metformin, commonly used to treat diabetes type 2, has recently been studied extensively for its potential as a cancer drug, inhibiting key metabolic pathways needed for cell growth.[47] Phenformin acts similar to metformin in cancer cell lines, but has higher potency.[45,46–48] Phenformin was discontinued in diabetes treatment in the early 1980s due to undesired side effects,[18] but its newly discovered beneficial effects in cancer treatment may outweigh the previously experienced risks.[46,49–53] Importantly, these side effects could be further mitigated by the use of a dedicated drug carrier, such as graphene nanosheets. On a structural level, phenformin contains a guanidine group, which could form hydrogen bonds between the amine groups in guanidine and the carboxyl groups on graphene sheets.[54,55] In addition, phenformin contains a phenol residue that could bind to graphene through pi–pi interactions due to delocalized electrons on the graphene surface.[54,55] Drug delivery of phenformin's analogue, metformin using carbon nanotubes in cancer cells has been reported,[56] as well as controlled metformin drug release using GO hydrogels in mice.[57,58] Moreover, GO has recently been used to selectively deliver metformin to triple-negative breast cancer,[59] demonstrating increasing interest and relevance for improving biguanide drug delivery using graphene-based drug carries.

Here, we report on the stability and binding properties of two graphene-based drug carriers, PEGylated graphene nanosheets (PGNS) and GO, in relation to the biguanide drug phenformin. This work is highly relevant for expanding the cancer drug repertoire and holds promise for overcoming challenges related to using metabolic drugs in cancer treatment.

RESULTS AND DISCUSSION

Characterization of PGNS and GO. To increase the solubility of PE-CVD graphene, we covalently attached poly(ethylene glycol) (PEGylation) onto PE-CVD graphene sheets. The PEGylation approach was used to retain the defect-free graphene properties of PE-CVD, while obtaining an irreversible increase in water solubility, but without introducing oxidations of the basal plane as in GO. This should preserve the pi electrons that are necessary for drug adsorption and yielding lower oxygenation levels in the PEGylated graphene nanosheets (PGNS). Throughout this work, we compare the PGNS to a commercially available GO from ACS materials.

The atomic ratio of oxygen to carbon, determined by X-ray fluorescence (XRF), was around 5 times lower in PGNS compared to GO (Table 1). This suggests that the PE-CVD production method, followed by the PEGylation process, does not introduce a high number of oxygen-carrying groups compared to that found in GO.

Table 1. Comparative Characterization of PGNS and GO

		PGNS	GO
Oxygen content (XRF carbon int. weighted)		0.023 ± 0.04	0.125 ± 0.08
D_r in diH$_2$O (μ^2/s)	pH 7.5	1.326 ± 0.18	1.131 ± 0.2
	pH 6.5	0.996 ± 0.2	1.114 ± 0.24
	pH 5	0.417 ± 0.03	0.718 ± 0.09
ZP in diH$_2$O (mV)	pH 7.5	-21 ± 4	-37.6 ± 6
	pH 6.5	-15 ± 2	-36.13 ± 6
	pH 5	-5 ± 2.5	-28.3 ± 2.9
AFM graphene layer height (nm)		$5–15$ nm	$1–3$ nm (detection limit)

*XRF characterization to estimate the relative oxygen ratio ($N = 3$, ±SD) normalized to carbon intensity-weighted content, dynamic light scattering (DLS) to assess diffusion coefficient (D_r) and ζ-potential (ZP) variation against pH change ($N = 3$, ±SD), and atomic force microscopy (AFM) to determine sheet height. Abbreviations: graphene oxide (GO), PEGylated graphene nanosheets (PGNS), X-ray fluorescence (XRF), dynamic light scattering (DLS).

Dynamic light scattering (DLS) was used to compare the effect of pH on the diffusion coefficient (D_r) and ζ-potential (ZP) of GO and PGNS. The ZP and D_r measurements showed no significant variation at pH 7.5 and 6.5 between PGNS and GO (Table 1 and Figure S1). However, at pH 5, the D_r was decreased for GO and was 3-fold lower for PGNS compared to pH 7.5. This substantial change in D_r indicates changes in either the shape or the hydrodynamic radius of the particle. The ZPs of PGNS and GO at physiological pH were -21.5 and -37.5 mV, respectively. The more negative ZP of GO is probably linked to its higher oxygen content compared to PGNS. Furthermore, acidic pH had a minimal effect on the ZP of GO compared to PGNS, the latter being almost neutral at pH 5 (Figure S1c). When dispersed in fetal bovine serum over 5 days, GO showed more signs of protein adsorption than PGNS. Thereafter, both GO and PGNS maintained their D_r and ZP levels compared to day 1 (Table S1).

Atomic force microscopy (AFM) was used for the shape characterization of both materials. The PGNS sample was found to consist of sheets that are relatively similar in size (mean diameter = 262 ± 75 nm) but, on average, showed smaller diameters than GO (mean diameter = 448 ± 226 nm) (Figures 1a and S2). The AFM scan also revealed possible solvent residues on top of the PEGylated graphene sheets, which could be caused by the solvent being trapped by the PEG chains during evaporation. The remaining solvent complicates the estimation of the layer numbers. GO was found to consist of primarily monolayer sheets of vastly varying size compared to PGNS (Figures 1b and S2). There was a high dispersity between sheet sizes, ranging from few nanometers to multiple micrometers in the largest sheet diameter.

The PE-CVD graphene used in this study was vertically grown on the substrate and therefore rendered few (~less than 10) layers thick sheets that were initially hydrophobic and not dispersible in water. However, after PEGylation, the resulting graphene sheets were stable and dispersed in deionized water for more than 1 week and could easily be redispersed by gentle shaking (Figure S3).

PGNS Provides Better Aqueous Dispersion Stability Than GO When Loaded with Phenformin. An important aspect of evaluating the use of nanoparticles for drug carrier application is its colloidal stability, particularly after drug loading. To assess the stability, time-resolved DLS measure-

B

65

Paper II - Improved pH-responsive release of phenformin from low defect graphene compared to graphene oxide
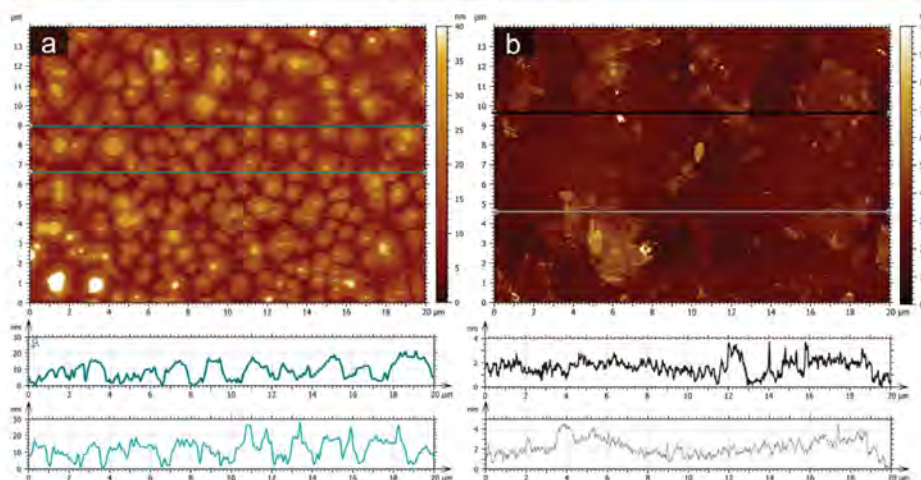
Figure 1. AFM characterization of (a) PGNS and (b) GO showing individual sheets of single and few layers with height using pseudo-coloring. Abbreviations: graphene oxide (GO), PEGylated graphene nanosheets (PGNS), and atomic force microscopy (AFM).

ments were conducted for GO and PGNS with the addition of phenformin. The underlying stability of both dispersions, prior to the addition of phenformin, is represented by the consistent baseline of intensity-based size measurements over a period of 165 min (Figure 2b). It can therefore be concluded that GO and PGNS maintained a stable size distribution in solution over the recorded measurement, with no detected graphene agglomerates formation. However, upon the addition of 1 mM phenformin to both dispersions, the Z-average size measurements of GO increased during the first hour, indicating the formation of larger agglomerates in the solution. These effects were not seen in PGNS within the same time frame under the same conditions.

To find the threshold of GO agglomeration induced by phenformin and identify possible agglomeration in PGNS that went undetected by DLS, we added increasing concentrations of phenformin (15.6 μM up to 1 mM) to both dispersions. Visually detected destabilization of GO sheets and formation of agglomerates were seen at concentrations of 250−1000 μM phenformin (Figure 2a) and confirmed by microscopy (Figure S4). Such agglomeration was not observed in PGNS at the same phenformin concentrations. A titration experiment was conducted to measure the extent of GO and PGNS stability upon increasing phenformin concentrations. Here, a centrifugation step was introduced to isolate the dispersed supernatant of GO and PGNS in a solution mixed with increasing concentrations of phenformin (15.6−1000 μM) after 24 h of interaction time. The graphene concentrations in the collected supernatants were calculated by integrating the area under the absorbance spectrum in the visible range. A decrease in measured supernatant graphene concentration would signify agglomeration due to the faster sedimentation of larger formed particles under equal centrifugal forces. We found that PGNS had lower levels of agglomeration compared with GO at concentrations of up to 1 mM phenformin (Figure 2c). Agglomeration of GO was dose-dependent and was detected

with phenformin concentrations down to 100 μM. PGNS also showed concentration-dependent agglomeration but at a slower rate than GO (Figure 2c). The addition of 250, 500, and 1000 μM phenformin resulted in supernatant concentrations relative to controls of 94, 90, and 86% for PGNS versus 64, 7.3, and 6.4% for GO, respectively (Figure 2c).

Depending on the pH of the solution, phenformin exists in the solution as either a divalent or monovalent ion. Therefore, addition of phenformin will increase the ionic strength of the solvent, in this case, water, and is expected to reduce the repulsive colloidal stability of graphene by reducing the strength of the electrical double layer surrounding the sheets. This double layer is also expected to be larger in GO due to higher oxygen content leading to increased electron density, which in turn would be more effective in overcoming the attractive forces that would otherwise bring the graphene sheets together.[60] For example, the higher stability in GO compared with reduced GO is due to decreased strength of the electrical double layer in reduced GO.[60] Similarly, the lower oxygen content on PE-CVD graphene would also result in a decreased electric double layer, making it unstable in water without the conjugation of PEG. However, contrary to GO, the addition of phenformin showed negligible effect on PGNS stability, most likely due to the PEGylation.

In support of this, other groups have demonstrated the agglomeration effect seen in GO by increasing the monovalent Na$^+$ ion concentrations to a critical coagulation concentration of 44−60 mM.[60,61] Furthermore, reports of divalent ions Ca^{2+} and Mg^{2+} interaction with GO[61] show critical coagulation concentrations comparable to the 1 mM phenformin concentrations used in our study, which supports our findings that phenformin compromises GO stability in solution. Moreover, it has been shown previously that steric stabilization using PEG prevents ion-mediated agglomeration,[62] supporting our observations that phenformin induced less agglomeration in PGNS than GO. The significance of this effect in the
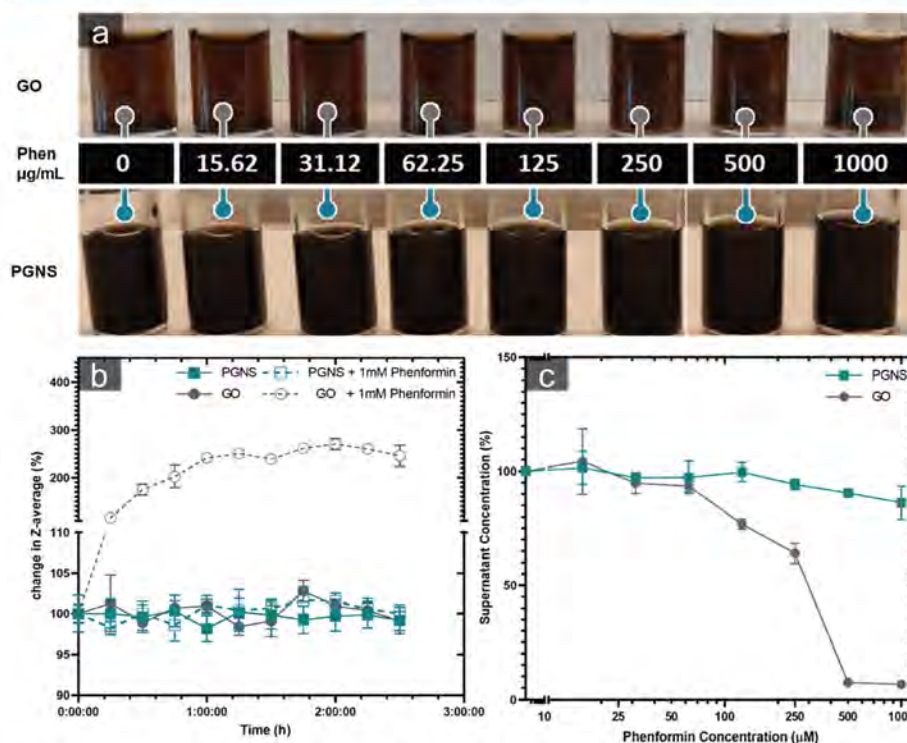
Figure 2. Reduced stability of GO compared to PGNS after the addition of phenformin to water dispersion. (a) Images of glass tubes containing GO (top) and PGNS (bottom) with a serial increase in phenformin concentrations (left: 0–1000 μg/mL) showing visible agglomeration in GO after 24 h. (b) Time-resolved intensity-weighed Z-average size estimation of GO and PGNS with and without the addition of phenformin, represented as a change from $T = 0$ ($N = 3$, ±SD). (c) GO and PGNS supernatant concentrations 24 h after the addition of increasing concentrations of phenformin. The supernatants were collected after gentle centrifugation of samples, and the integrated area under the absorbance spectrum between 400 and 900 nm is displayed as % from control to indicate concentration ($N = 3$, ±SD). Abbreviations: graphene oxide (GO), PEGylated graphene nanosheets (PGNS).

bloodstream is critical for the choice of nanoparticles in drug delivery. The ionic destabilization, here represented by phenformin, gives an indication of the stability of graphene if exposed to the naturally occurring electrolytes in the bloodstream. Blood electrolytes, such as sodium and calcium cations, maintained at concentrations over 100 and 2 mmol/L respectively,[63] may pose a concern toward the stability of repulsively stabilized nanoparticles such as GO. However, from our data (Figure 2), this can be overcome using steric stabilization.

Kinetics of Phenformin Adsorption onto PGNS and GO. Phenformin has the potential to bind with a graphene sheet by either pi interactions with the hydrophobic basal plane of graphene or via the interaction between the amine group of the phenformin and the carboxylic groups of graphene. Microscale thermophoresis (MST), time-correlated fluorescence imaging, and time-resolved absorption measure-

ments were used to understand the kinetics and affinity of the interaction of phenformin with graphene dispersions.

MST traces were collected after 24 h of phenformin interaction in a titration series (0–1 mM) with PGNS and GO to calculate the binding at each concentration. As MST relies on the temperature-induced changes in fluorescence to calculate binding, PGNS was covalently labeled with an Atto-488 dye, while the autofluorescence of GO was sufficient to calculate the binding. Hill's slope-fitted fractional binding curves showed 4.5 times higher binding affinity of phenformin toward PGNS compared to GO with k_d values of 3.625 ±0.551 and 16.25 ± 2.138 μM, respectively (Figure 3).

To monitor the binding kinetics at an equilibrium state, the adsorption of 50 μM phenformin was monitored over time on 0.5 and 1 mg/mL of GO and PGNS, respectively. There was rapid drug adsorption within the first 4–8 h (Figure 3), where GO dispersions reached 50% binding 1.3 times faster than

D

Paper II - Improved pH-responsive release of phenformin from low defect graphene compared to graphene oxide
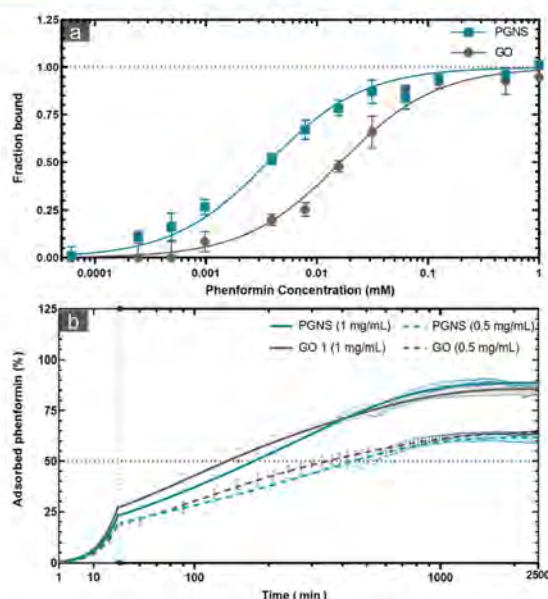
Figure 3. Binding affinity and kinetics of phenformin from PGNS and GO. (a) MST-derived fractional binding of a series concentrations of phenformin up to 1 mM onto GO and PGNS, specific binding curves with Hill's slope. (b) Kinetic measurements reflecting the % of phenformin adsorption on GO and PGNS. The analysis was done using GO and PGNS at two different concentrations of 0.5 and 1 mg/mL. The graphs show the continued measurements of free phenformin removed over 24 h from an initial ($T = 0$) concentration of 50 μM (10.26 μg/mL). ($N = 2$ and 3, ±standard error of mean (SEM) for PGNS and GO, respectively). Abbreviations: microscale thermophoresis (MST), graphene oxide (GO), PEGylated graphene nanosheets (PGNS).

PGNS at both concentrations tested (Table 2). However, PGNS reached equilibrium before GO, 1.4 times faster at 1

Table 2. Phenformin Kinetic Diffusion Parameters for PGNS and GO

	PGNS		GO	
Concentration (mg/mL)	1	0.5	1	0.5
Time to plateau (h)	18.5	20.5	26	41
Time to 50% (h)	2.86	7.23	2.23	5.62
Fast diffusion ratio (%)	24.55%	29.51%	51.65%	54.25%

"Recorded times needed for each condition to reach an adsorption milestone; two-phase association kinetics fit results after 48 h phenformin adsorption measurements to calculate the contribution of each phase of the adsorption. Abbreviations: graphene oxide (GO), PEGylated graphene nanosheets (PGNS).

mg/mL, and 2 times faster at 0.5 mg/mL. This indicates a rapid binding mechanism of phenformin to GO that becomes saturated as phenformin adsorption reaches ~50%, a mechanism apparently less predominant in PGNS. Such binding could reflect the direct interaction between the phenformin amines and the carboxyl groups. Therefore, a two-phase association model was used to calculate the contribution of this fast adsorption phase for GO and PGNS. Approximately 25% of the total phenformin binding

was attributed to the fast phase in PGNS compared to 50% in GO. This relative increase could also be explained by the amine carboxyl interaction.

The binding was studied further as a function of the fluorescence lifetime of fluorescein. Graphene is known to quench the fluorescence of fluorescein donor molecules allowing their use as a fluorescence lifetime imaging microscopy—fluorescence resonance energy transfer (FLIM-FRET) pair.[64,65] The initial binding of equal fluorescein concentrations onto PGNS and GO was 32.15 and 17.66%, respectively. Since the lifetime of fluorescein is affected by pH (Figure S5), we tracked the change of fluorescein binding onto PGNS and GO after the addition of phenformin. The binding was reduced to 20.3 and 6.37% in PGNS and GO, respectively. A spatial resolution of the binding efficiency showed that the displacement of fluorescein by phenformin appears to be more considerable in the nonagglomerated regions in GO, suggesting a higher phenformin binding in these regions (Figure 4).

In addition to agglomeration, the difference in oxygen content and the extent of surface defects could play a critical role in the discrepancy of phenformin interactions with GO versus PGNS. The measured 5-fold higher oxygen content in GO (Table 1) means more sheet defects and consequently disturbed pi electrons.[10] Thus, the probability of carboxylic groups, and their interaction with phenformin's amines, should

E

Paper II - Improved pH-responsive release of phenformin from low defect graphene compared to graphene oxide
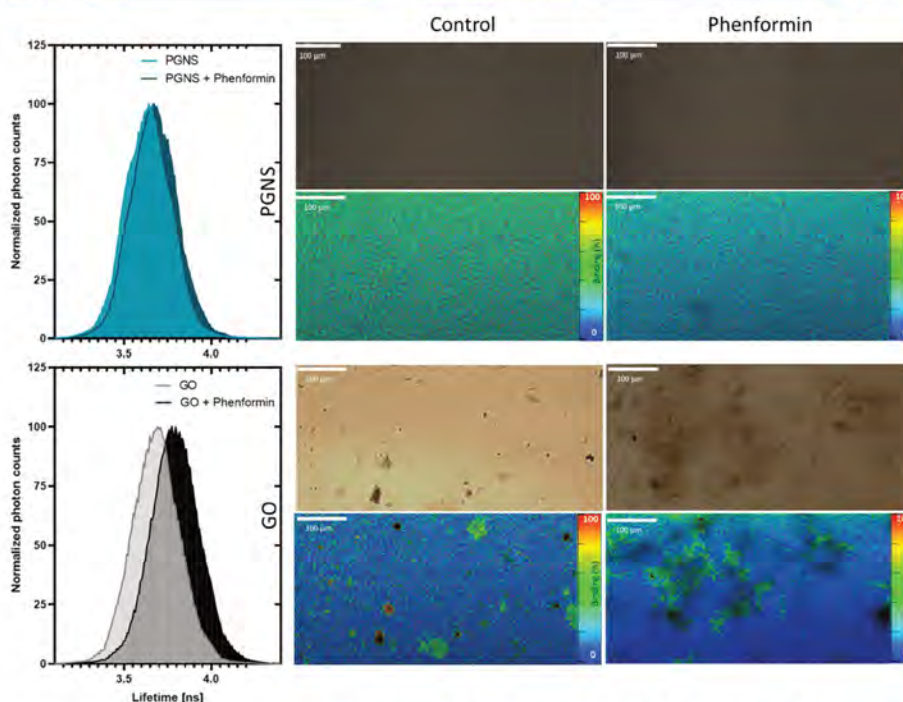
Figure 4. Fluorescence lifetime distributions of fluorescein mixed with PGNS and GO before and after adding 1 mM phenformin (left). Representative images at 20× magnification using bright-field microscopy and specially resolved FLIM-FRET with pseudo-color coding of fluorescein binding efficiency using GO and PGNS as photon acceptors before and after the addition of 1 mM phenformin (right). Abbreviations: microscale thermophoresis (MST), graphene oxide (GO), PEGylated graphene nanosheets (PGNS), fluorescence lifetime imaging microscopy-fluorescence resonance energy transfer (FLIM-FRET).

increase. This interaction is detectable by DLS in the absence of graphene (Figure S6). On the other hand, the removal of oxygen correlates with an increase in the sp^2 hybrid orbital fraction on the graphene surface.[66] Therefore, a less defected basal plane as in PGNS would allow for more pi−pi and cation−pi interactions with phenformin. However, the lower number of carboxylic groups on PE-CVD graphene limits their interaction with external amines compared to GO. In addition, a proportion of these groups are converted into amides during the covalent attachment of PEG in PGNS, decreasing their concentration even further. In contrast, the addition of the oxygen-rich PEG arms in PGNS adds a new mechanism and binding opportunity for phenformin. This may happen as we found that the ZP of PEG alone is attenuated after phenformin addition (Figure S7).

Dissociation Rates of Phenformin from Graphene at Different pH Levels. The effect of pH on the release profile of phenformin from GO and PGNS was studied after 24 h of interaction. The amount of unbound phenformin was measured at pH values that simulate shifts between normal tissues and tumor microenvironment of pH 5, 6.8, and 7.4 with increasing graphene concentrations.

A change in phenformin adsorption capacity onto graphene was affected by pH in both PGNS and GO (Figure 5a). There was an increased release of phenformin in acidic pH compared to physiological pH 7.4. This increase was on average 2.2 and 4.4 times higher at pH 5 than pH 7.4 in GO and PGNS, respectively. More specifically, the release of phenformin from GO was increased 24.2% (±7.1%) and 14.2% (±5.7%) at pH 5 compared with 7.4 at concentrations of 62.125 and 125 μg/mL, respectively. In comparison, the increase in PGNS was 35.2% (±5.9%) and 35.4% (±5.2%) for the same concentrations.

These results correspond to the change in ZP of PGNS and GO at pH values ranging from 3 to 11.5 (Figures 5b and S1). The shift toward positive ZP corresponding to more basic pH levels was steeper in PGNS compared to GO, spanning over a 3.8-fold increased charge range in the tested pH values. An increased positive electrostatic potential at the shear planes of PNGS could cause an enhanced release of the positively charged phenformin at acidic pH values, compared to GO. The
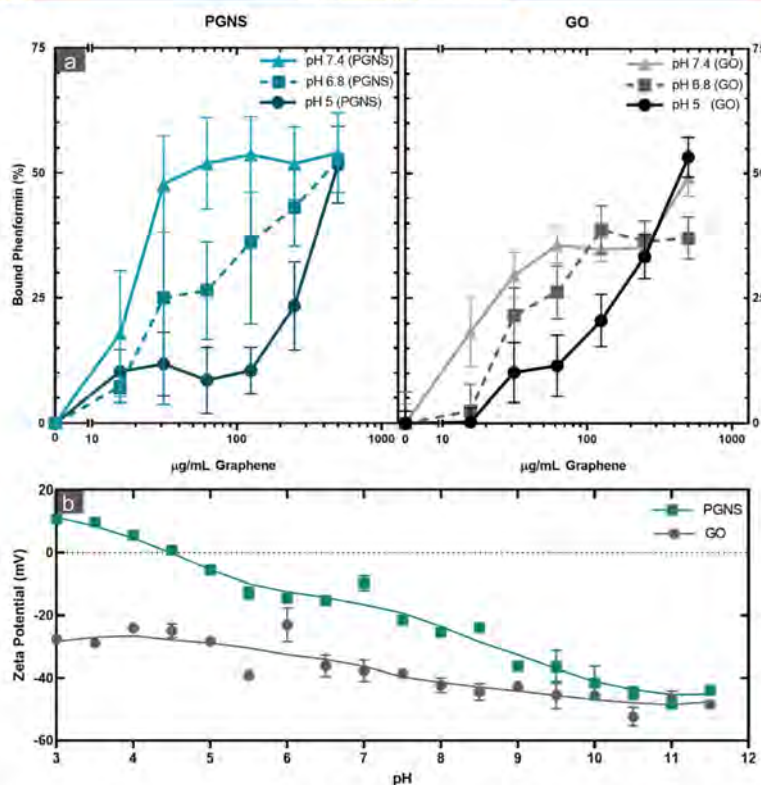
Figure 5. pH-dependent release of phenformin from PGNS and GO. (a) Percentage (%) of bound of phenformin at pH 5, 6.8, and 7.4 is represented at increasing concentrations of PGNS and GO after 24 h measured by high-performance liquid chromatography (HPLC) determination of the unbound filtrate ($\pm$SEM, $N = 3$). (b) ZP values of GO and PGNS water dispersions as a function of pH ($\pm$SEM, $N = 3$). Abbreviations: high-performance liquid chromatography (HPLC), ζ-potential (ZP), graphene oxide (GO), PEGylated graphene nanosheets (PGNS).

decrease in negative charges appeared to correlate with the pH-dependent release of the adsorbed phenformin in PGNS and GO (Figures 5b and S1). Thus, as the pH drops lower than physiological level, similar to that observed in the microenvironment of tumor or lysosomes,[21] more phenformin is released.

The difference in the modular affinity between phenformin and GO or PGNS at acidic versus basic pH values could be due to a combination of different interaction mechanisms between phenformin and graphene. In GO, the degree of protonation of carboxylic groups on GO and guanidinium in phenformin might be a key factor. At neutral pH levels, carboxylic groups are more likely to interact with the protonated biguanide core of phenformin.[67] However, this type of interaction is less likely under acidic conditions. Carboxyl groups are increasingly protonated, leading to lower binding and the consequent release of phenformin. Previous

studies demonstrating the pH-dependent drug release of the cancer drug doxorubicin from GO have ascribed this effect to weakened hydrogen bonding under acidic conditions.[41,43,44,68,69] While it could be argued that PGNS is also affected by the same mechanism, the lower density of carboxylic groups on its surface should limit this contribution compared to GO. Therefore, this might not explain the enhanced pH-dependent release observed in our experiment using PGNS. However, the higher capacity to participate in pi interactions due to the low-defected surface, such as in PGNS, makes it more relevant for the adsorption of phenformin than in GO. The interaction with the basal plane of graphene could occur through either pi–pi interactions with the phenol ring or cation–pi interactions with the amine group of phenformin. Cation–pi interactions, in particular, are known to increase in strength with increasing pH.[70] Thus, the increased probability

G

of establishing pi−interaction can provide a reason for the higher pH-responsiveness in PGNS compared to GO.

Additionally, the PEG arms in PGNS could be involved in the pH-responsive binding of phenformin. While PEG could interact with phenformin itself (Figure S7), this ability can be limited by possible PEG adsorption onto the graphene surface. Poly(ethylene glycols) have been shown to adsorb onto activated carbons in a pH-dependent manner, where the adsorption was at its lowest at pH 5.[71]

■ CONCLUSIONS

We show that using covalent PEGylation, PE-CVD graphene sheets can be modified to overcome its hydrophobicity and provide better colloidal stability in the presence of the metabolic drug phenformin. Furthermore, we show that phenformin adsorption capacity is increased in the PEG-functionalized graphene compared to GO, likely due to higher pi- and PEG-mediated interaction possibilities. Most importantly, the pH-responsive phenformin release is not only conserved in nonoxidized graphene sheets but appears to be enhanced in PGNS. Finally, this work shows that PEGylated pristine graphene may be a better carrier than oxidized graphene for drug delivery of phenformin and warrants further exploration in cancer model systems.

■ METHODS

Preparation of PGNS and GO. PE-CVD graphene flakes (10 mg, as obtained from CealTech, Stavanger, Norway) were dispersed in DiH$_2$O and sonicated in a glass vial for 10 min until dispersion. The pH of the dispersion was adjusted to 5.5 with HCl. Graphene (1:5 wt %) and monofunctional 2K mPEG-Amine (50 mg, Biochempeg, MA) were added to the washed PE-CVD graphene and sonicated with the graphene for 5 min. The cross-linking was then mediated by adding 1.5 mg of 1-ethyl-3-(3-dimethylaminopropyl) carbodiimide (EDC) (Merck KGaA, Darmstadt, Germany) to the mixture under sonication for 30 min. The dispersion was left under constant agitation overnight. The excess EDC and mPEG were then removed by dialysis for 48 h using 30 mL of Slide-A-Lyzer Dialysis Cassettes (Thermo Scientific, Massachusetts) in DiH$_2$O that is replaced after 2, 6, and 24 h. The PEG−graphene suspension was sequentially sonicated in a bath sonicator and then washed with DiH$_2$O using 100 kDa Vivaspin (Sartorius AG, Göttingen, Germany) centrifugal concentrators three times. Thereafter, the UV−vis spectrum of the filtrate was controlled for the absence of absorbance peaks differentiating from a blank DiH$_2$O control (WL: 200−900 nm).

Commercially available graphene oxide prepared by modified Hummer's method (GNO1W001, ACS Material, LLC, Pasadena) was used in this study. A 1 mg/mL water dilution was made in DiH$_2$O that is then cross-filtrated using Vivaflow 50 (Sartorius AG, Göttingen, Germany) to neutralize the pH and eliminate any existing contaminants.

Characterization. *X-ray Fluorescence (XRF).* PGNS and GO suspension (50 µL) was placed dropwise on a silver membrane filter (Cat. No. 1145348, Osmonics, Inc., Minnetonka). The samples were dried at 50 °C for >30 min and measured on an S4 PIONEER X-ray spectrometer (Bruker AXS GmbH, Karlsruhe, Germany) the following day. To calculate the relative oxygen content, the intensity values from carbon and oxygen of blank filters were subtracted from the

samples. To compensate for variations in the amount of PGNS and GO placed on the filters, the oxygen content of all filters was normalized based on the measured carbon content. The relative oxygen content was then calculated by dividing the resulting relative oxygen content of GO by PGNS.

Atomic Force Microscopy (AFM). For analysis, 20 µL of the suspensions were placed on a mica substrate and evaporated at 50 °C for >30 min and allowed to cool before analysis. The sample was analyzed in repulsive mode on an MFP-3D-BIO (Asylum Research, Oxford Instruments, California). Noise filtration was performed using two-dimensional fast Fourier transform (2D-FFT) filtering in Gwyddion 2.57. Analysis of sheet diameter distribution is based on the radius from the center of mass calculated from a minimum of 150 sheets segmented by height.

Dynamic Light Scattering (DLS). DLS-based surface charge and intensity-weighted sizes of PGNS and GO were measured using Zetasizer Nano ZSP (Malvern Panalytical, Malvern, United Kingdom) with an inline MPT-2 degassed titrator. The titration compartment containing 10 mL of GO or PGNS was kept under constant agitation and real-time pH measurement to adjust the pH at each titration step using HCL and NaOH.

Stability Study. *UV−Vis Spectroscopy.* Phenformin (Cayman Chemical, Michigan, United States) was added in increasing concentrations (15 µM to 1 mM) to 1 mg/mL of PGNS and GO suspensions. After 24 h, 3000 RCF centrifugation for 10 min was performed to sediment larger agglomerates. The supernatants were collected, and their concentration was measured using UV−vis spectroscopy by integrating the area under the spectrum in the visible range between 400 and 900 nm.

DLS. Size measurement of PE-CVD graphene and graphene oxide at 100 µg/mL concentration was carried out continuously over time using DLS (Malvern Panalytical Ltd, UK) for 150 min with and without 1 mM phenformin. The calculated sizes were normalized to the initial measured size at $T = 0$.

Phenformin Binding Kinetics. *UV−Vis Kinetic Measurements.* In plastic UV cuvettes, 1 mL of 50 µM phenformin (the concentration based on a pilot experiment showing equilibrium reached within 24 h under same parameters without graphene) was separated from 400 mL of water suspensions of PGNS and GO at concentrations of 500 and 1000 µg/mL using a 20K MWCO RC membrane. Continuous absorbance measurements at 233 nm were taken (15 min intervals) using a Shimadzu UV-1800 UV−visible spectrophotometer. The decrease in absorbance correlated with the decrease of phenformin in the lower compartment and its binding to graphene. The adsorption of phenformin is then calculated after background subtraction (based on water-only internal control) and the ratios of interpolated measured values by the maximum phenformin concentration of 10.26 µg/mL.

Fluorescence Lifetime-Based FLIM-FRET. Lifetimes of (15 µg/mL) fluorescein (Merck, Darmstadt, Germany) in exposure to 100 µg/mL of graphene with and without the addition 0.5 and 1 mM of phenformin was recorded using a Leica TCS SP8 falcon platform (Leica Microsystems, Mannheim, Germany). The lifetime decays were collected and fitted to a two-exponential tail fit decay to calculate the intensity-based mean lifetimes and the FLIM-FRET changes corresponding to phenformin doses (Tables S2 and S3).

Microscale Thermophoresis (MST). First, fluorescent PGNS were produced similar to the production of PGNS described in

H

Paper II - Improved pH-responsive release of phenformin from low defect graphene compared to graphene oxide

the Preparation of PGNS and GO section. However, 10% of the added Monofunctional 2K mPEG-Amine was substituted with an ATTO-488-Amine (ATTO-TEC, Siegen, Germany) dye to obtain a green fluorescent PGNS for MST analysis. The k_d of GO and PGNS was determined via microscale thermophoresis (MST; Monolith NT.115, Nano Temper). Series concentrations of phenformin (0−1 mM) in DiH$_2$O were mixed with GO or Atto-488-PGNS to a final concentration of 50 μg/mL. Afterward, each of the mixtures was pulled into a capillary and set into the Monolith NT.115 capillary compartment. MST power (40%) was used in combination with the blue LED power to determine the MST traces. The change in the thermophoresis of the fluorescence correlates with higher phenformin binding at each concentration used. MST traces derived fraction bound values were plotted against the phenformin molar concentration in MO. Affinity analysis software was used and k_d was calculated from the dose−response curve.

High-Performance Liquid Chromatography (HPLC). The binding of phenformin at different pH levels is determined via HPLC. Phenformin (50 μM) was mixed with a series dilution of PGNS and GO (15−500 μg/mL) in triplicate at 3 pH levels of 5, 6.8, and 7.4. After 24 h, 300 μL of the mixture was moved to a 10 kDa MWCO filtration plate and centrifuged over a collection plate at 500 rpm until complete filtration. Each filtrate (100 μL) was then measured for unbound phenformin at 233 nm using HPLC (Hitachi High Technologies, Tokyo, Japan) over Phenyl-Hexyl 2.7 μm column using a gradient of DiH$_2$O and acetonitrile (30:70%) as the mobile phase.

ASSOCIATED CONTENT

Supporting Information

The Supporting Information is available free of charge at https://pubs.acs.org/doi/10.1021/acsomega.1c03283.

ζ-Potential pH dependence for graphene nanoparticles (Figure S1); AFM-based size estimation of graphene nanoparticles (Figure S2); PGNS and GO prolonged dispersion stability in water (Figure S3); bright-field microscopy images at 5× magnification of 100 μg/mL of GO and PGNS at concentrations of 0, 0.5, and 1 mM of phenformin (Figure S4); fluorescence arrival time histograms showing the effect of pH on the lifetime of fluorescein in 2-(N-morpholino)ethanesulfonic acid (MES) buffer (Figure S5); ζ-potential changes toward more positive charges of carboxymethylcellulose (Figure S6); ζ-potential of mPEG-amine in water before and after adding phenformin (Figure S7); stability of GO and PGNS in DI water versus fetal bovine serum (FBS) (Table S1); lifetime fit values for fluorescein decays with GO and PGNS (Table S2); FLIM-FRET fit values for fluorescein decays with GO and PGNS (Table S3) (PDF)

AUTHOR INFORMATION

Corresponding Author

Hanne Røland Hagland − *Department of Chemistry, Biosciences and Environmental Technology, University of Stavanger, 4021 Stavanger, Norway;* orcid.org/0000-0002-7470-1358; Email: Hanne.r.hagland@uis.no

Authors

Abdelnour Alhourani − *Department of Chemistry, Biosciences and Environmental Technology, University of Stavanger, 4021 Stavanger, Norway*

Jan-Lukas Forde − *Centre for Pharmacy, Department of Clinical Science, University of Bergen, 5007 Bergen, Norway; Department of Internal Medicine, Haukeland University Hospital, 5021 Bergen, Norway*

Lutz Andreas Eichacker − *Department of Chemistry, Biosciences and Environmental Technology, University of Stavanger, 4021 Stavanger, Norway*

Lars Herfindal − *Centre for Pharmacy, Department of Clinical Science, University of Bergen, 5007 Bergen, Norway*

Complete contact information is available at:
https://pubs.acs.org/10.1021/acsomega.1c03283

REFERENCES

(1) Yang, K.; Feng, L.; Liu, Z. The advancing uses of nano-graphene in drug delivery. *Expert Opin. Drug Delivery* 2015, 12, 601−612.
(2) Coleman, J. N. Liquid exfoliation of defect-free graphene. *Acc. Chem. Res.* 2013, 46, 14−22.
(3) Liu, Z.; Robinson, J. T.; Sun, X.; Dai, H. PEGylated nanographene oxide for delivery of water-insoluble cancer drugs. *J. Am. Chem. Soc.* 2008, 130, 10876−10877.
(4) Jong, W. H.; de Borm, P. J. A. Drug delivery and nanoparticles: Applications and hazards. *Int. J. Nanomed.* 2008, 3, 133−149.
(5) Tian, B.; Wang, C.; Zhang, S.; Feng, L.; Liu, Z. Photothermally enhanced photodynamic therapy delivered by nano-graphene oxide. *ACS Nano* 2011, 5, 7000−7009.
(6) Sun, X.; Liu, Z.; Welsher, K.; Robinson, J. T.; Goodwin, A.; Zaric, S.; Dai, H. Nano-Graphene Oxide for Cellular Imaging and Drug Delivery. *Nano Res.* 2008, 1, 203−212.
(7) Tran, T. H.; Nguyen, H. T.; Pham, T. T.; Choi, J. Y.; Choi, H.-G.; Yong, C. S.; Kim, J. O. Development of a Graphene Oxide Nanocarrier for Dual-Drug Chemo-phototherapy to Overcome Drug Resistance in Cancer. *ACS Appl. Mater. Interfaces* 2015, 7, 28647−28655.
(8) Yang, X.; Zhang, X.; Liu, Z.; Ma, Y.; Huang, Y.; Chen, Y. High-Efficiency Loading and Controlled Release of Doxorubicin Hydrochloride on Graphene Oxide. *J. Phys. Chem. C* 2008, 112, 17554−17558.
(9) Tian, W.; Li, W.; Yu, W.; Liu, X. A Review on Lattice Defects in Graphene: Types, Generation, Effects and Regulation. *Micromachines* 2017, 8, No. 163.
(10) Banhart, F.; Kotakoski, J.; Krasheninnikov, A. V. Structural defects in graphene. *ACS Nano* 2011, 5, 26−41.
(11) Backes, C.; Abdelkader, A. M.; Alonso, C.; Andrieux-Ledier, A.; Arenal, R.; Azpeitia, J.; Balakrishnan, N.; Banszerus, L.; Barjon, J.; Bartali, R.; Bellani, S.; Berger, C.; Berger, R.; Ortega, M. M. B.; Bernard, C.; Beton, P. H.; Beyer, A.; Bianco, A.; Bøggild, P.; Bonaccorso, F.; Barin, G. B.; Botas, C.; Bueno, R. A.; Carriazo, D.; Castellanos-Gomez, A.; Christian, M.; Ciesielski, A.; Ciuk, T.; Cole, M. T.; Coleman, J.; Coletti, C.; Crema, L.; Cun, H.; Dasler, D.; Fazio, D. de.; Diez, N.; Drieschner, S.; Duesberg, G. S.; Fasel, R.; Feng, X.; Fina, A.; Forti, S.; Galiotis, C.; Garberoglio, G.; García, J. M.; Garrido,

Paper II - Improved pH-responsive release of phenformin from low defect graphene compared to graphene oxide

the Preparation of PGNS and GO section. However, 10% of the added Monofunctional 2K mPEG-Amine was substituted with an ATTO-488-Amine (ATTO-TEC, Siegen, Germany) dye to obtain a green fluorescent PGNS for MST analysis. The k_d of GO and PGNS was determined via microscale thermophoresis (MST; Monolith NT.115, Nano Temper). Series concentrations of phenformin (0–1 mM) in DiH_2O were mixed with GO or Atto-488-PGNS to a final concentration of 50 μg/mL. Afterward, each of the mixtures was pulled into a capillary and set into the Monolith NT.115 capillary compartment. MST power (40%) was used in combination with the blue LED power to determine the MST traces. The change in the thermophoresis of the fluorescence correlates with higher phenformin binding at each concentration used. MST traces derived fraction bound values were plotted against the phenformin molar concentration in MO. Affinity analysis software was used and k_d was calculated from the dose–response curve.

High-Performance Liquid Chromatography (HPLC). The binding of phenformin at different pH levels is determined via HPLC. Phenformin (50 μM) was mixed with a series dilution of PGNS and GO (15–500 μg/mL) in triplicate at 3 pH levels of 5, 6.8, and 7.4. After 24 h, 300 μL of the mixture was moved to a 10 kDa MWCO filtration plate and centrifuged over a collection plate at 500 rpm until complete filtration. Each filtrate (100 μL) was then measured for unbound phenformin at 233 nm using HPLC (Hitachi High Technologies, Tokyo, Japan) over Phenyl-Hexyl 2.7 μm column using a gradient of DiH_2O and acetonitrile (30:70%) as the mobile phase.

■ ASSOCIATED CONTENT

⊕ Supporting Information

The Supporting Information is available free of charge at https://pubs.acs.org/doi/10.1021/acsomega.1c03283.

ζ-Potential pH dependence for graphene nanoparticles (Figure S1); AFM-based size estimation of graphene nanoparticles (Figure S2); PGNS and GO prolonged dispersion stability in water (Figure S3); bright-field microscopy images at 5× magnification of 100 μg/mL of GO and PGNS at concentrations of 0, 0.5, and 1 mM of phenformin (Figure S4); fluorescence arrival time histograms showing the effect of pH on the lifetime of fluorescein in 2-(N-morpholino)ethanesulfonic acid (MES) buffer (Figure S5); ζ-potential changes toward more positive charges of carboxymethylcellulose (Figure S6); ζ-potential of mPEG-amine in water before and after adding phenformin (Figure S7); stability of GO and PGNS in DI water versus fetal bovine serum (FBS) (Table S1); lifetime fit values for fluorescein decays with GO and PGNS (Table S2); FLIM-FRET fit values for fluorescein decays with GO and PGNS (Table S3) (PDF)

■ AUTHOR INFORMATION

Corresponding Author

Hanne Roland Hagland − *Department of Chemistry, Biosciences and Environmental Technology, University of Stavanger, 4021 Stavanger, Norway;* ● orcid.org/0000-0002-7470-1358; Email: Hanne.r.hagland@uis.no

Authors

Abdelnour Alhourani − *Department of Chemistry, Biosciences and Environmental Technology, University of Stavanger, 4021 Stavanger, Norway*

Jan-Lukas Forde − *Centre for Pharmacy, Department of Clinical Science, University of Bergen, 5007 Bergen, Norway; Department of Internal Medicine, Haukeland University Hospital, 5021 Bergen, Norway*

Lutz Andreas Eichacker − *Department of Chemistry, Biosciences and Environmental Technology, University of Stavanger, 4021 Stavanger, Norway*

Lars Herfindal − *Centre for Pharmacy, Department of Clinical Science, University of Bergen, 5007 Bergen, Norway*

Complete contact information is available at:
https://pubs.acs.org/10.1021/acsomega.1c03283

■ REFERENCES

(1) Yang, K.; Feng, L.; Liu, Z. The advancing uses of nano-graphene in drug delivery. *Expert Opin. Drug Delivery* **2015**, *12*, 601−612.

(2) Coleman, J. N. Liquid exfoliation of defect-free graphene. *Acc. Chem. Res.* **2013**, *46*, 14−22.

(3) Liu, Z.; Robinson, J. T.; Sun, X.; Dai, H. PEGylated nanographene oxide for delivery of water-insoluble cancer drugs. *J. Am. Chem. Soc.* **2008**, *130*, 10876−10877.

(4) Jong, W. H.; de Borm, P. J. A. Drug delivery and nanoparticles: Applications and hazards. *Int. J. Nanomed.* **2008**, *3*, 133−149.

(5) Tian, B.; Wang, C.; Zhang, S.; Feng, L.; Liu, Z. Photothermally enhanced photodynamic therapy delivered by nano-graphene oxide. *ACS Nano* **2011**, *5*, 7000−7009.

(6) Sun, X.; Liu, Z.; Welsher, K.; Robinson, J. T.; Goodwin, A.; Zaric, S.; Dai, H. Nano-Graphene Oxide for Cellular Imaging and Drug Delivery. *Nano Res.* **2008**, *1*, 203−212.

(7) Tran, T. H.; Nguyen, H. T.; Pham, T. T.; Choi, J. Y.; Choi, H.-G.; Yong, C. S.; Kim, J. O. Development of a Graphene Oxide Nanocarrier for Dual-Drug Chemo-phototherapy to Overcome Drug Resistance in Cancer. *ACS Appl. Mater. Interfaces* **2015**, *7*, 28647−28655.

(8) Yang, X.; Zhang, X.; Liu, Z.; Ma, Y.; Huang, Y.; Chen, Y. High-Efficiency Loading and Controlled Release of Doxorubicin Hydrochloride on Graphene Oxide. *J. Phys. Chem. C* **2008**, *112*, 17554−17558.

(9) Tian, W.; Li, W.; Yu, W.; Liu, X. A Review on Lattice Defects in Graphene: Types, Generation, Effects and Regulation. *Micromachines* **2017**, *8*, No. 163.

(10) Banhart, F.; Kotakoski, J.; Krasheninnikov, A. V. Structural defects in graphene. *ACS Nano* **2011**, *5*, 26−41.

(11) Backes, C.; Abdelkader, A. M.; Alonso, C.; Andrieux-Ledier, A.; Arenal, R.; Azpeitia, J.; Balakrishnan, N.; Banszerus, L.; Barjon, J.; Bartali, R.; Bellani, S.; Berger, C.; Berger, R.; Ortega, M. M. B.; Bernard, C.; Beton, P. H.; Beyer, A.; Bianco, A.; Bøggild, P.; Bonaccorso, F.; Barin, G. B.; Botas, C.; Bueno, R. A.; Carriazo, D.; Castellanos-Gomez, A.; Christian, M.; Ciesielski, A.; Ciuk, T.; Cole, M. T.; Coleman, J.; Coletti, C.; Crema, L.; Cun, H.; Dasler, D.; Fazio, D. de.; Díez, N.; Drieschner, S.; Duesberg, G. S.; Fasel, R.; Feng, X.; Fina, A.; Forti, S.; Galiotis, C.; Garberoglio, G.; García, J. M.; Garrido,

Paper II - Improved pH-responsive release of phenformin from low defect graphene compared to graphene oxide

J. A.; Gibertini, M.; Gölzhäuser, A.; Gómez, J.; Greber, T.; Hauke, F.; Hemmi, A.; Hernandez-Rodriguez, I.; Hirsch, A.; Hodge, S. A.; Huttel, Y.; Jepsen, P. U.; Jimenez, I.; Kaiser, U.; Kaplas, T.; Kim, H.; Kis, A.; Papagelis, K.; Kostarelos, K.; Krajewska, A.; Lee, K.; Li, C.; Lipsanen, H.; Liscio, A.; Lohe, M. R.; Loiseau, A.; Lombardi, L.; Francisca López, M.; Martin, O.; Martín, C.; Martínez, L.; Martin-Gago, J. A.; Ignacio Martinez, J.; Marzari, N.; Mayoral, A.; McManus, J.; Melucci, M.; Méndez, J.; Merino, C.; Merino, P.; Meyer, A. P.; Miniussi, E.; Miseikis, V.; Mishra, N.; Morandi, V.; Munuera, C.; Muñoz, R.; Nolan, H.; Ortolani, L.; Ott, A. K.; Palacio, I.; Palermo, V.; Parthenios, J.; Pasternak, I.; Patane, A.; Prato, M.; Prevost, H.; Prudkovskiy, V.; Pugno, N.; Rojo, T.; Rossi, A.; Ruffieux, P.; Samori, P.; Schué, L.; Setijadi, E.; Seyller, T.; Speranza, G.; Stampfer, C.; Stenger, I.; Strupinski, W.; Svirko, Y.; Taioli, S.; Teo, K. B. K.; Testi, M.; Tomarchio, F.; Tortello, M.; Treossi, E.; Turchanin, A.; Vazquez, E.; Villaro, E.; Whelan, P. R.; Xia, Z.; Yakimova, R.; Yang, S.; Yazdi, G. R.; Yim, C.; Yoon, D.; Zhang, X.; Zhuang, X.; Colombo, L.; Ferrari, A. C.; Garcia-Hernandez, M. Production and processing of graphene and related materials. *2D Mater.* 2020, 7, No. 022001.

(12) Lim, J. Y.; Mubarak, N. M.; Abdullah, E. C.; Nizamuddin, S.; Khalid, M.; Inamuddin. Recent trends in the synthesis of graphene and graphene oxide based nanomaterials for removal of heavy metals—A review. *J. Ind. Eng. Chem.* 2018, 66, 29–44.

(13) Tiliakos, A.; Cucu, A.; Ceaus, C.; Trefilov, A. M. I.; Stamatin, I. In *Graphite Oxide Post-Synthesis Processing Protocols*, 2nd CommScie International Conference "Challenges for Sciences and Society in the Digital Era"; International Journal of Science Communication, 2015.

(14) Lavin-Lopez, M. P.; Romero, A.; Garrido, J.; Sanchez-Silva, L.; Valverde, J. L. Influence of Different Improved Hummers Method Modifications on the Characteristics of Graphite Oxide in Order to Make a More Easily Scalable Method. *Ind. Eng. Chem. Res.* 2016, 55, 12836–12847.

(15) Yang, K.; Feng, L.; Shi, X.; Liu, Z. Nano-graphene in biomedicine: theranostic applications. *Chem. Soc. Rev.* 2013, 42, 530–547.

(16) Vranic, S.; Rodrigues, A. F.; Buggio, M.; Newman, L.; White, M. R. H.; Spiller, D. G.; Bussy, C.; Kostarelos, K. Live Imaging of Label-Free Graphene Oxide Reveals Critical Factors Causing Oxidative-Stress-Mediated Cellular Responses. *ACS Nano* 2018, 12, 1373–1389.

(17) Lammel, T.; Boisseaux, P.; Fernández-Cruz, M.-L.; Navas, J. M. Internalization and cytotoxicity of graphene oxide and carboxyl graphene nanoplatelets in the human hepatocellular carcinoma cell line Hep G2. *Part. Fibre Toxicol.* 2013, 10, No. 27.

(18) Liao, K.-H.; Lin, Y.-S.; Macosko, C. W.; Haynes, C. L. Cytotoxicity of Graphene Oxide and Graphene in Human Erythrocytes and Skin Fibroblasts. *ACS Appl. Mater. Interfaces* 2011, 3, 2607–2615.

(19) Boyd, D. A.; Lin, W.-H.; Hsu, C.-C.; Teague, M. L.; Chen, C.-C.; Lo, Y.-Y.; Chan, W.-Y.; Su, W.-B.; Cheng, T.-C.; Chang, C.-S.; Wu, C.-I.; Yeh, N.-C. Single-step deposition of high-mobility graphene at reduced temperatures. *Nat. Commun.* 2015, 6, No. 6620.

(20) Huang, X.; Yin, Z.; Wu, S.; Qi, X.; He, Q.; Zhang, Q.; Yan, Q.; Boey, F.; Zhang, H. Graphene-based materials: synthesis, characterization, properties, and applications. *Small* 2011, 7, 1876–1902.

(21) De, M.; Ghosh, P. S.; Rotello, V. M. Applications of Nanoparticles in Biology. *Adv. Mater.* 2008, 20, 4225–4241.

(22) Alexis, F.; Pridgen, E.; Molnar, L. K.; Farokhzad, O. C. Factors affecting the clearance and biodistribution of polymeric nanoparticles. *Mol. Pharmaceutics* 2008, 5, 505–515.

(23) Sydykov, B.; Oldenhof, H.; Sieme, H.; Wolkers, W. F. Storage stability of liposomes stored at elevated subzero temperatures in DMSO/sucrose mixtures. *PLoS One* 2018, 13, No. e0199867.

(24) Akbarzadeh, A.; Rezaei-Sadabady, R.; Davaran, S.; Joo, S. W.; Zarghami, N.; Hanifehpour, Y.; Samiei, M.; Kouhi, M.; Nejati-Koshki, K. Liposome: classification, preparation, and applications. *Nanoscale Res. Lett.* 2013, 8, No. 102.

(25) Chen, C.; Han, D.; Cai, C.; Tang, X. An overview of liposome lyophilization and its future potential. *J. Controlled Release* 2010, 142, 299–311.

(26) Ageitos, J. M.; Chuah, J.-A.; Numata, K. Design Considerations for Properties of Nanocarriers on Disposition and Efficiency of Drug and Gene Delivery. In *Nanomedicines: Design, Delivery and Detection/ edited by Martin Braddock, AstraZeneca Research and Development*; Braddock, M., Ed.; RSC Drug Discovery, 2041–3203; Royal Society of Chemistry, Macclesfield, U.K., 2016; Chapter 1, Vol. 51; pp 1–22. DOI: 10.1039/9781782622536-00001.

(27) Moosavian, S. A.; Bianconi, V.; Pirro, M.; Sahebkar, A. Challenges and pitfalls in the development of liposomal delivery systems for cancer therapy. *Semin. Cancer Biol.* 2021, 69, 337–348.

(28) Nel, A. E.; Mädler, L.; Velegol, D.; Xia, T.; Hoek, E. M. V.; Somasundaran, P.; Klaessig, F.; Castranova, V.; Thompson, M. Understanding biophysicochemical interactions at the nano-bio interface. *Nat. Mater.* 2009, 8, 543–557.

(29) Rosenblum, D.; Joshi, N.; Tao, W.; Karp, J. M.; Peer, D. Progress and challenges towards targeted delivery of cancer therapeutics. *Nat. Commun.* 2018, 9, No. 1410.

(30) Byrne, J. D.; Betancourt, T.; Brannon-Peppas, L. Active targeting schemes for nanoparticle systems in cancer therapeutics. *Adv. Drug Delivery Rev.* 2008, 60, 1615–1626.

(31) Coleman, B. R.; Knight, T.; Gies, V.; Jakubek, Z. J.; Zou, S. Manipulation and Quantification of Graphene Oxide Flake Size: Photoluminescence and Cytotoxicity. *ACS Appl. Mater. Interfaces* 2017, 9, 28911–28921.

(32) Khan, U.; O'Neill, A.; Porwal, H.; May, P.; Nawaz, K.; Coleman, J. N. Size selection of dispersed, exfoliated graphene flakes by controlled centrifugation. *Carbon* 2012, 50, 470–475.

(33) Liu, Y.; Zhang, D.; Pang, S.; Liu, Y.; Shang, Y. Size separation of graphene oxide using preparative free-flow electrophoresis. *J. Sep. Sci.* 2015, 38, 157–163.

(34) Geng, H.; Yao, B.; Zhou, J.; Liu, K.; Bai, G.; Li, W.; Song, Y.; Shi, G.; Doi, M.; Wang, J. Size Fractionation of Graphene Oxide Nanosheets via Controlled Directional Freezing. *J. Am. Chem. Soc.* 2017, 139, 12517–12523.

(35) Sun, X.; Luo, D.; Liu, J.; Evans, D. G. Monodisperse chemically modified graphene obtained by density gradient ultracentrifugal rate separation. *ACS Nano* 2010, 4, 3381–3389.

(36) Yang, K.; Wan, J.; Zhang, S.; Tian, B.; Zhang, Y.; Liu, Z. The influence of surface chemistry and size of nanoscale graphene oxide on photothermal therapy of cancer using ultra-low laser power. *Biomaterials* 2012, 33, 2206–2214.

(37) Yan, Y.; Ding, H. pH-Responsive Nanoparticles for Cancer Immunotherapy: A Brief Review. *Nanomaterials* 2020, 10, No. 1613.

(38) Cote, L. J.; Kim, J.; Tung, V. C.; Luo, J.; Kim, F.; Huang, J. Graphene oxide as surfactant sheets. *Pure Appl. Chem.* 2010, 83, 95–110.

(39) Paulista Neto, A. J.; Fileti, E. E. Elucidating the amphiphilic character of graphene oxide. *Phys. Chem. Chem. Phys.* 2018, 20, 9507–9515.

(40) Kim, J.; Cote, L. J.; Kim, F.; Yuan, W.; Shull, K. R.; Huang, J. Graphene Oxide Sheets at Interfaces. *J. Am. Chem. Soc.* 2010, 132, 8180–8186.

(41) Huang, C.; Hu, X.; Hou, Z.; Ji, J.; Li, Z.; Luan, Y. Tailored graphene oxide-doxorubicin nanovehicles via near-infrared dye-lactobionic acid conjugates for chemo-photothermal therapy. *J. Colloid Interface Sci.* 2019, 545, 172–183.

(42) Deng, W.; Qiu, J.; Wang, S.; Yuan, Z.; Jia, Y.; Tan, H.; Lu, J.; Zheng, R. Development of biocompatible and VEGF-targeted paclitaxel nanodrugs on albumin and graphene oxide dual-carrier for photothermal-triggered drug delivery in vitro and in vivo. *Int. J. Nanomed.* 2018, 13, 439–453.

(43) Wang, L.; Yu, D.; Dai, R.; Fu, D.; Li, W.; Guo, Z.; Cui, C.; Xu, J.; Shen, S.; Ma, K. PEGylated doxorubicin cloaked nano-graphene oxide for dual-responsive photochemical therapy. *Int. J. Pharm.* 2019, 557, 66–73.

74

(44) Xie, M.; Zhang, F.; Peng, H.; Zhang, Y.; Li, Y.; Xu, Y.; Xie, J. Layer-by-layer modification of magnetic graphene oxide by chitosan and sodium alginate with enhanced dispersibility for targeted drug delivery and photothermal therapy. *Colloids Surf., B* **2019**, 176, 462–470.

(45) Krishnamurthy, S.; Ng, V. W. L.; Gao, S.; Tan, M.-H.; Yang, Y. Y. Phenformin-loaded polymeric micelles for targeting both cancer cells and cancer stem cells in vitro and in vivo. *Biomaterials* **2014**, 35, 9177–9186.

(46) Chong, C. R.; Chabner, B. A. Mysterious metformin. *Oncologist* **2009**, 14, 1178–1181.

(47) Wheaton, W. W.; Weinberg, S. E.; Hamanaka, R. B.; Soberanes, S.; Sullivan, L. B.; Anso, E.; Glasauer, A.; Dufour, E.; Mutlu, G. M.; Budinger, G. S.; Chandel, N. S. Metformin inhibits mitochondrial complex I of cancer cells to reduce tumorigenesis. *eLife* **2014**, 3, No. e02242.

(48) Kwong, S. C.; Brubacher, J. Phenformin and lactic acidosis: a case report and review. *J. Emerg. Med.* **1998**, 16, 881–886.

(49) Berstein, L. M. Modern approach to metabolic rehabilitation of cancer patients: Biguanides (phenformin and metformin) and beyond. *Future Oncol.* **2010**, 6, 1313–1323.

(50) Zhao, H.; Swanson, K. D.; Zheng, B. Therapeutic Repurposing of Biguanides in Cancer. *Trends Cancer* **2021**, 7, 714–730.

(51) Garcia Rubiño, M. E.; Carrillo, E.; Ruiz Alcalá, G.; Domínguez-Martín, A. A.; Marchal, J.; Boulaiz, H. Phenformin as an Anticancer Agent: Challenges and Prospects. *Int. J. Mol. Sci.* **2019**, 20, No. 20133316.

(52) Di Magno, L.; Manni, S.; Di Pastena, F.; Coni, S.; Macone, A.; Cairoli, S.; Sambucci, M.; Infante, P.; Moretti, M.; Petroni, M.; Nicoletti, C.; Capalbo, C.; Smaele, E.; de Di Marcotullio, L.; Giannini, G.; Battistini, L.; Goffredo, B. M.; Iorio, E.; Agostinelli, E.; Maroder, M.; Canettieri, G. Phenformin Inhibits Hedgehog-Dependent Tumor Growth through a Complex I-Independent Redox/Corepressor Module. *Cell Rep.* **2020**, 30, 1735–1752.e7.

(53) Masoud, R.; Reyes-Castellanos, G.; Lac, S.; Garcia, J.; Dou, S.; Shintu, L.; Abdel Hadi, N.; Gicquel, T.; El Kaoutari, A.; Diémé, B.; Tranchida, F.; Cormareche, L.; Borge, L.; Gayet, O.; Pasquier, E.; Dusetti, N.; Iovanna, J.; Carrier, A. Targeting Mitochondrial Complex I Overcomes Chemoresistance in High OXPHOS Pancreatic Cancer. *Cell Rep. Med.* **2020**, 1, No. 100143.

(54) Yang, K.; Feng, L.; Shi, X.; Liu, Z. Nano-graphene in biomedicine: theranostic applications. *Chem. Soc. Rev.* **2013**, 42, 530–547.

(55) Tao, H.; Zhang, Y.; Gao, Y.; Sun, Z.; Yan, C.; Texter, J. Scalable exfoliation and dispersion of two-dimensional materials – an update. *Phys. Chem. Chem. Phys.* **2017**, 19, 921–960.

(56) Yoo, S.; Hou, J.; Yi, W.; Li, Y.; Chen, W.; Meng, L.; Si, J.; Hou, X. Enhanced Response of Metformin towards the Cancer Cells due to Synergism with Multi-walled Carbon Nanotubes in Photothermal Therapy. *Sci. Rep.* **2017**, 7, No. 1071.

(57) Tao, C.; Wang, J.; Qin, S.; Lv, Y.; Long, Y.; Zhu, H.; Jiang, Z. Fabrication of pH-sensitive graphene oxide–drug supramolecular hydrogels as controlled release systems. *J. Mater. Chem.* **2012**, 22, 24856–24861.

(58) Chengnan, L.; Pagneux, Q.; Voronova, A.; Barras, A.; Abderrahmani, A.; Plaisance, V.; Pawlowski, V.; Hennuyer, N.; Staels, B.; Rosselle, L.; Skandrani, N.; Li, M.; Boukherroub, R.; Szunerits, S. Near-infrared light activatable hydrogels for metformin delivery. *Nanoscale* **2019**, 11, 15810–15820.

(59) Jing, L.; Shao, S.; Wang, Y.; Yang, Y.; Yue, X.; Dai, Z. Hyaluronic Acid Modified Hollow Prussian Blue Nanoparticles Loading 10-hydroxycamptothecin for Targeting Thermochemotherapy of Cancer. *Theranostics* **2016**, 6, 40–53.

(60) Gudarzi, M. M. Colloidal Stability of Graphene Oxide: Aggregation in Two Dimensions. *Langmuir* **2016**, 32, 5058–5068.

(61) Chowdhury, I.; Duch, M. C.; Mansukhani, N. D.; Hersam, M. C.; Bouchard, D. Colloidal properties and stability of graphene oxide nanomaterials in the aquatic environment. *Environ. Sci. Technol.* **2013**, 47, 6288–6296.

(62) Angelopoulou, A.; Voulgari, E.; Diamanti, E. K.; Gournis, D.; Avgoustakis, K. Graphene oxide stabilized by PLA-PEG copolymers for the controlled delivery of paclitaxel. *Eur. J. Pharm. Biopharm.* **2015**, 93, 18–26.

(63) Shrimanker, I.; Bhattarai, S. StatPearls: *Electrolytes*; StatPearls Publishing LLC, 2021.

(64) Lin, W.; Tian, B.; Zhuang, P.; Yin, J.; Zhang, C.; Li, Q.; Shih, T.-M.; Cai, W. Graphene-Based Fluorescence-Quenching-Related Fermi Level Elevation and Electron-Concentration Surge. *Nano Lett.* **2016**, 16, 5737–5741.

(65) Chu, S.-W. Optical microscopy approaches angstrom precision, in 3D! *Light: Sci. Appl.* **2019**, 8, No. 117.

(66) Bagri, A.; Mattevi, C.; Acik, M.; Chabal, Y. J.; Chhowalla, M.; Shenoy, V. B. Structural evolution during the reduction of chemically derived graphene oxide. *Nat. Chem.* **2010**, 2, 581–587.

(67) Guo, D.-S.; Zhang, H.-Q.; Ding, F.; Liu, Y. Thermodynamic origins of selective binding affinity between p-sulfonatocalix4,5arenes with biguanidiniums. *Org. Biomol. Chem.* **2012**, 10, 1527–1536.

(68) Depan, D.; Shah, J.; Misra, R. Controlled release of drug from folate-decorated and graphene mediated drug delivery system: Synthesis, loading efficiency, and drug release response. *Mater. Sci. Eng., C* **2011**, 31, 1305–1312.

(69) Fong, Y. T.; Chen, C.-H.; Chen, J.-P. Intratumoral Delivery of Doxorubicin on Folate-Conjugated Graphene Oxide by In-Situ Forming Thermo-Sensitive Hydrogel for Breast Cancer Therapy. *Nanomaterials* **2017**, 7, No. 388.

(70) Ma, J. C.; Dougherty, D. A. The Cation-pi Interaction. *Chem. Rev.* **1997**, 97, 1303–1324.

(71) Pietrelli, L. Effect of MW and pH on poly(ethylene glycol) adsorption onto carbon. *Adsorption* **2013**, 19, 897–902.

Paper III - Graphene-based phenformin carriers for cancer treatment, a comparative study between oxidized and pegylated pristine graphene in human cells and zebrafish

This paper is not in Brage due to copyright restrictions